AN ANALYSIS OF THE RADIATION BUDGET IN TWO TROPICAL CONTINENTAL ATMOSPHERIC COLUMNS

By

ALLISON BETH COLLOW

A dissertation submitted to the

Graduate School – New Brunswick

Rutgers, The State University of New Jersey

In partial fulfillment of the requirements for the degree of

Doctor of Philosophy

Graduate Program in Atmospheric Science

Written under the direction of

Mark Miller

And approved by

_____

_____

_____

_____

New Brunswick, NJ

May 2015

ABSTRACT OF THE DISSERTATION

An Analysis of the Radiation Budget in Two Tropical Continental Atmospheric Columns

by ALLISON BETH COLLOW

Dissertation Director:

Mark Miller

Many uncertainties remain in the relationship between clouds, aerosols, and radiation, especially in locations along tropical margins. Two regions of particular interest because of their perceived susceptibility to climate change are the Sahel region of West Africa and the Amazon Rainforest of Brazil. Both the Sahel and the Amazon Rainforest have two distinct seasons with varying cloudiness, but the impacts of this cloudiness upon the regional radiation budgets are only vaguely understood. With this in mind, the Atmospheric Radiation Measurement Program's Mobile Facility #1 collected a full year of surface based observations in Niamey, Niger in the central Sahel and Manacapuru, Brazil in the Amazon Rainforest. These surface observations were complemented by top of the atmosphere observations from the Geostationary Earth Radiation Budget instrument and Clouds and the Earth's Radiant Energy System. This dissertation presents observations from these deployments with focus on the diurnal cycle of meteorology and the accompanying radiation budget at the surface, top of the atmosphere, and within the atmospheric column itself in the Sahel and upon the seasonal cycle in the Amazon. Cloud radiative effects (CREs) are examined in detail. Although both regions are located in the tropics and share some common features, their climates

and radiation budgets are very different. Among the conclusions of this work are that clouds reflect incoming solar insolation and prevent the loss of longwave radiation to space in both locations, though the large loading of water vapor and abundance of clouds in the Amazon create a more substantial impact at the boundaries of the atmospheric column. It is demonstrated that CREs are dominated by the shortwave spectrum in the Sahel and by the longwave spectrum in the Amazon Rainforest. It is further demonstrated that CREs are themselves a diurnally varying signal that cannot be appropriately quantified by instantaneous measurements from polar orbiting satellites, but that can be quantified by geostationary satellites equipped with broadband radiometers. Sensitivity to the averaging period employed in the analysis of CREs is also demonstrated, further reinforcing the notion that instantaneous measurements of CREs are likely to produce significant misrepresentations of these effects.

ACKNOWLEDGMENTS

Research for this dissertation was funded by the Department of Energy's Atmospheric System Research program award DE-FG02-08ER64531. Data used in this study were obtained from the Atmospheric Radiation Measurement Program sponsored by the U.S. Department of Energy, Office of Science, Office of Biological and Environmental Research, Climate and Environmental Sciences Division.

Portions of this dissertation appear in Collow et al. (2015)

I would also like to thank

Lynne Trabachino for providing quality controlled rainfall and Microwave radiometer profiler-Merged Sounding data for Niamey, Niger, thermodynamic profiles in Manacapuru, Brazil, as well as the creation of Figure 2.5,

Bryan Raney for assisting with computer codes,

my research advisor – Dr. Mark Miller,

my committee members – Dr. Alan Robock, Dr. Jim Miller, and Dr. Virendra Ghate,

and my husband, Tom, for his support and science discussions

TABLE OF CONTENTS

LIST OF FIGURES

CHAPTER 1: INTRODUCTION

1.1 Overview

Evidence suggests that the climate is changing as a result of anthropogenic emissions of greenhouse gases (IPCC, 2013). Greenhouse gases include carbon dioxide, methane, and water vapor, which change the radiative balance within the Earth-Atmosphere system by absorbing longwave (LW) radiation, heating the troposphere, and emitting a larger amount of radiation toward the surface, thereby preventing some LW radiation from leaving the system at the top of the atmosphere (TOA). Observations show an average increase in global average surface temperature of 0.85°C between 1880 and 2012 (IPCC, 2013). It is expected that the surface temperature will continue to increase in the coming years in response to human influences. Along with an increase in surface temperature, other aspects of the climate system have been changing, such as an increase in extreme events. For example, observations suggest an increase in the frequency of heat waves in Europe, Asia, and Australia and an increase in the frequency or intensity of precipitation events in North America and Europe (IPCC, 2013). While these changes are occurring, many uncertainties within the climate system remain.

General circulation models (GCMs) are one of the tools used to help increase our understanding of the climate system and how the climate may change in the future. The Coupled Model Intercomparison Project 5 (CMIP5) has developed a suite of near and long-term climate simulations with varying levels of greenhouse forcing with the goal of increasing understanding of the climate system and climate change (Taylor et al., 2012). But, the area with the lowest level of confidence in these simulations is representations of the processes by which aerosols interact with clouds and radiation budget (IPCC, 2013).

Regions located within convective margins, or regions with a large gradient in precipitation, are thought to be more sensitive to climate change (Neelin et al., 2006). One such area is the Sahel region of West Africa (Figure 1.1). Nestled between the Sahara Desert and the Atlantic Ocean, the Sahel is home to one of the tightest moisture gradients on Earth as well as a population density similar to the east coast of the United States. The population is extremely sensitive to changes in climate, as they depend on rainfall for their livelihood. Precipitation only occurs a few months out of the year in connection with the wet phase of the West African Monsoon (WAM). A reduction in strength or failure of the wet phase often results in a decrease in rainfall that is detrimental to the population who depend on agriculture for food and their economy (Kandji et al., 2006). A low crop yield resulting from suppressed precipitation can lead to food security concerns, famine, mass migration, and hundreds of thousands of deaths (Hengsdijk and Keulen, 2002; Kandji et al., 2006).

Figure 1.1: Map of West Africa with the Sahel region shaded in pink (ArcGIS).

Changes in the WAM associated with known climate forcing mechanisms such as the North Atlantic Oscillation (NAO) and El Niño Southern Oscillation (ENSO) are thought to be important modulators of precipitation over the Sahel (Li et al. 2012; Joly and Voldoire, 2009), but the exact causes of droughts in the region are not fully understood. A catastrophic 5-year drought that occurred from 1968 through 1973 was linked to changes in the intensity of individual rainfall events rather than a variation in the northward progression of the Intertropical Convergence Zone (ITCZ; Nicholson, 1981). Rainfall deficits between 1971 and 1990 have been linked to a decrease in observed rainfall events, though the cause for these deficits is unknown (Le Barbé et al., 2002). The potential sensitivity to climate change in this and other regions highlights the need for a complete understanding of the current climate and how it might change in the future.

Another region with potential climate change sensitivities is the Amazon Rainforest of Brazil (Figure 1.2). This rainforest is home to one of the largest concentrations of plant and animal species on the planet and plays a pivotal role in Earth's biosphere. Apart from the consequences of fossil fuel consumption, which is largely focused in the Northern Hemisphere, the rainforest has in recent years been subject to human influences in the form of clear-cutting and subsequent biomass burning. These landscape modifications have been concentrated around the periphery of the rainforest in regions known collectively as the ring-of-fire, and the resulting deforestation has been linked to changes in the distribution of precipitation in clear-cut areas and to changes in the regional radiation budget as a consequence of biomass burning aerosol. In addition to this aerosol contrast, deforestation has been an ongoing concern for Amazonia and is hypothesized to alter the amount of

rainfall in the area (Chue et al., 1994, Cauduro Dias de Paiva and Clarke, 1995, D'Almeida et al, 2007).

Figure 1.2: Map of the northern half of South America showing the location of Manaus and the Amazon Rainforest (ArcGIS).

Due to its unique location the Amazon rainforest, Manaus, Brazil, and its surrounding area have generated scientific interest, especially in the 1980s and 1990s (Figure 1.2). The region downwind of Manaus is of particular interest due to its pristine environment which is at times countered by aerosols from biomass burning and industry when the wind is from the proper direction. When present, these aerosols have the potential to serve as cloud condensation nuclei (CCN) and thereby impact the radiation budget, either directly or indirectly. In the past 20 years data collection in Amazonia has been limited even though deforestation and climate change are occurring, whereupon it is

desirable to collect data that can be used to verify the output from GCMs and improve our understanding of the climate in a tropical rainforest and how it has changed over the years.

An important aspect of the climate system and the radiation budget is the diurnal cycle. It is imperative that GCMs are capable of capturing the diurnal cycle accurately. Past studies have highlighted the difficulty in simulating the diurnal cycle in some GCMs and accurate portrayal of the cycle is a good test of GCM physics (DelGenio and Yao, 1988). Many factors that can influence the radiation budget are on timescales of less than one day. It has been shown that radiative forcing at the surface is dependent on constituents with sub-seasonal variations, including water vapor, clouds and aerosols (Miller et al. 2009). In addition, Milton et al. (2008) showed that on seasonal and diurnal time scales models have a difficult time representing the radiation balance, especially in the shortwave (SW), indicating we need a better understanding of the factors that control radiation transfer. It is challenging for GCMs to accurately simulate the WAM due to the complex interplay between the radiation, convection, land-surface and atmosphere coupling, and large-scale and mesoscale flow features that conspire to produce clouds and precipitation in the region (Koster et al., 2005; Miller et al., 2012). Many previous studies on the energy budget show a global, annual mean, which are not capable of assessing these factors in the radiation budget as well as average out characteristics that may only impact a particular region. Studies such as Trenberth et al. (2009) do not consider regional energy budgets and diurnal cycles with a temporal resolution that is compatible with the atmospheric structures that modulate it.

There have been past attempts to quantify energy budgets on regional and local scales in the tropics (Miller and Slingo, 2007, McFarlane et al., 2008, Slingo et al., 2009,

Miller et al., 2012). These studies have produced heating rate profiles or "bulk" measurements of the net radiative heating of the column, which is known as Radiative Flux Divergence (RFD). A positive value of RFD implies radiative heating within the column, while a negative value implies radiative cooling. One of the first direct measurements of RFD is shown by Miller and Slingo (2007), focusing on Niamey, Niger, Africa, which lies in the West African Sahel region. Data from a single day with a resolution of 15 minutes demonstrated the impact of clouds on the downwelling SW radiation, and the variability in the SW RFD due to changing cloud cover was easily detected. Slingo et al. (2009) later expanded this study to provide a seasonal view over Niamey and while not on a diurnal time scale, this study demonstrated that water vapor in the wet season prevents a portion of LW radiation at the surface and within the lower troposphere from exiting at the TOA and that wet season clouds reflect, absorb, and scatter incoming SW radiation, preventing a portion from reaching the surface. Miller et al. (2012) presented a detailed analysis of the annual progression of RFD, cloud radiative forcing (CRF) and cloud radiative effect (CRE) over Niamey using observations. In their study, CRF was used to denote the impact of clouds at the surface and TOA, while CRE was used to denote the impact of clouds on the atmospheric column. However in this study, as well as others, CRE is used for all three locations. The observed monthly RFD was compared to that projected in several GCMs included in CMIP3. It was shown that clouds cause a slight net warming at the TOA (~20-40 W m^{-2}) and more substantial net cooling at the surface (~-30-100 W m^{-2}) resulting in a net warming within the atmosphere between 30 and 70 W m^{-2} depending on the month. It was demonstrated that the regional radiation budgets portrayed in many commonly used GCMs over the Sahel contained improper partitioning of radiant energy between the

surface and the atmosphere. It was also shown that some GCMs produce credible estimates of the net RFD and net CRE due to compensating errors.

McFarlane et al. (2008) used observations made on the islands of Nauru and Manus in the Tropical Western Pacific to investigate the impact of clouds on SW radiation. They reported that low clouds tend to increase SW absorption in the column compared to clear skies and that middle and high level clouds can either increase or decrease absorption depending on their location, particle size, and water vapor within the column. Their study suggested that averaging over the course of a day makes it difficult to detect variability in the absorption of radiation by clouds as the averaged data showed less than 5 W m^{-2} of absorption in many cases. Parding et al. (2011) also examined SW absorption within clouds using ground and satellite measurements. The study showed that in order to reduce temporal and spatial mismatches in the data between the two boundaries, a three-hour average must be used.

Miller et al. (2012), McFarlane et al. (2008), and Parding et al. (2011) provide a solid framework from which to investigate the details of the energy budget within an atmospheric column on a regional scale. It is desirable to expand the scope of the studies by combining specific attributes of these studies to seasonal and diurnal time scales. It is also important to investigate and contrast different locations within the tropics as characteristics can widely vary from location to location. Previous studies have shown the radiation budget and its controls in one tropical location may not be indicative of that in another. Lack of a comprehensive knowledge of the tropical climate is a weakness in our understanding of the global energy budget so more detailed studies, such as the current one, are needed. To our knowledge, the diurnal cycle of the RDF and atmospheric CRE for

an entire year using only observations has not been published in the past, making this dissertation new and unique.

1.2 Climate in the Sahel Region of West Africa

The climate in the Sahel region of West Africa is heavily influenced by the phase of the WAM in addition to yearly variations in its duration and strength. The WAM is marked by two distinct seasons; a dry season from October to April and a wet season from May to September. During the dry season, the surface winds are predominantly northerly from the Sahara Desert bringing in dry and hot air to the region. Very little cloud cover is observed during the dry season, most of which is due to advection of high level tropical cirrus clouds. These dry season cirrus clouds have a cloud fraction of ~20% and thickness of one km (Kollias et al., 2009). Due to the increased heating in the Northern Hemisphere summer, a heat low forms over the Sahara Desert causing a large pressure gradient between this low and the Santa Helena anticyclone over the southern Atlantic Ocean (Sultan and Janicot, 2003). The surface winds controlled by this pressure gradient undergo backing to the west resulting in the advection of cool air from the tropical Atlantic to the region. This westerly wind is maintained through September and these monsoonal winds converge with dry Harmattan winds along the intertropical front (ITF; Lélé and Lamb, 2010). The ITF is a distinct feature from the ITCZ and remains north of the ITCZ. The passage of the ITF at a given location in the central Sahel indicates the "pre-onset" of the monsoon and is characterized by the advection of moist air, with minimal precipitation. Following a quasi-stable period in May and June, the ITCZ propagates northward from 5 to 10°N and a Hadley-type circulation sets up, initiating the onset of the wet season when the majority of the precipitation occurs (Sultan and Janicot, 2003).

The wet season of the monsoon is also marked by other changes in dynamics and winds aloft. The tropical easterly jet located at 200 hPa strengthens as the wet season progresses, peaking in August when convection and rainfall also peak. In addition, the African easterly jet (AEJ) located at 700 mb calms (Sultan et al., 2003, Sultan and Janicot, 2003). The AEJ forms in response to two diabatically forced meridional circulations: heating and dry convection in the Sahara Desert and deep convection associated with the ITCZ. Vertical shear within the AEJ allows for squall lines and mesoscale convective complexes (MCCs) to maintain their strength or intensify (Thorncroft and Blackburn, 1999, Parker et al., 2005a).

These changes in dynamics and circulation associated with the WAM over West Africa characterize the climate. As a result of the WAM, the advection of cooler moist air into the Sahel's lower troposphere feeds convection during the wet season, along with evaporation from the surface after the initial onset (Bock et al., 2008). This convection produces clouds, precipitation, and the growth of surface vegetation that decreases the surface albedo. Precipitation is generally observed from May to September, with the climatological maximum in August (Lebel and Ali, 2009). The wet season ends as the Northern Hemisphere summer heating subsides and collapses the Saharan heat low, thereby reversing the large-scale pressure gradient between the tropical Atlantic and the Sahara desert and, once again, producing hot, dry northerly winds over the Sahel region.

The wet season of the WAM is marked by a large increase in moisture, but rainfall is not a daily occurrence as the majority of the precipitation is associated with larger scale features such as MCCs and easterly waves. Precipitation often occurs in bursts followed

by days without any rainfall and minimal cloud cover. A steady decrease in the lifting condensation level (LCL) is observed in the wet season and it reaches its lowest level in August. The height of the LCL exhibits a large correlation with rainfall, while large values of convective available potential energy do not show any correlation with precipitation in this region (Kollias et al., 2009).

Diurnal variability is a robust signal in the Sahel region as demonstrated in past studies. During the day, when the convective boundary layer is deeper, monsoonal winds are relatively weak (Parker et al., 2005b; Abdou et al., 2009; Pospichal et al., 2010). This allows for moisture to mix vertically as the lower atmosphere heats and turbulent mixing is strong. Overnight, monsoonal winds strengthen as boundary layer turbulence weakens and horizontal advection becomes important (Parker et al., 2005b). These nighttime winds take on a southwesterly flow as the nocturnal jet between 200 and 400 m in altitude sets up north of the ITCZ and south of the ITF (Sultan et al., 2007; Lothon et al., 2008; Abdou et al., 2009). Enhanced nocturnal monsoonal winds increase moisture advection and in combination with destabilization caused by radiative cooling leads to a nocturnal maximum in precipitation that peaks during the early morning hours (Peyrillé and Lapore, 2007; Lothon et al., 2008). The majority of this precipitation is associated with MCCs that are enhanced by the shear in the nocturnal jet (Laing & Fritsch, 1993; Mohr, 2004). This change in diurnal winds in the boundary layer and thermodynamics are important mechanisms for the monsoon system and the climate in the Sahel.

The presence of clouds and water vapor during the wet season of the WAM can be seen in the surface and TOA radiative fluxes, as well as the net cooling of the column (i.e. RFD). Unless a direction is indicated, a positive net flux is entering the atmospheric

column, while a negative net flux is leaving the column. The surface downwelling LW flux increases by an average of about 30 W m^{-2} with the largest increase in May and June. The upwelling LW flux at the surface shows a large correlation to surface temperature and averages roughly 475 W m^{-2} during the wet season. The net surface LW is heavily influenced by column water vapor, with the minimum occurring in May and gradually increasing to almost 50 W m^{-2} in August. Both the upwelling and downwelling components of the surface SW flux decrease in the wet season, despite the seasonal increase in solar insolation. Clouds and water vapor reflect and absorb solar insolation, preventing it from reaching the surface. In addition, the surface albedo decreases due to the darkening of the surface from the growth of vegetation that results from rainfall. These two influences result in a reduction in the net surface SW flux that can exceed -100 W m^{-2} (Slingo et al., 2009, Miller et al., 2009).

An increase in the net surface LW flux is balanced by a decrease in the outgoing LW flux at the TOA during the wet season. Less LW radiation is able to exit to space with more LW radiation emitted isotropically by clouds and water vapor. In addition, clouds increase the albedo of the atmosphere, causing more SW radiation to be reflected and increasing the outgoing TOA SW flux (Slingo et al., 2009). SW fluxes are controlled by the annual progression of solar insolation, clouds, aerosols, water vapor, and seasonal changes in albedo, while the LW fluxes are controlled by the temperature of the surface and atmosphere, clouds, aerosols, and water vapor.

The radiative fluxes at the surface and TOA contain significant information, but they do not show how much radiation is absorbed or used for heating within the atmosphere. The daily and month average net column cooling (RFD) were presented by

Slingo et al. (2009) and Miller et al. (2012). The SW column radiative heating increases once water vapor and clouds are present in the wet season due to absorption. However, at the same time there is a coincident small decrease in the LW column radiative cooling. As a result, the net column cooling has an annual mean of 52 W m^{-2}, with a range 25 W m^{-2} around the mean. Clouds tend to have a large effect on the radiative fluxes at the column boundaries (surface and TOA), but a relatively smaller effect on the net column cooling. The surface SW CRF can reach a cooling of 140 W m^{-2} at the height of the wet season. There is a more subtle impact at the TOA and in the LW fluxes.

Aerosols and dust are a common feature of the Sahel region and must be considered when analyzing the radiation budget. Dry season mineral dust, primarily composed of kaolinite and gypsum, has been observed to have aerosol optical depths (AODs) at 500 nm exceeding 2 during dust storms (Turner et al., 2008). The AOD in this region can be quite variable, ranging from 0.08 to 2.5. Dust is usually located near the surface, between 0 and 2 km, while biomass burning aerosols are found between 2 and 6 km (McFarlane et al, 2009). These aerosols result in a heating of the bottom kilometer of ~4 K day^{-1} and ~2 K day^{-1} between 1 and 5 km. This warming in the atmosphere is compensated by a cooling at the surface and because downwelling radiation is absorbed and scattered, a decrease of the downwelling component of the SW surface flux is observed (McFarlane et al, 2009, Mallet et al., 2009). Aerosols can also reduce the amplitude of the diurnal cycle of precipitation (Kim et al., 2010).

At the surface, latent and sensible heat fluxes are an important component of the energy budget in the Sahel, especially during the day in the wet season. Latent and sensible heat are negligible overnight during both seasons. Once the wet season rainfall wets the

surface, evaporation of moisture from the bare soil and evapotranspiration (as the surface greens) result in an average latent heat flux of 49.2 W m^{-2}. The diurnal peak in the latent heat flux occurs just after local noon at 125 W m^{-2}. Sensible heat also peaks at noon in both seasons with a diurnal average of 65 W m^{-2} in the dry season and 55 W m^{-2} in the wet season. A maximum sensible heat flux over 200 W m^{-2} in the dry season indicates the large amount of heating that occurs (Miller et al, 2009).

1.3 Climate in the Amazon Rainforest of Brazil

Measurements from the Amazon Rainforest are quite rare and due to its unique location, Manaus, Brazil, which is a city of 2 million located within the rainforest (Figure 1.2), and the surrounding area has generated scientific interest, especially in the 1980s and 1990s. Like other regions in the tropics, the climate in Manaus is characterized by wet and dry seasons and is, on the whole, extremely moist with values of integrated water vapor exceeding 40 kg m^{-2} in the dry season (Rao et al. 1996). The dry season, occurring in July and August, tends to have more convective clouds than the wet season, with a monthly average rainfall of 100 mm (Culf et al, 1998, Machado et al., 2004). Characterized by more frequent rainfall events, December through April is considered to be the wet season with an average rainfall between 200 and 300 mm (Culf et al, 1998, Negri et al., 2000, Malhi et al., 2002, Machado et al., 2004). These data suggest an annual peak in rainfall in May that exceeds 400 mm. The majority of dry season rainfall events in Manaus occur in the afternoon, while they occur in the evening in the wet season (Negri et al., 2000, Machado et al., 2002, Machado et al., 2004, Rickenbach, 2004). Observations also indicate a secondary nocturnal maximum often associated with large scale squall lines (Rickenbach, 2004). Cloud fraction reaches its daily maximum hours after the peak in rainfall (Machado

et al., 2002). Although moderate precipitation events are quite common and convective in nature, Amazonia does not experience as many intense storms as other equatorial regions over land (Zipser et al., 2006). It has been suggested that the long convective season in this region results from a continually moist boundary layer and the lack of an inversion, which is associated with large scale circulation changes due to equatorial sea surface temperatures.

Aside from rainfall patterns, numerous studies have analyzed the surface radiation budget in Amazonia and many have focused upon influence of biomass burning on solar insolation (Eck et al., 1998, Schafer et al., 2001, Rosario et al., 2011). Increased cloudiness during the wet season results in a decrease in the solar radiation reaching the surface with an approximate downwelling flux of 175 W m^{-2} from February through March (Culf et al., 1998, Malhi et al., 2002). This decrease in solar radiation occurs on a diurnal time scale with a reduction in insolation of 125 W m^{-2} at the diurnal maximum observed around local noon (Hahmann and Dickinson, 1997, Malhi et al., 2002). Simulations of cloud radiative forcing suggest that almost triple the amount of SW radiation can reach the surface in the absence of clouds (Culf et al., 1998), although clouds are not the only feature within the atmosphere that can impact downwelling SW radiation in this region. The aerosol single scattering albedo at both 440 and 870 nm can exceed 0.9 on average and the AOD at 440 nm can exceed unity when smoke is present (Schafer et al., 2002, Rosario et al., 2011), although the likelihood of smoke over Manaus is relatively small. With a surface albedo around 0.13 in the surrounding region, or smaller, due to dense vegetation, some of the downwelling solar radiation is reflected at the surface resulting in a daily maximum

absolute value of the net surface SW flux of about 625 W m^{-2} in the dry season and 500 W m^{-2} in the wet season (Giambelluca et al., 1997, Culf et al., 1998, Malhi et al., 2002).

Previous studies have not directly measured the surface upwelling and downwelling components of the LW radiative flux. As a result, these studies calculate the net LW flux by subtracting the net SW flux from the net all-wavelength flux (Culf et al., 1998, Malhi et al., 2002). Cloudiness and large values of water vapor prevent LW radiation from escaping to space, sending much radiation back to the surface, resulting in small values of net LW radiation at the surface. The net LW flux at the surface is relatively minuscule compared to the net SW flux and through the course of the year, the average monthly values of net LW flux leaving the surface never exceeds an absolute value of 30 W m^{-2} (Culf et al., 1998). Overnight the LW flux is slightly negative and only deviates from this value in the afternoon in the wet season and during sunlight hours in the dry season (Malhi et al., 2002). As a result of the small net LW flux, the net surface flux is positive during the day (the surface absorbs radiation) and minuscule at night (Mahli et al., 2002). To date, little work has been done incorporating radiative fluxes measured at the top of the atmosphere with those measured at the surface therein creating a need for an understanding of the cross atmosphere radiation budget over the Amazon.

The sensible and latent heat fluxes are important components of the surface energy budget due to the large amount of moisture at the surface. The sensible heat flux has a minimum around 6 pm local time in both seasons with a value of -40 W m^{-2} in the wet season and -80 W m^{-2} in the dry season (Figure 1.3b; Hahmann and Dickinson, 1997). There is a gradual increase as the night progresses until the sun rises and the sensible heat increases drastically until it peaks at noon in the wet season with a maximum of 400 W m^{-2}

and at 2 pm in dry season with a maximum of 150 W m^{-2} (Figure 1.3b and d; Hahmann and Dickinson, 1997). Like the sensible heat flux, the latent heat flux is influenced by solar insolation, which drives turbulent transport. Latent heat is constant overnight in both seasons with a value just above zero (Figure 1.3a and c). Both wet and dry season maxima occur at noon and exceed 300 W m^{-2} (Hahmann and Dickinson, 1997).

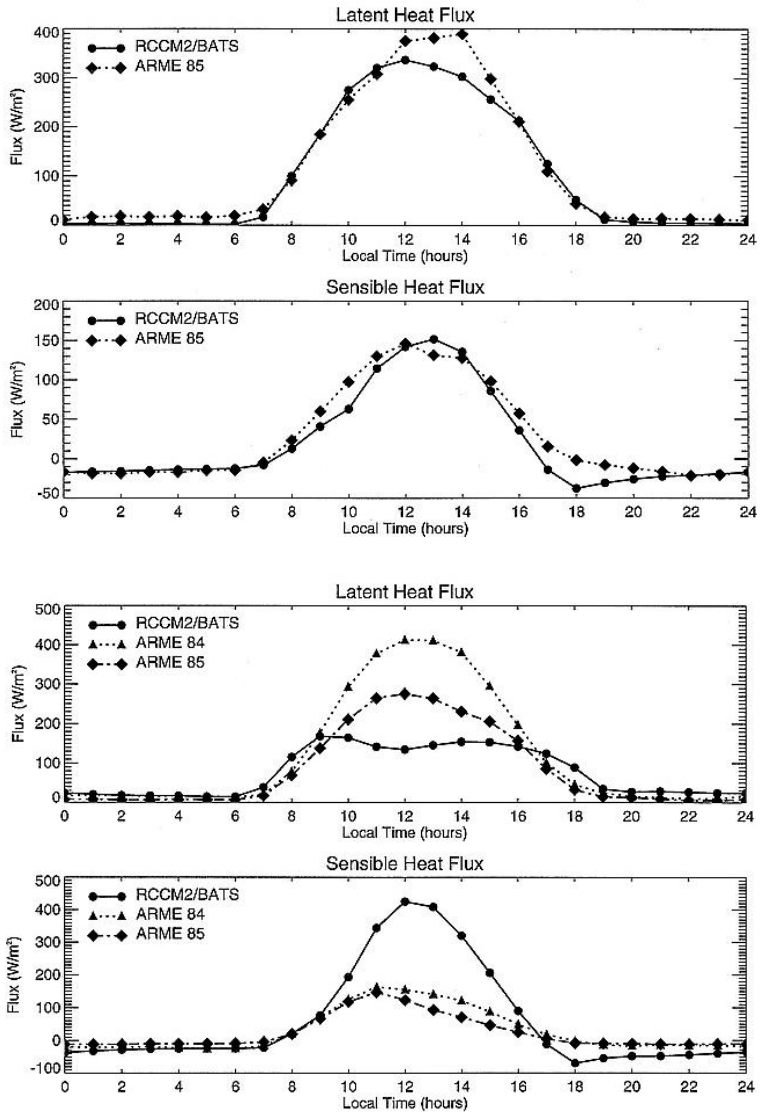

Figure 1.3: The diurnal cycle of (a) latent and (b) sensible heat flux in the Amazon Rainforest in April 1985 and in (c and d) August 1985 (Figures 5 and 6 from Hahmann and Dickinson, 1997).

The Amazon River and its tributaries are large bodies of water that can influence the surface wind field in the area. This river breeze can influence the local climate and weather. River breeze circulations have been previously documented in the Tapajós River and Amazon River near Santarém and the Negro River and Solimões River near Manaus (Oliveira and Fitzjarrald, 1992, Dias et al., 2004; Figure 1.4). This feature is more prevalent in the dry season. Daytime heating of the land surface causes the land to be warmer during the day, but the river to be warmer overnight. Similar to a sea breeze circulation, a low level low pressure perturbation develops over the warmer surface resulting in convergence of low level air and rising motion, which descends over the cooler surface. This diurnal change in pressure results in a 180° wind shift between the daytime and nighttime hours.

(a)

(b)

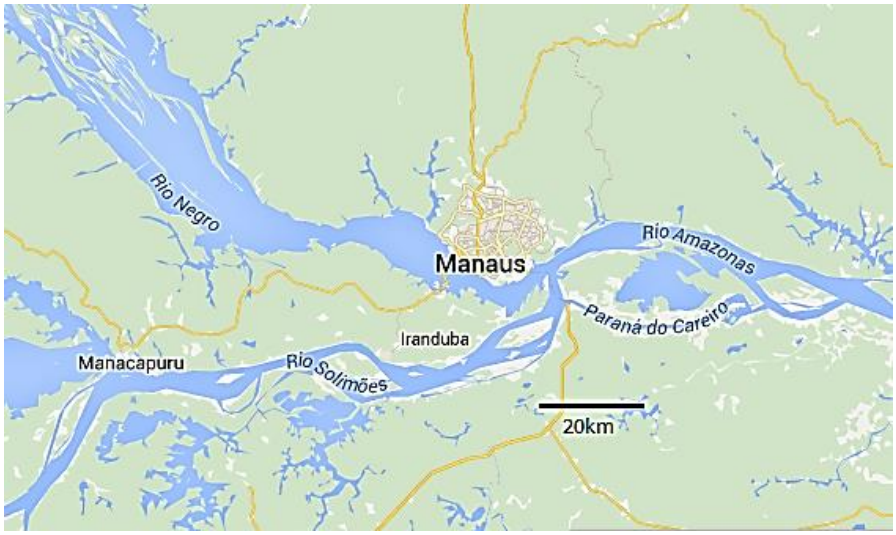

Figure 1.4: (a) Map showing the location of the Amazon River and Rio Tapajós in relation to Santarem. (b) Map showing the location of the Rio Negro and Rio Solimões in relation to Manaus (Google Maps).

1.4 Atmospheric Radiation Measurement Program's Mobile Facility (AMF)

The AMF is a suite of instruments deployed by the Department of Energy that travels to climate-change-sensitive locations to obtain measurements necessary for the study of climate (Miller and Slingo, 2007, Mather and Voyles, 2013). It became operational in 2005 and was deployed internationally for the first time in 2006 when it was stationed

in Niamey, Niger (13.52 °N, 2.11 °E, 207 m alt; Figure 1.5) (Miller and Slingo, 2007, Mather and Voyles, 2013). This deployment was part of a larger field campaign with the African Monsoon Multidisciplinary Analyses, entitled Radiative Divergence using AMF, Geostationary Earth Radiation Budget Instrument (GERB), and African Monsoon Multidisciplinary Analyses Stations. Throughout this campaign, the AMF was stationed at the Niamey Airport, with a secondary site located roughly 50 km to the east in Banazambou. Throughout 2014 and 2015, the AMF will be located in Manacapuru, Brazil (3.21 °S, 60.60 °W, 50 m alt) as part of the Green Ocean Amazon (GOAmazon) campaign (Figure 1.6). These data sets are the backbone of this dissertation.

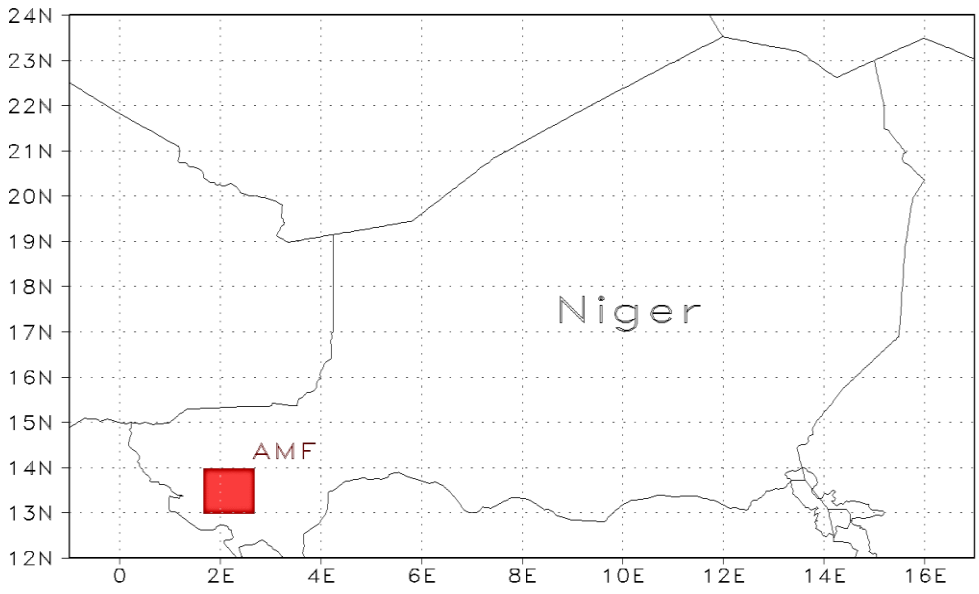

Figure 1.5: Map of Niger showing the location of the AMF in 2006.

A main focus of the AMF is the measurement of radiation and its controls. Eppley hemispheric pyranometers and pyrgeometers measure upwelling LW and SW radiation 18 m above ground level with a temporal resolution of 1 minute. A multifilter rotating shadowband radiometer also measures downwelling SW radiation but with the added

benefit of separating direct and diffuse radiation into five narrowband spectral regions in the visible and near infrared wavelength band so that aerosol optical depth can be calculated. Surface latent and sensible heat fluxes are derived from measurements collected using an eddy correlation system, however these measurements are unavailable for the wet season in the Amazon and are therefore not presented for that region.

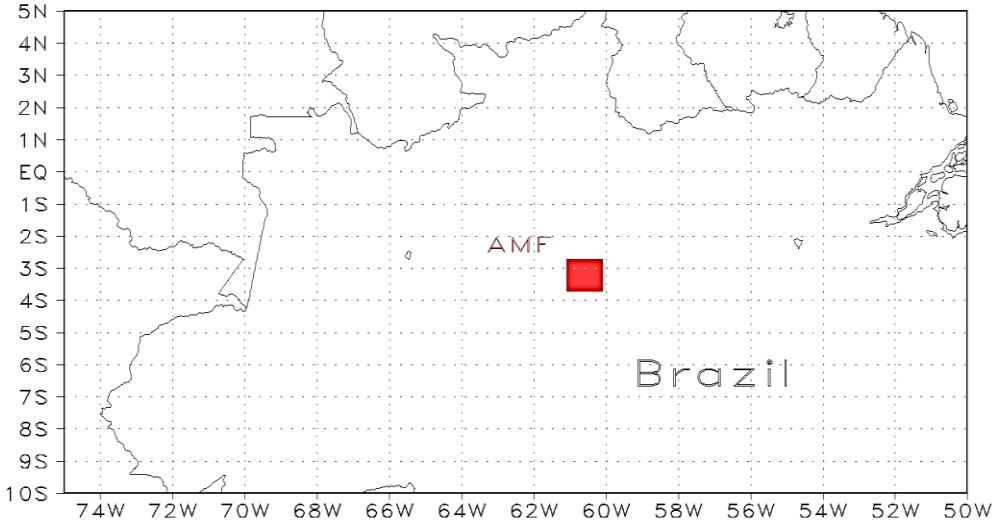

Figure 1.6: Map of Brazil showing the location of the AMF in 2014.

A standard AMF deployment includes measurements of all standard meteorological quantities at the surface using instruments mounted on a 10 m tower (Miller and Slingo, 2007). These measurements include in situ temperature at 2 m in altitude, wind speed and direction at 10 m in altitude, relative humidity at 2 m in altitude, and rain rate every minute with respective accuracies of 0.4 °C, 2%, 3°, 2%, and 0.1 mm hr^{-1} (ARM Climate Research Facility, 2011). Rawindsondes were launched every 6 hours giving profiles of temperature, moisture, pressure, and wind speed and direction (Miller and Slingo, 2007). In addition to rawindsondes, integrated water vapor and cloud liquid water are measured by a line of sight microwave radiometer using emissions at 23.8 and 31.4 GHz every 20 seconds (Morris,

2006). A microwave radiometer profiler (MWRP) measures temperature with an infrared thermometer and emissions in the microwave V-band with an accuracy of 0.5°C and water vapor (Liljegren, 2002). The MWRP was not operational in Manacapuru, Brazil during 2014 however was present in Niamey, Niger for the duration of the West African deployment. A 915 MHz radar wind profiler measures wind speed and direction with height with a temporal resolution of 6 minutes and a spatial resolution of 75 m (Coulter, 2012a). The wind profiler cycles between five directions and two pulse length settings and is capable of measuring speed within 1 m s^{-1} and direction within 3° (Coulter, 2012a).

Clouds can have a significant impact on the radiation budget and are therefore sampled in detail using AMF instrumentation. A micropulse lidar (MPL) and laser ceilometer measure cloud base height, while a 95 GHz vertically pointing cloud radar measures the profiles of other cloud properties. The cloud radar has a temporal resolution of 2 seconds and an uncertainty in reflectivity of 0.5 dB (Widener and Johnson, 2006). The MPL has a temporal resolution of 30-60 s and a resolution of 30m (Coulter, 2012b), while the laser ceilometer has a temporal resolution of 30 seconds and a range resolution of 15 meters (Morris, 2012). These three instruments were combined to create the Active Remotely-Sensed Cloud Locations (ARSCL) value added product. A more detailed description of the AMF and its deployment in Niamey, Niger can be found in Miller and Slingo (2007).

1.5 GERB

Located aboard the European Space Agency's Meteosat-8, GERB collects near-real-time broadband SW ($\lambda < 4$ μm) and LW ($\lambda > 4$ μm) TOA radiances and fluxes every 15 minutes for its entire field of view with a spatial resolution of 50 km. GERB works in

conjunction with the Spinning Enhanced Visible and Infrared Imager (SEVIRI), which examines the geometry of the radiance field to provide radiative fluxes (Sandford et al., 2003, Harries et al., 2005). Measurements of the total radiation emitted in the spectral band between 0.32 and 100 μm, and reflected SW broadband radiation from 0.32 to 4 μm are collected by the GERB/SEVIRI combination (Sandford et al., 2003, Harries et al., 2005). The LW broadband radiation is then calculated from the total radiation minus the SW radiation (Harries et al., 2005). The field of view of GERB moves from east to west allowing for extensive coverage of the tropics and midlatitudes centered over Africa (Sandford et al. 2003).

Instrument uncertainties are known to satisfy RFD calculations (Miller et al., 2012). Onboard calibration units allow for the instrument to recalibrate in between each measurement taken, with three measurements every 40 ms. After data are collected, they are geolocated, rectified, converted to fluxes, and binned or averaged (Sandford et al., 2003, Harries et al., 2005).

An angular dependence model is used to convert the observed radiances into fluxes (DeWitte et al., 2000, Clerbaux et al., 2008). Multiple sources of error combine to create an uncertainty in the resulting radiative flux, but the absolute uncertainty in outgoing LW radiation is estimated to be 0.96% and the uncertainty for SW radiation estimated to be 2.25% (Russell et al., 2006). The GERB instrument was shut down for up to 6 hours every night during the eclipse seasons when the Earth eclipsed the sun, allowing GERB sensors to cool rapidly. It was also shut down for about an hour each day around 11:30 am local time to prevent sun glint, which incorporated the periods of February 9 to April 23, 2006 and August 18 to October 30, 2006 (Harries et al., 2005). In addition, GERB sensors did

not collect any data for the period between September 24, 2006 and October 9, 2006 (Slingo et al., 2009). Unless noted, GERB data were available for the rest of 2006 and used in this dissertation. The absence of the late September and early October data should not have produced a major impact on the calculated statistics presented in this study. Minor impacts may be present, particularly around noon due to the prevention of sun glint at the solar maximum. As a result of a failed launch of a new satellite, GERB has not been operational since January 2013 and can therefore not be used in conjunction with the AMF observations in Brazil.

1.6 Clouds and the Earth's Radiant Energy System (CERES)

Similar to GERB, CERES contains a broadband radiometer aboard a satellite with the goal of measuring radiances and fluxes at the TOA. CERES measures radiation between 0.2 and 100 μm, with the cutoff between the SW and LW channels at 5 μm at a spatial resolution of 20 km (Weilicki et al., 2006). CERES data used in this study were taken from observations made aboard the Aqua and Terra satellites, both on near polar orbits that cross the equator at 10:30 am and 1:30 pm local time. Just like GERB, CERES' radiances are used in conjunction with an imager, in this case the Moderate Resolution Imaging Spectroradiometer, and are converted to radiative fluxes using an angular dependence model (Loeb et al., 2005).

1.7 Rapid Radiative Transfer Model (RRTM)

Interpretation of the impacts of the boundary fluxes and clouds and aerosols in atmospheric columns may be estimated using a radiation transfer model. The LW and SW radiative fluxes and cooling rates calculated using RRTM are based upon detailed calculations made using a Line-By-Line Radiative Transfer Model. The Line-By-Line

Radiative Transfer Model is used to obtain absorption coefficients (Mlawer et al., 1997) and the correlated-k method is used to make calculations that have an accuracy comparable to line-by-line codes without performing as many operations by using a set of absorption coefficients that vary by wavenumber. This is done by mapping the absorption coefficients $k(v)$, where v is frequency, from a spectral space to a variable defined space. This allows for temperature, pressure, and relative molecular concentrations to change from layer to layer and impact $k(v)$ differently. Each spectral band resolved in RRTM must have at most two species with considerable absorption. A layer by layer radiative transfer calculation is performed for each interval according to the Schwartzchild equation, $R'=R_0+(B_{eff} - R_0)A$, where R' and R_0 are the outgoing and incoming radiances, B_{eff} is the Planck function, and A is absorptance. The RRTM code can account for numerous atmospheric gases including water vapor, carbon dioxide, ozone, nitrous oxide, methane, CFC-11, CFC-12, CFC-22, and CCl_4 in addition to the effects of liquid and ice clouds (Mlawer et al., 1997, Mlawer and Clough, 1998).

Radiation transfer calculations performed using RRTM were set up for this study using the following options. The LW and SW versions of the model were run separately and the output was combined to analyze the net radiation budget. Measured surface temperature from the surface meteorology system at the AMF was used. Average temperature and relative humidity was adjusted for the 42 layers above the surface based on derived values from the MWRP-Merged Sounding Product developed by Lynne Trabachino (Trabachino and Miller, 2014). Surface emissivity was assumed to be unity and Lambertian reflection occurred at the surface. In the SW model, cloud fraction was always equal to unity if there was a cloud present. RRTM was run every 5 seconds, which

is the temporal resolution of the cloud radar. If the ARSCL algorithm detected a cloud within those five seconds, the cloud fraction was assumed to be 100%. Otherwise, a zero percent cloud fraction was used. The results were then hour averaged.

For both LW and SW, cloud water path, ice fraction, ice effective radius, and liquid effective radius was calculated using the method presented in Dunn et al. (2011) and currently used in Microbase, which is a retrieval algorithm utilizing constrained data from a cloud radar and other instruments. The accuracy of this retrieval algorithm has been evaluated using radiative closure experiments and it is known to be accurate enough to adequately represent radiation transfer through clouds. It has been used in past studies (Mather et al. 2007) to estimate tropical heating rate profiles. Complete validation of such an algorithm is not possible using in-situ measurements, but its reliance upon cloud liquid water path and its use in the tropical atmosphere are consistent with its capability. All clouds that are colder than -16 °C were considered to be comprised entirely of ice, while all clouds above 0 °C were liquid. A linear fractionation scheme was used to partition particle phase in the region between 0 and 16 °C. On days that exhibit deep convection with moderate precipitation events, it is not possible to measure the location of the cloud top with an accuracy that is sufficient for modeling the radiation. In addition the MWRP does not work properly when it is raining. As a result, radiation calculations were not performed when these conditions were present.

1.8 Calculations and Methodology

Unlike measurements from the AMF, GERB and CERES, some variables of interest must be calculated. Solar insolation was calculated using the Sun position algorithm as described by Reda and Andreas (2008) and another calculated quantity is the

height of the LCL, which was computed as outlined in Bolton (1980). The large scale vertical velocity at 700 mb (ω_{700}), as reported by the National Centers for Environmental Prediction (NCEP) reanalysis was used in this study.

To reduce random error and uncertainties associated with GERB and AMF instruments, all AMF meteorological data were averaged into 1-hour bins and all radiation variables into 3-hour bins for the diurnal cycle. All quantities were subsequently classified by season with the wet season incorporating July, August, and September for Niamey, Niger as done by Miller et al. (2009), and the dry season in Niamey, Niger including January through March as done by Milton et al. (2008). Since the cloud radar and wind profiler become operational in March 2006, only the wet season has been analyzed for their respective fields in Niamey, Niger. Since CERES does not have a temporal resolution that can be used for a diurnal cycle study, observations in the Amazon were averaged by month to analyze the seasonal cycle of all variables. The diurnal cycle of meteorology and surface radiative fluxes were computed using the same averaging technique as for Niamey, Niger. The wet season is defined as January, February, and March, while the dry season includes July, August, and September in Manacapuru, Brazil. TOA radiative fluxes were computed using

$$F_{SW\_TOA} = I_0 - SW\uparrow_{TOA} \tag{1.1}$$

$$F_{LW\_TOA} = -LW\uparrow_{TOA}, \tag{1.2}$$

where I_0 is the TOA solar insolation, $SW\uparrow_{TOA}$ is the upwelling SW radiation at the TOA, and $LW\uparrow_{TOA}$ is the upwelling LW radiation at the TOA. The surface net SW and LW radiative fluxes, F_{SW} and F_{LW}, were calculated using

$$F_{SW} = SW\uparrow_{surface} - SW\downarrow_{surface} \tag{1.3}$$

$$F_{LW} = LW\uparrow_{surface} - LW\downarrow_{surface}, \quad (1.4)$$

where $SW\uparrow_{surface}$ is the upwelling SW radiation at the surface, $SW\downarrow_{surface}$ is the downwelling SW radiation at the surface, $LW\uparrow_{surface}$ is the upwelling LW radiation at the surface, and $LW\downarrow_{surface}$ is the downwelling LW radiation at the surface This sign convention has been chosen so the radiative fluxes could be analyzed in context of the RFD with any radiative flux entering the column as a positive quantity or any radiative flux leaving the column at one of the boundaries as a negative quantity. Therefore, a positive radiative flux denotes a gain to the Earth-Atmosphere system.

The cross-atmospheric RFD, which quantifies the surplus or deficit of radiation across the column that heats or cools it, was also calculated using

$$RFD_{SW} = I_0 - SW\uparrow_{TOA} + SW\uparrow_{surface} - SW\downarrow_{surface} \quad (1.5)$$

$$RFD_{LW} = LW\uparrow_{surface} - LW\downarrow_{surface} - LW\uparrow_{TOA} \quad (1.6)$$

$$RFD_{net} = RFD_{SW} + RFD_{LW} \quad (1.7)$$

where I_0 is the TOA solar insolation, $SW\uparrow_{TOA}$ is the upwelling SW radiation at the TOA, $SW\uparrow_{surface}$ is the upwelling SW radiation at the surface, $SW\downarrow_{surface}$ is the downwelling SW radiation at the surface, $LW\uparrow_{surface}$ is the upwelling LW radiation at the surface, $LW\downarrow_{surface}$ is the downwelling LW radiation at the surface, and $LW\uparrow_{TOA}$ is the upwelling LW radiation at the TOA. The RFD is negative when there is a radiation deficit in the column indicating cooling and positive when it indicates warming. Following the calculation of RFD, CRE was calculated at the TOA, the surface, and within the atmospheric column (atmospheric CRE) by comparing clear sky conditions to all sky conditions using the following equations

$$CRE_{TOA} = LW\uparrow_{TOA,clear} - LW\uparrow_{TOA} + SW\uparrow_{TOA,clear} - SW\uparrow_{TOA} \quad (1.8)$$

$$CRE_{Surface} = LW\downarrow_{surface} - LW\downarrow_{surface,clear} + SW\downarrow_{surface} - SW\downarrow_{surface,clear} \quad (1.9)$$

$$CRE_{Atmosphere} = CRE_{TOA} - CRE_{surface} + SW\uparrow_{surface} - SW\uparrow_{surface,clear}. \quad (1.10)$$

We used the technique similar to Ramanathan et al. (1989), Cess et al. (1995) and Miller et al. (2012) to identify clear sky conditions from the observations of SW and LW flux at the surface and TOA. This technique relies on an analysis of the SW radiative flux at the TOA and surface versus the cosine of the solar zenith to determine a linear relationship representing the clear sky scenario over the course of each month. This relationship was then used calculate a clear sky TOA and surface net SW flux for each hour bin during that month. For the LW, the minimum observed downwelling flux at the surface for each hour bin in the given month is the clear sky value, while the maximum upwelling flux is used for the TOA. A detailed description of this technique can be found in the appendix of Miller et al (2012). A three hour average was used to compute the RFD and CREs to reduce the spatial and temporal mismatch between measurements at the surface and TOA, as recommended by Parding et al. (2011).

1.9 Scientific Questions and Outline of Work

The impact of clouds and aerosols on the radiation budget remains a subject of uncertainty and scientific debate. The goal of this study is to determine what controls and influences the regional radiation budget in the Sahel region of West Africa and the Amazon Rainforest of Brazil on a diurnal or seasonal time scale, focusing on the surface, TOA, and absorption within the atmosphere, and how these regional radiation budgets compare. The scientific questions that are answered are as follows:

1. What role does water vapor play in modulating the diurnal cycle of the radiation budget during the wet season over the West African Sahel?

2. To what extent does the type of cloud present influence the diurnal radiation budget at the TOA, surface, and within the atmospheric column over the West African Sahel and the monthly average radiation budget in the Amazon Rainforest of Brazil?

3. How does the CRE compare in the West African Sahel region and Amazon Rainforest of Brazil?

4. How will the radiation budget in the West African Sahel region respond to projected changes in climate, such as an increase or decrease in cloud fraction and thickness?

Work that was done to answer these science questions is presented in chapters 2, 3, and 4 of this dissertation. Chapter 2 presents a detailed case study on the diurnal cycle of meteorology, thermodynamics, dynamics, and radiation in Niamey, Niger throughout 2006. This analysis complements a previous study that examines the monthly mean radiation budget (Miller et al., 2012). A unique focus is the diurnal cycle of the column RFD and CRE at the TOA, surface, and within the atmospheric column. Such an analysis has not been attempted in the past because there were no measurements available.

Observations of meteorology, thermodynamics, and radiation in Manacapuru, Brazil in the year 2014 are presented in chapter 3. Monthly averages were used to determine impacts of the radiation budget on a seasonal time scale.

In chapter 4 the observations in chapter 2 are used as a framework to determine how the radiation budget might change in response to small changes in the climate system. Output from CMIP5 were analyzed and inserted into the Rapid Radiative Transfer model to assess individual components of the changing climate. In addition, detailed descriptions

of the current energy budget and the possible future energy budget in Niamey, Niger are shown.

The final chapter concludes with a summary of the work done and the significance it has in the field of climate research. The main focus of this chapter is a comparison between the radiation budget and its controls in Niamey, Niger and Manacapuru, Brazil as well as observational techniques. Ideas for future work are also presented.

CHAPTER 2: Diurnal Cycle Meteorology, Clouds, and Radiation in the West African Sahel Region

Many uncertainties remain in the relationship between clouds, aerosols, and the radiation budget, especially in under-sampled regions like the Sahel. Factors that influence the radiation budget such as clouds and aerosols often exhibit a diurnal cycle and it is therefore imperative that the radiation budget be examined on a diurnal time scale. The following chapter presents results on the diurnal cycle of surface meteorology, cloud coverage, thermodynamic profiles, and radiation in Niamey, Niger from the year 2006. Local hour in Niamey, Niger is one hour ahead of Coordinated Universal Time. The diurnal cycle of meteorology can be found in section 2.1, clouds, aerosols, and radiation in section 2.2, and the effect of clouds on the radiation budget in section 2.3. This work has been submitted for publication in the *Quarterly Journal of Royal Meteorological Society*.

2.1 Diurnal cycle of meteorology

Diurnal signals in the surface air temperature, mixing ratio, and wind speed (Figures 2.1a-c) for the wet and dry seasons are symptomatic of a typical diurnal cycle driven by solar heating that is characterized by a convective daytime boundary layer and a stable nocturnal boundary layer. Surface air temperature follows a diurnal pattern that is typical for a semi-arid region with its maximum temperature observed at mid-day and its minimum just before dawn (Figure 2.1a). There is a greater range of surface air temperature during the dry season (6°C during the wet season and 14°C during the dry season) due to less cloudiness and water vapor in the atmosphere compared to the wet season (discussed later).

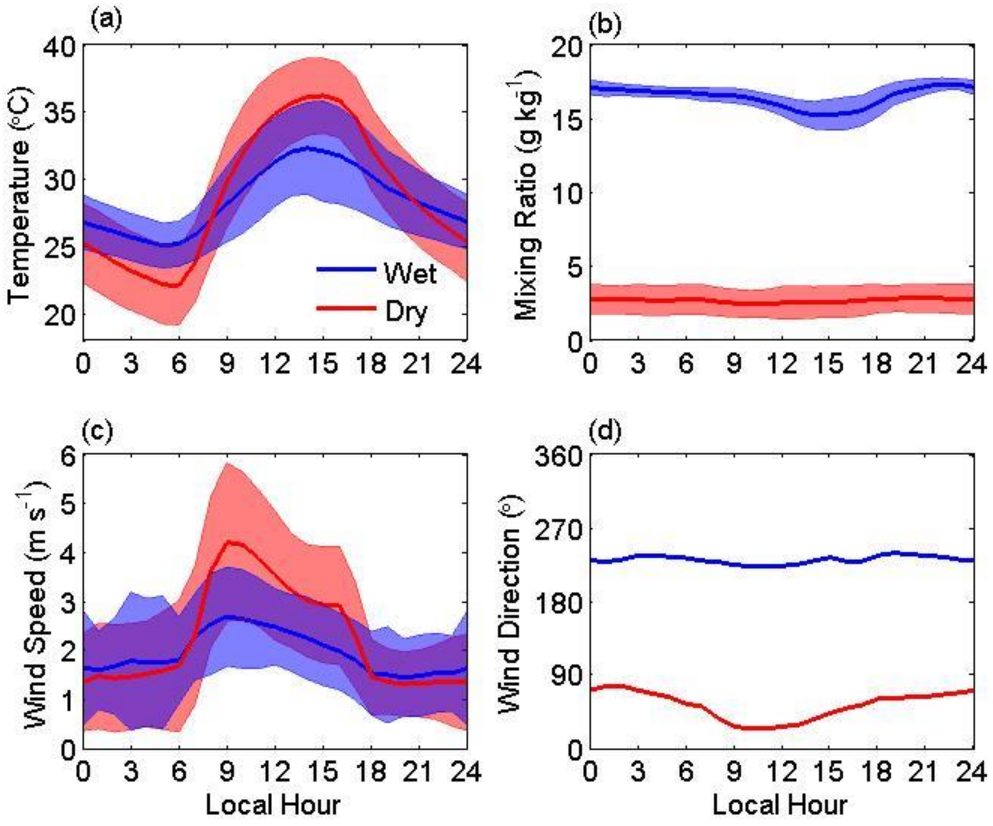

Figure 2.1: The diurnal cycle of (a) air temperature at 2 m, (b) mixing ratio at 2 m, (c) wind speed at 10 m, and (d) wind direction at 10 m for the 2006 wet (blue) and dry (red) season in Niamey, Niger. Shading represents plus or minus one standard deviation.

There is a negligible diurnal cycle in the mixing ratio during the dry season and it remains virtually constant at ~4 g kg^{-1} (Figure 2.1b), which is consistent with a dry soil and a lack of precipitation and moisture advection. In contrast, a diurnal cycle with a range of ~2 g kg^{-1} and a minimum in the afternoon (1500 h) is observed during the wet season. Nighttime in the Sahel during 2006 is characterized by calm winds during both the wet and dry seasons (Figure 2.1c), while daytime winds tend to be stronger. The range of the daytime wind speed increase is substantially higher during the dry season and surface winds increase by nearly 3 m s^{-1} during that season. Wind speeds exhibit a rapid increase

in the morning during both seasons, but decline abruptly during the late afternoon during the dry season rather than declining steadily as in the wet season. Winds at the surface are predominantly from the southwest during the wet season with little diurnal variability and a mean value of 220° (Figure 2.1d). During the dry season the winds are from the east during the night (~70°) and more northerly during the daytime. The daytime cycles of mixing ratio and winds are consistent with water vapor ventilation and momentum transport, characteristic of a deepening, entraining convective boundary layer.

Wind speed and direction profiles for the lower portion of the boundary layer measured with the radar wind profiler (Figure 2.2) provide a more complete picture of the diurnal cycle of wind structure during the wet season (Lothon et al., 2008). Layering is obvious in the wind direction during the wet season with abrupt and substantial directional wind shear observed just above 1 km, indicating a monsoonal layer near the surface and the Saharan Air Layer (SAL) above (Figure 2.2a). Despite this directional wind shear in the wet season boundary layer, wind velocities are rather uniform through the observable portion of the boundary layer (Figure 2.2b). A wet season nocturnal jet centered at 0.6 km with a southwesterly flow nearing 10 m s^{-1} has been reported by previous studies in the wet season that forms as a result of the pressure gradient force associated with the intensified heat low interacting with the Coriolis force (Parker et al., 2005; Lothon et al. 2008, Kalapureddy et al., 2009). We find a similar jet, though slightly lower in altitude with an average wind speed around 8 m s^{-1}.

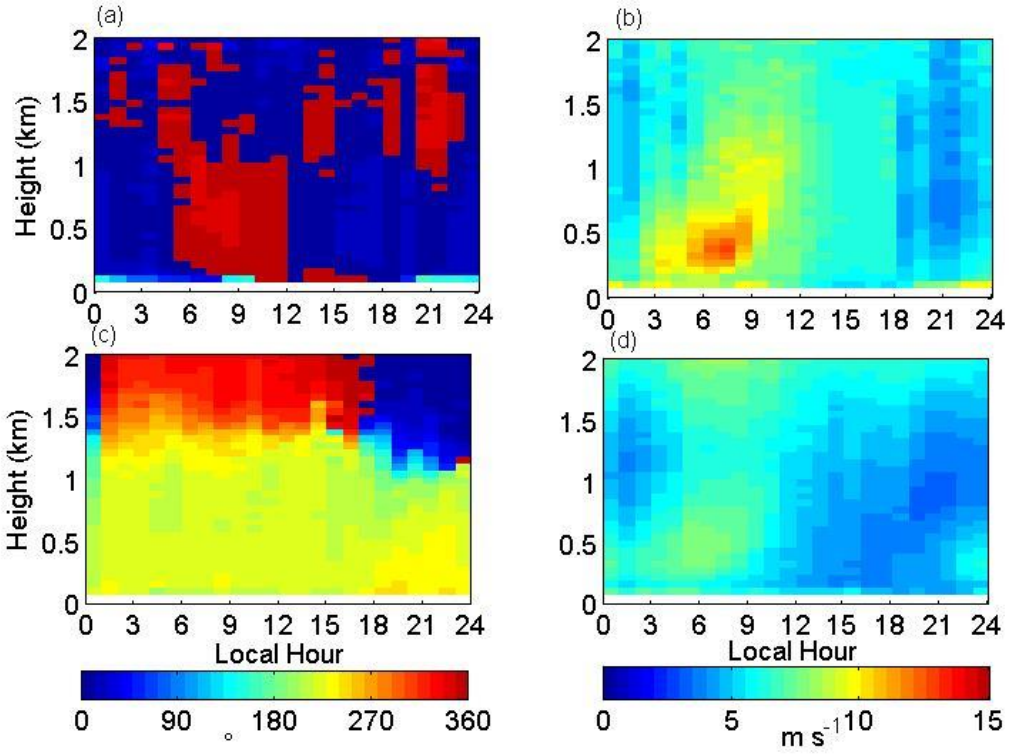

Figure 2.2: The diurnal cycle of (a) wind direction and (b) wind speed for the 2006 dry season and (c) wind direction and (d) wind speed for the 2006 wet season.

Wind speed increases observed in the developing Sahelian boundary layer during the early morning of the wet and dry seasons differ substantially as the wet season experiences much less acceleration. The main difference in the energetics between the two seasons are the sensible and latent heat fluxes. The diurnal cycles of the latent and sensible heat fluxes peak around local noon (Figures 2.3a & 2.3b) in good agreement with the results reported in Miller et al. (2009) and Gounou et al. (2012). The sensible heat fluxes are negligibly small during the night during both seasons. Latent heat flux is always positive indicating that moisture originates from the surface and is transported into the atmosphere and exhibits a diurnal cycle both during the wet and dry seasons, though vastly different in range. The wet season latent heat flux has a maximum of 63 W m^{-2} at noon with relatively

constant value overnight and an abrupt, unexplained dip observed at 0500 h. In contrast, a minimal diurnal change in latent heat flux is observed during the dry season.

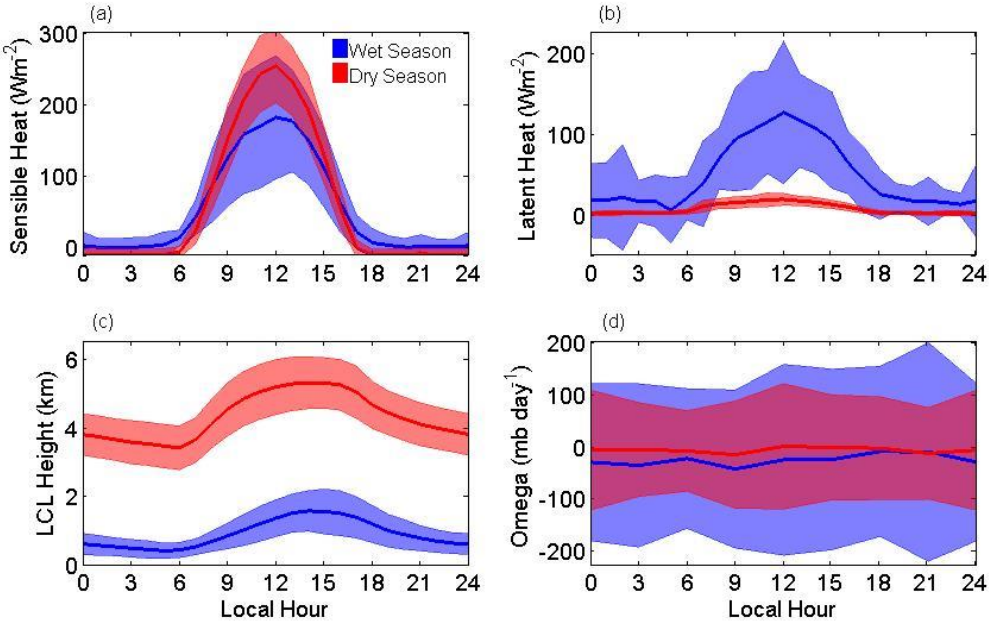

Figure 2.3: The diurnal cycle of (a) surface sensible heat flux, (b) surface latent heat flux, (c) LCL height, and (d) 700 mb omega for the 2006 wet (blue) and dry (red) seasons in Niamey, Niger. Shading represents plus or minus one standard deviation.

The higher values of latent heat flux during the wet season compared to the dry season are mostly attributed to evaporation of soil moisture and transpiration from vegetation (Miller et al., 2009). A mix of bare soil and small shrubs and grasses characterize the site and appropriately the daily average latent heat flux observed during the wet season is in between observations in the Sahel presented by Timouk et al. (2009) for a grassland and bare soil surface. The larger maximum sensible heat flux during the dry season is also consistent with the results for a grassland from their study, but the wet season diurnal cycle compares more favorably with their semi-desert regime. The wet season latent and sensible heat may also be comparable to those observed in millet fields, which are common in the

Sahel, by Ramier et al. (2009). Their observations in a fallow have generally higher values of the latent heat flux and lower for sensible heat, likely due to the larger presence of a greater concentration of vegetation that the average in the Sahel. This suggests that evapotranspiration is more dominant in the energy budget in a fallow field than over the integrated Sahel landscape.

Two variables of critical importance in boundary layer and cloud development are the surface LCL and the synoptic scale vertical motion (denoted hereafter as omega, ω). Cloud development and base height are dependent upon the LCL height in a convective boundary layer. The diurnal cycle of the LCL height (Figure 2.3c) follows that of the surface temperature and moisture and is, accordingly, about 2 km lower during the wet season due to lower temperatures and increased moisture (Kollias et al., 2009). Referring to Figure 2c, the LCL lies firmly within the surface southwesterly flow regime during the night, but reaches the directional shear zone sometime in the late morning and rises into the SAL during mid-day. Clouds forming while the LCL lies below the shear zone will undoubtedly experience significant directional shear if they develop vertically. Later analysis of the diurnal variation in the thermodynamic cross-sections and cloud structures will further delineate the position of the LCL relative to the SAL.

Negative ω at 700 mb indicating upward motion at this level, which corresponds to approximately 3 km in height, is diagnosed by the NCEP reanalysis during both seasons (Figure 2.3d). This constant upward motion is consistent with Niamey's location beneath the tropical upwelling branch of the Hadley cell circulation. The synoptic-scale ω at 700 mb exhibited little change on diurnal time-scales during the dry season and had an average value of -10 mb day^{-1}, while it had a stronger diurnal cycle reaching a maximum uplift of

-42 mb day^{-1} in the morning during the wet season, corresponding with the morning minimum in LCL and maximum in cloud fraction (Figure 2.4a).

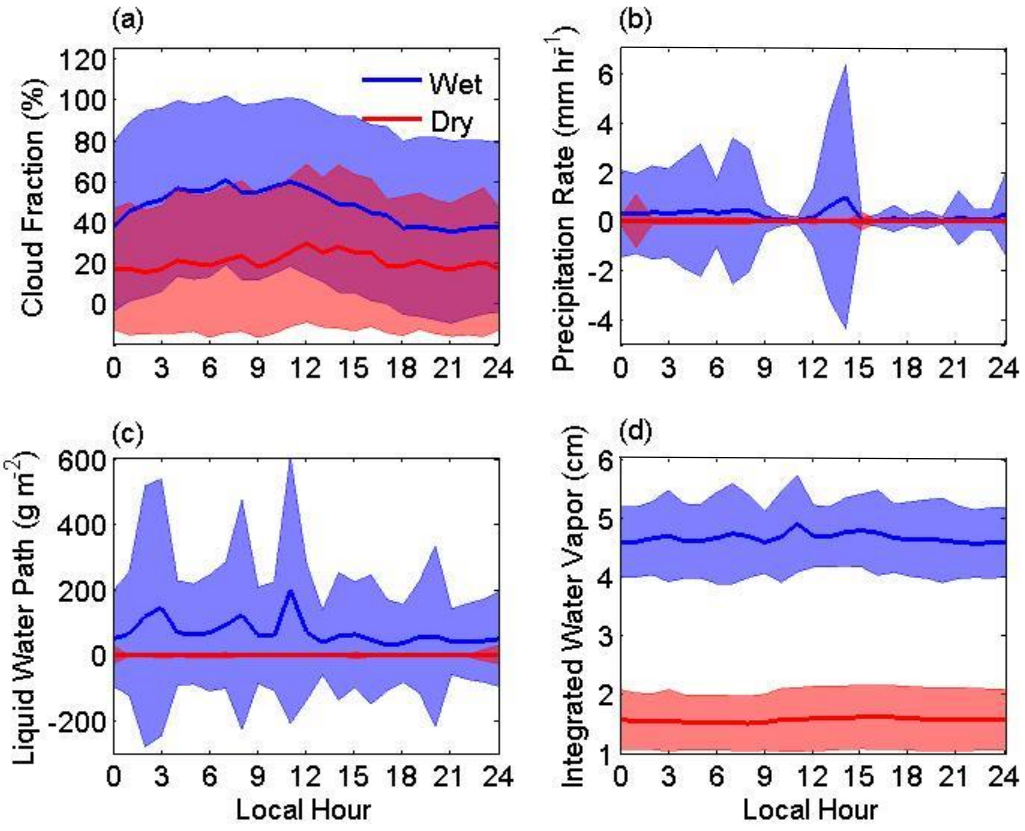

Figure 2.4: The diurnal cycle of (a) cloud fraction, (b) precipitation rate, (c) liquid water path, and (d) integrated water vapor for the 2006 wet (blue) and dry (red) in Niamey, Niger. Shading represents plus or minus one standard deviation.

Cloud coverage refers to the fraction of time a cloud was observed within a one hour period with no distinction as to cloud location within the column and the observed diurnal cycles for the dry and wet season are shown in Figure 2.4a. A modest diurnal cycle peaking around midday is observed during the dry season, but a more substantial diurnal cycle with a diurnal range in cloud coverage of 30% is observed during the wet season with large standard deviations in both seasons. Maximum cloud coverage during the wet season

is observed around dawn followed by a gradual decrease in the late morning and early afternoon to a late evening value of ~38%. This wet season diurnal cycle is observed to reciprocate the diurnal cycle of the LCL (Figure 2.3c); the lowest LCL heights are observed at dawn along with the maximum cloud coverage. A strong relationship between monthly average LCL and cloud coverage was noted in a past study (Kollias et al., 2009), so the current result suggests that this relationship extends downscale to the diurnal cycle. Monthly average rainfall rate, which has been shown to correlate well with the LCL in past studies, has a complicated diurnal pattern that cannot be easily associated with the diurnal cycle of LCL or cloud coverage (Fig 4b). The rainfall rate is relatively constant from midnight until 0700 h at a value of ~0.3 mm $hour^{-1}$. Apart from the peak in rainfall at 1300 h (1 mm $hour^{-1}$), associated with a few late season large precipitation events, the rainfall is negligible from 0900 h until midnight. A nocturnal preference for rainfall from midnight until 0700 h is consistent with the results by Rickenback et al. (2009) and Bouniol et al. (2012). There was no rainfall recorded during the dry season.

The observed diurnal cycle of cloud coverage does not correlate well with that of the liquid water path (LWP; Figure 2.4c), which is to be expected since the cloud field includes both ice and mixed phase clouds not measured by the microwave radiometer. During the dry season, the LWP can be considered negligible as it was always below the instrument uncertainty of 25 g m^{-2}. Several prominent peaks are superimposed upon a background value of ~50 g m^{-2} during the wet season. These peaks in the LWP on diurnal timescales are also not correlated with rainfall rate suggesting that most of the wet season precipitation originates from mixed-phase cumulonimbus clouds. Further, the spiked behavior of the LWP in the earlier part of the day is indicative of the intermittent presence

of boundary layer warm cumulus clouds. The microwave radiometer does not report LWP during precipitating conditions due to accumulation of water on the radiometer dome.

The atmospheric column integrated water vapor did not exhibit a diurnal cycle in either season (Figure 2.4d) and was almost constant at a value of 1.6 cm during dry season and 4.75 cm during the wet season, in good agreement with Bock et al. (2008). This constancy indicates a relatively uniform layer of water vapor through the cycle upon which phase changes and vertical transports are superimposed by local processes. Diurnal changes in liquid water path (Figure 2.4c), in surface latent heat flux (Figure 2.3b) and in surface mixing ratio (Figure 2.1b) suggest considerable vertical mixing and redistribution of water vapor, but the constancy of the integrated water vapor seems to imply that horizontal advection is not varying on diurnal time scales.

A low-level influx of water vapor during the wet season and the omnipresent SAL are major components of the WAM. Their role in the diurnal cycle is analyzed by subtracting the seasonal mean profile from the dry season and wet season diurnal cycle of temperature, T, mixing ratio, q, and equivalent potential temperature, θe, and then subtracting the dry season anomaly from the wet season anomaly (Figures 2.5a-c). By doing so it is easier to analyze the anomaly in the diurnal cycle without being hindered by the large difference between the two seasons. Layering within the column is clearly present in the temperature anomaly profile with the monsoonal layer in the bottom 1km and the SAL between 2 and 4 km (Figure 2.5a). Although the mean profiles have been removed, there is still a slight influence from the variation in the diurnal cycle of solar insolation. The wet season has a period of increased warming at the surface relative to the dry season prior to the time of the maximum surface temperature. While the surface is warmer at this

time, the atmosphere is cooler above the SAL. This coupling is then reversed in the afternoon hours.

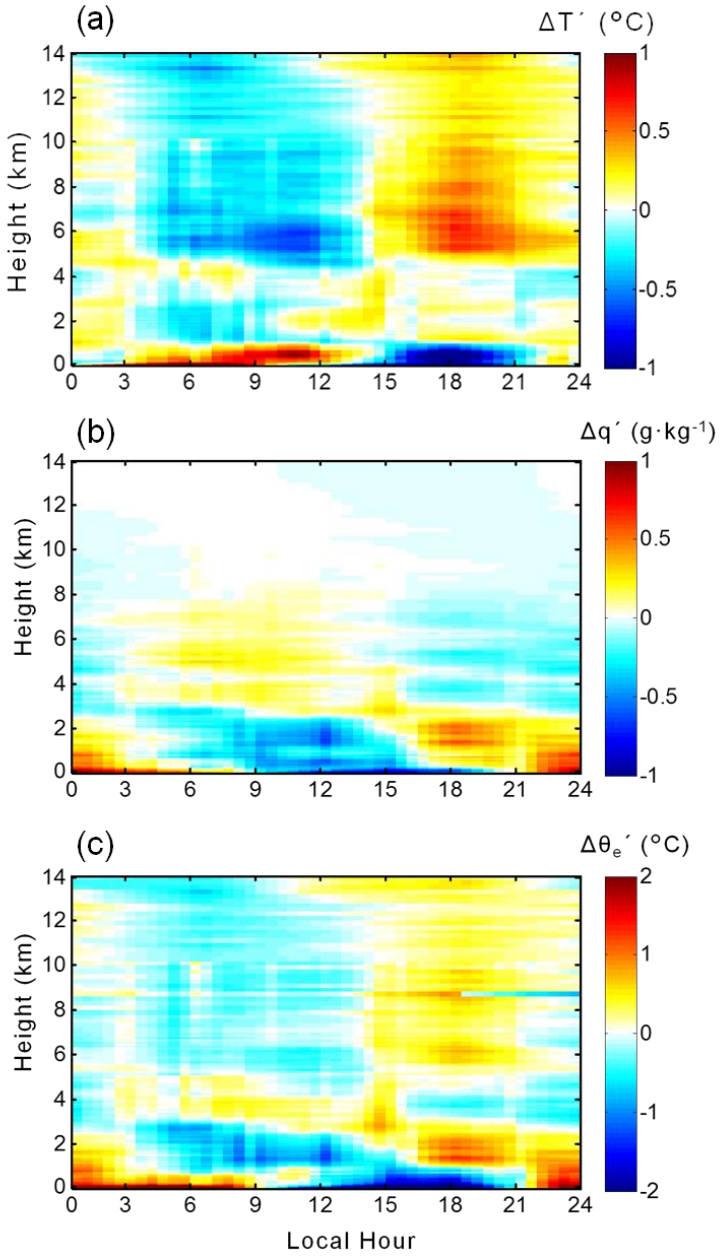

Figure 2.5: Time-height cross section of the anomaly in the diurnal cycle for the 2006 wet season minus dry season of MWRP Merged Sounding (a) temperature, (b) mixing ratio, and (c) equivalent potential temperature in Niamey, Niger. This figure was created by Lynne Trabachino.

Overnight during the wet season, the boundary layer contains more moisture, especially in the bottom 1 km (Figure 2.5b). Coincident with the increased nocturnal convection and precipitation, the moister air in the wet season is relocated to between 4 and 8 km as the boundary layer deepens, however the anomaly is not as large as overnight. The amount of vapor within the column does not change, but rather spreads out throughout the column, resulting in a smaller anomaly in the morning hours. Drier air from the SAL aloft becomes mixed with the surface air mass resulting in the largest negative anomaly in the diurnal cycle and column during the daytime in the bottom 2 km. As the day progresses, the positive moisture anomaly moves closer to the surface until it becomes stationary overnight.

The influence of specific humidity on equivalent potential temperature is readily apparent below the SAL, while temperature becomes important aloft (Figure 2.5c). Beginning around 0300 h a positive θ_e anomaly is present between 3 and 5 km. Just like the diurnal cycle in the profile for specific humidity, the larger values of θ_e in the wet season decrease in altitude throughout the day until becoming stagnant overnight highlighting the instability of the boundary layer overnight. Above 5 km the coupling from the temperature anomaly is present with a negative anomaly in the morning and a positive anomaly in the afternoon and evening hours.

2.2 Clouds, Aerosols, and Radiation

Seasonal radiation throughput over the Sahel is complicated by the presence of drastic differences in column integrated water vapor (Figure 2.4d), large aerosol loads, ubiquitous cirrus, and shallow and deep convection during the wet season. We analyze the diurnal cycles of the cross-column radiation budget using coincident radiation

measurements made at the surface and TOA every 15 minutes. These 15-minute radiation measurements are averaged over 3 hours to reduce random errors associated with the radiance-to-flux algorithms that are used to construct the satellite broadband irradiance measurements and to insure that sampling discordance between the surface and satellite measurements were minimized. The 3 hour temporal resolution of these measurements is consistent with changes in diurnal cloudiness and aerosol load that influence the diurnal cycle of radiation throughput, as shown within this section (Parding et al., 2011). We begin by analyzing the diurnal cycles of cloud fraction and aerosol after having established in Figure 2.4d that there is no diurnal cycle in water vapor mixing ratio that will impact the diurnal cycles of clear sky radiation.

Cloud fraction refers to the vertical profile of the layer-to-layer cloud coverage and the diurnal cycle of cloud fraction during the wet season is shown in Figure 2.6. High level cloudiness (>7 km) is observed over the Sahel during both seasons though cloud fractional coverage is, in general, relatively low during the dry season. When high cloudiness is present during the dry season, it tends to occur during the late afternoon (maximum at ~ 1500 h) as a solitary layer. High cloudiness is more prevalent during the wet season (Figure 2.6b; maximum ~20%) and it almost always occurs in association with clouds that have bases at lower levels with similar cloud fraction implying that it is associated with deep convection. Morning hours are clearly favored for high cloudiness and all other cloud types during the wet season. Mid-level clouds are present during the majority of the diurnal cycle (0300 and 1800 h) during this season and are most prevalent between 0800 h and noon. The wet season distribution of mid-level clouds is not uniform in time, however, because mid-level clouds occurring in mid-afternoon (around 1500 h at ~6 km) in the wet

season are only observed during August. Boundary layer clouds follow a diurnal cycle similar to that of mid-level clouds during the wet season, with prominence from 0300 to 1800 h. Although Bouniol et al. (2012) have suggested the inadequacy of ARM instruments to observe high level cirrus clouds, good agreement between the AMF observed monthly cloud fraction and that reported by International Satellite Cloud Climatology Project was found by Miller et al. (2012). However, evidence presented in Figure 2.6 seems to suggest that optically thin cirrus may have been present in the area even when the AMF instrumentation detected clear conditions in the column above the site.

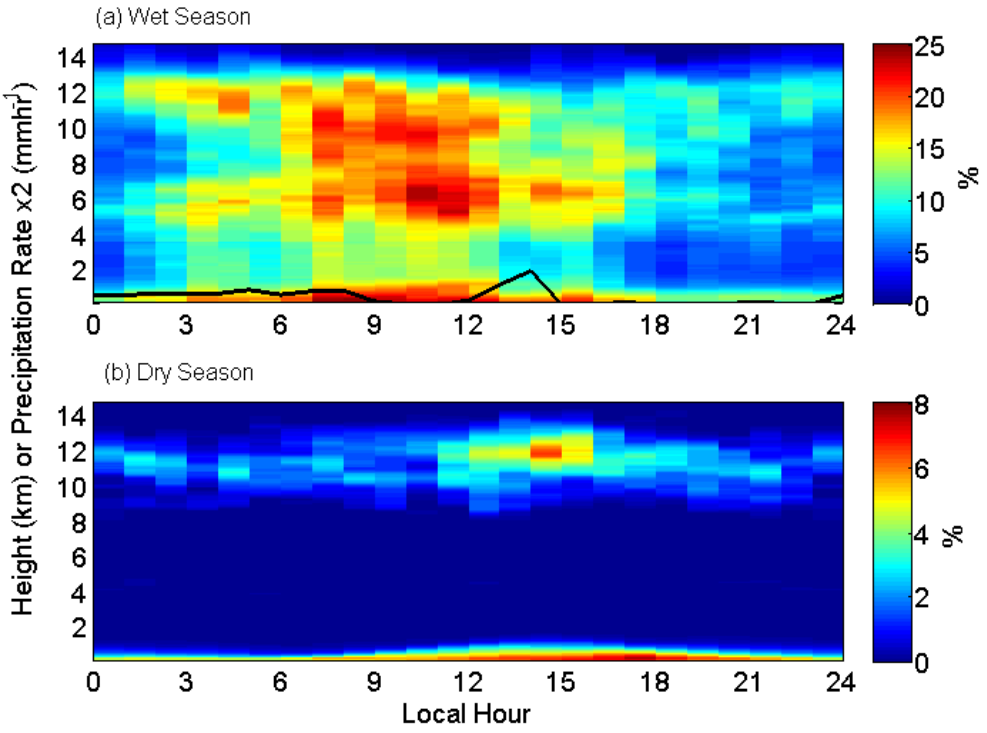

Figure 2.6: Cloud fraction as a function of time and height during the 2006 (a) wet season and (b) dry season in colors and precipitation rate in the solid black line in Niamey, Niger.

Significant near-surface echoes are observed during the morning hours of the wet season when the LCL lies below 1 km at dawn and rises to ~2 km by noon whereby we cannot exclude the possibility that these echoes originate from some combination of dust,

smoke plumes from fires, and shallow cumulus clouds. We refer to Bouniol et al. (2012) for additional details and a month-by-month look at the diurnal cycle of cloud coverage and cloud type.

There are two main sources of aerosol present over the Sahel: dust and the byproducts of combustion from heating, cooking, and mosquito deterrent fires. These fires are most frequent at dawn and dusk as suggested by peaks in condensation nuclei measured by the AMF during these periods (not shown). Dust is ubiquitous in the lower atmosphere over the Sahel and is likely to be the dominant aerosol control on radiation throughput. Large dust storms occurred in 2006 during the dry season, which resulted in the largest AOD of the year (McFarlane et al. 2009). The daytime AOD as measured by the multi-filter shadowband radiometer when the sky was clear or when the Sun's disk was visible between clouds at four wavelengths for the wet season is shown in Figure 2.7. Some caution must be exercised when interpreting these measurements because there were many more opportunities to measure AOD in clear conditions during the dry season because there were fewer clouds. Wet season measurements are supposed to represent relatively "cloud-free" conditions, but our ability to adequately filter cases when extremely thin cirrus is present is probably less than perfect and this shortcoming is most likely to significantly influence the statistical integrity of measurements made during the wet season. Aerosols absorb and reflect more radiation at 500 nm than longer SW wavelengths, and the least at 870 nm, and this leads to a progression of AOD to smaller and smaller values as the observation wavelength is increased. We assume that there is no diurnal cycle in ozone, which would impact the 615 and 674 nm channels, but the total AOD in these bands is impacted by the total column ozone. A pronounced diurnal cycle in the AOD is observed

during the wet season when skies are presumably clear (Figure 2.7). Magnitudes of the AOD during the wet season diurnal cycle are higher than expected and exhibit a peak at noon, which may be a result of the high AOD spikes shown by McFarlane et al. (2009) or the result of thin cirrus cloud cover above the dust and aerosol layer. One of the most confusing and intriguing issues confronting the radiation transfer community is separation of the radiative impacts of dust from those of thin cirrus over the Sahel. The increasing separation between the 870 nm and 500 nm AODs implies an increasing amount of smaller aerosol particles present in the column as the morning progresses.

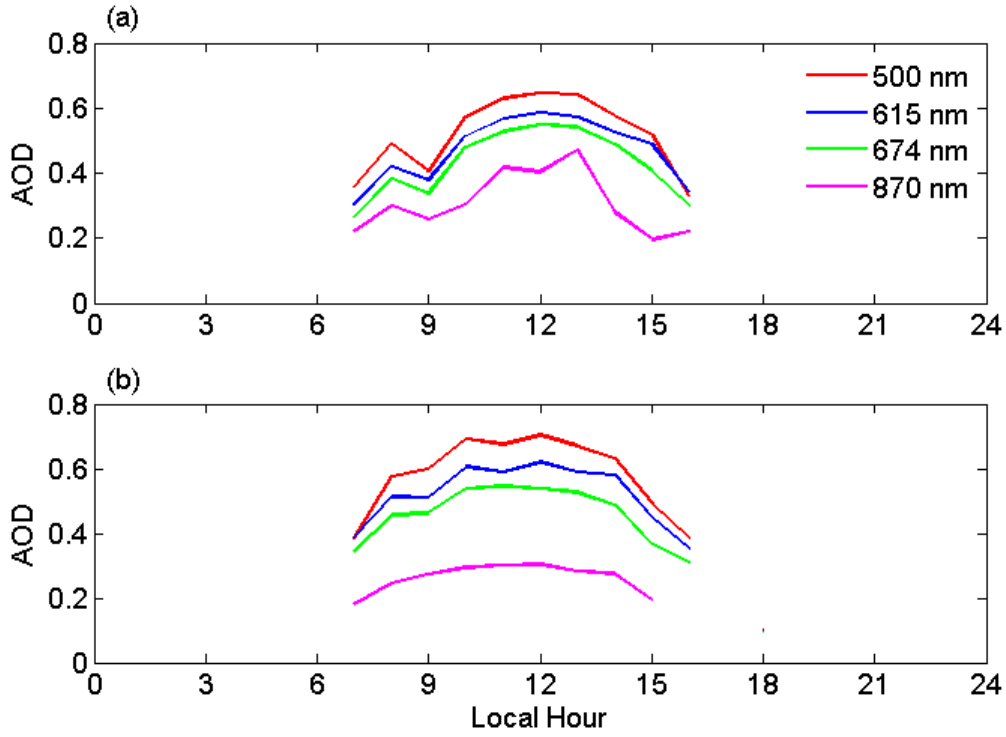

Figure 2.7: AOD at 500 nm, 615 nm, 674 nm, and 870 nm for the (a) wet season and (b) dry season for the year 2006 in Niamey, Niger.

Aerosols and, especially, clouds exhibit pronounced diurnal cycles over the Sahel and, as such, are expected to exert some influence on the diurnal cycle of atmospheric radiation throughput. Our analysis of this radiation throughput begins by examining the

irradiance at the TOA and surface and the difference between these irradiances, which has been previously defined as the Radiative Flux Divergence. Once the TOA and surface radiative fluxes and the RFD have been computed, they can be categorized by virtue of the cloud cover to determine how clouds impact them, which we term the Cloud Radiative Effects. This terminology has been chosen to be consistent with McFarlane et al. (2013), which modifies past terminology referring to the TOA and surface CRE's as "forcing".

The GERB reported diurnal cycle of TOA radiative fluxes, ARM observed surface radiative fluxes, and RFD for the dry and wet seasons are shown in figure 2.8. A positive radiative flux at the TOA denotes warming of the Earth-atmosphere system while a negative flux denotes cooling of the Earth-atmosphere system. The SW TOA flux is positive signifying daytime heating (Figure 2.6a) and the LW TOA flux is negative through the diurnal cycle signifying cooling of the system (Figure 2.6b). Solar insolation modulates the SW TOA flux during both seasons with sunrise around 6 am and sunset around 6 pm and a peak around noon. It is higher during the wet season due to increased solar insolation during the summer months, though attenuated to some extent by the increased albedo from an increase in cloud cover. A subtle diurnal cycle is seen in the TOA LW flux during the dry season with a minimum around noon (~ -305 W m^{-2}) and an otherwise relatively constant magnitude of ~-270 W m^{-2}. This shift in diurnal outgoing LW radiation is consistent with the land non-convective regime as shown by Taylor (2012) due to the diurnal fluctuations in temperature. A negligible diurnal cycle is observed during the wet season when the LW TOA flux maintains a near constant magnitude of ~ -240 W m^{-2}. These wet season measurements are consistent with measurements and calculations by McFarlane et al. (2013) over the Tropical Western Pacific and are very close to the global

annual average shown by Stephens et al. (2012). Cooling in the LW is higher during the dry season due to less cloud cover and water vapor and a higher surface temperature.

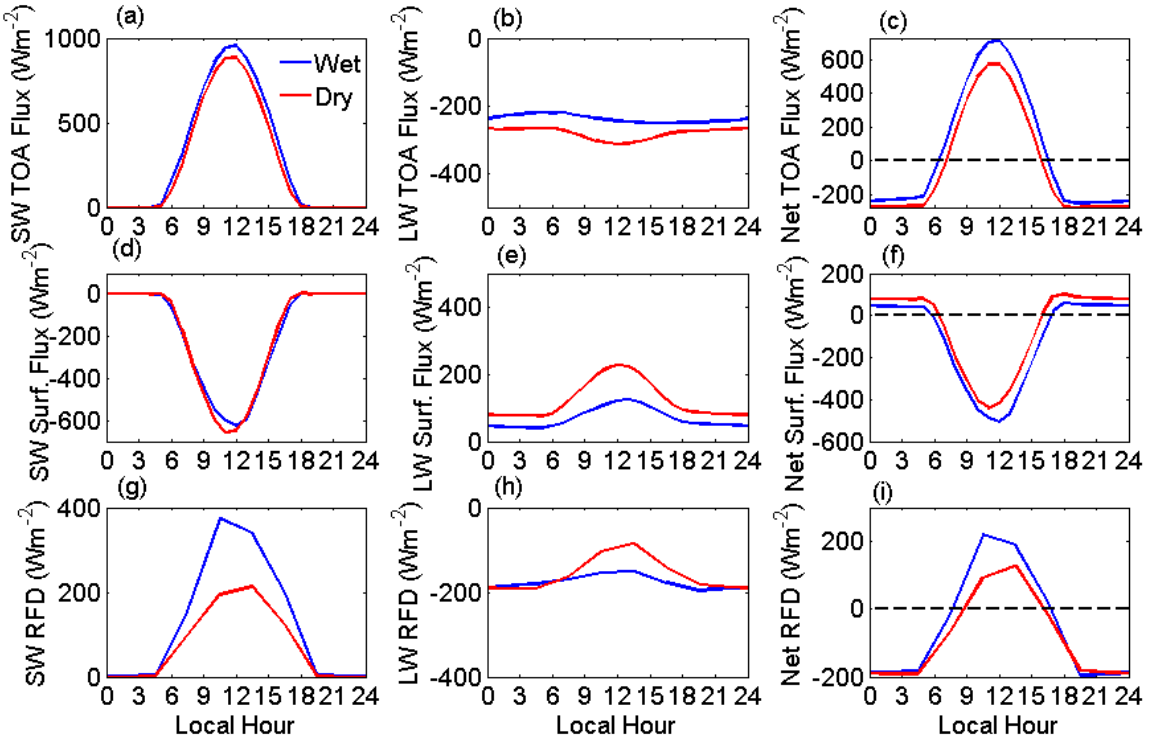

Figure 2.8: The diurnal cycle of the TOA (a) SW, (b) LW, and (c) net radiative fluxes, surface (d) SW, (e) LW, and (f) net radiative fluxes, and (g) SW, (h) LW, and (i) net RFD for the 2006 wet (blue) and dry (red) seasons in Niamey, Niger.

The net radiative flux at the TOA over the Sahel was always higher during the wet season. There was increased SW radiative heating during the daytime and less LW cooling during the nighttime (Figure 2.8c). The asymmetry of the diurnal signal differs in the SW and LW between the two seasons; the LW signal is symmetric about local noon while the SW signal is asymmetric with a peak in the afternoon (~0300 h). This wet season SW asymmetry is well correlated with the afternoon reduction in cloud coverage (Figure 2.6) and is thereby likely to have been modulated by changes in cloud albedo. Changes in cloud

albedo are also likely to dominate the difference in the diurnal cycle of the net TOA radiation flux between the two seasons. The clear suggestion is that the difference in the diurnal cycle of radiation at TOA between the two seasons is related to changes in cloud cover during the wet season. To summarize, the variability in the net TOA flux during the wet season seems strongly coupled to column cloudiness that is supplied by local convection, while in the dry season it is driven by a combination of surface temperature (LW) and dust load (SW). These TOA diurnal signals are superimposed upon a diurnally quiescent increase in the absorption of radiation due to the increase in integrated water vapor during the wet season.

The net SW surface flux in Niamey, Niger is negative during both seasons indicating a gain of radiative energy to the surface (Figure 2.8d) and there is a strong diurnal cycle modulated by insolation. Despite higher solar insolation during the wet season, a near equal amount of SW radiation reaches the surface in the dry season because there is less cloudiness and less water vapor to impede SW radiation passing through the atmosphere. There is a decrease in the surface albedo during the wet season as a result of the "greening" of the Sahel, so a larger percentage of the radiation reaching the surface is absorbed. These radiative impacts evidently offset because the diurnal cycle of the SW flux at the surface is almost the same in the wet and dry seasons.

A similar diurnal cycle in the surface net LW flux is exhibited during dry and wet seasons and the flux is positive during both seasons, signifying a loss of energy by the surface to the atmosphere (Figure 2.8e). This loss is larger at all times during the dry season because there is less water vapor and cloudiness to emit outgoing LW toward the surface. The nighttime values of the surface net LW flux were around 75 W m^{-2} during the

dry season and ~50 W m^{-2} during the wet season. Daytime high temperatures are significantly greater during the dry season (Figure 2.1a), which leads to a surface LW flux of ~225 W m^{-2} during midday in the dry season, while only ~125 W m^{-2} during the wet season.

The net surface radiative flux (Figure 2.8f) is negative at night during both seasons and positive during the day. Hence, the surface loses energy at night through LW loss to the atmosphere (and ultimately to space) and during the day it gains radiative energy, which is lost to the atmosphere through the sensible and latent heat fluxes (Figure 2.3a-b) and by conduction into the soil. We refer to Miller et al. (2009) for further discussion regarding the surface energy budget. Quantitatively, these results agree extremely well with those presented by Guichard et al. (2009). Since their study focused on the year 2003 in a region slightly to the northwest, this could indicate that the surface radiation budget for Niamey, Niger in 2006 was representative of the Sahel region.

To isolate the absorption and emission of radiation within the atmosphere as an independent entity, we calculated the RFD (Figures 2.8g-i). The SW RFD was always positive signifying heating of the atmosphere due to the absorption of solar radiation by water vapor and aerosols during the daylight hours and this heating is enhanced during the wet season due to a greater amount of water vapor. Predictably, the shape of the SW RFD broadly follows the input of solar insolation with a peak of ~375 W m^{-2} in the wet season and peak of ~200 W m^{-2} during the dry season. The LW RFD is always negative denoting cooling of the atmosphere by LW emission to space and the diurnal cycle of LW RFD is similar during both seasons with peaks (minimal cooling) around noon (Figure 2.8h). The

LW RFD is almost constant overnight with an average nighttime values around 185 W m^{-2} during both seasons.

The net RFD over the Sahel is negative at night (Figure 2.8i) as LW radiation emitted to space dominates over the net LW surface flux and positive during a portion of the day when the absorption of SW radiation by water vapor and aerosols dominates emission of LW radiation to space. Correlation coefficients between the net RFD and numerous meteorological factors were calculated, but none, including cloud coverage, showed a significant correlation on a diurnal time scale for either season. This result does not imply that clouds have no impact upon the net RFD but rather that the combination of clouds and clear sky RFD on 3-hour time scales exhibits no correlation.

There is little difference between the diurnal cycles of LW RFD during the two seasons, but a significant difference in the diurnal cycle of SW RFD. The sharp increase in SW RFD during the wet season daytime is primarily due to increased water vapor absorption. There is virtually no difference in the net RFD at night between the two seasons. This observation may seem at odds with the significant difference in water vapor loading (Figure 2.4d), but is explained by the cooler nocturnal surface temperatures during the dry season. There is less LW emission from the surface to the atmosphere during dry season nighttime hours due to cooler surface temperatures and more surface emission to the atmosphere from the surface during the wet season, but the increased surface emission during the wet season is offset by downward emission of LW from the vapor laden lower atmosphere.

2.3 Cloud Radiative Effect

A negative value of TOA CRE denotes cooling of the Earth-atmosphere system by the clouds, while a positive value denotes heating (Figures 2.9a-c). The SW TOA CRE is negative during both seasons because clouds reflect incoming solar radiation. The diurnal cycle of SW TOA CRE for both seasons (Figure 2.9a) follows the same pattern due to the diurnal cycle of solar insolation, however the wet season SW TOA CRE (-75 W m^{-2} around 8am) is over twice as negative as the dry season SW TOA CRE (-35 W m^{-2} around 8am). Weak diurnal cycles in the LW TOA CRE are observed during both seasons (Figure 2.9b). Peaks in the LW TOA CRE are out of phase by approximately 6 hours with the wet season peak occurring around dawn and leading the dry season peak.

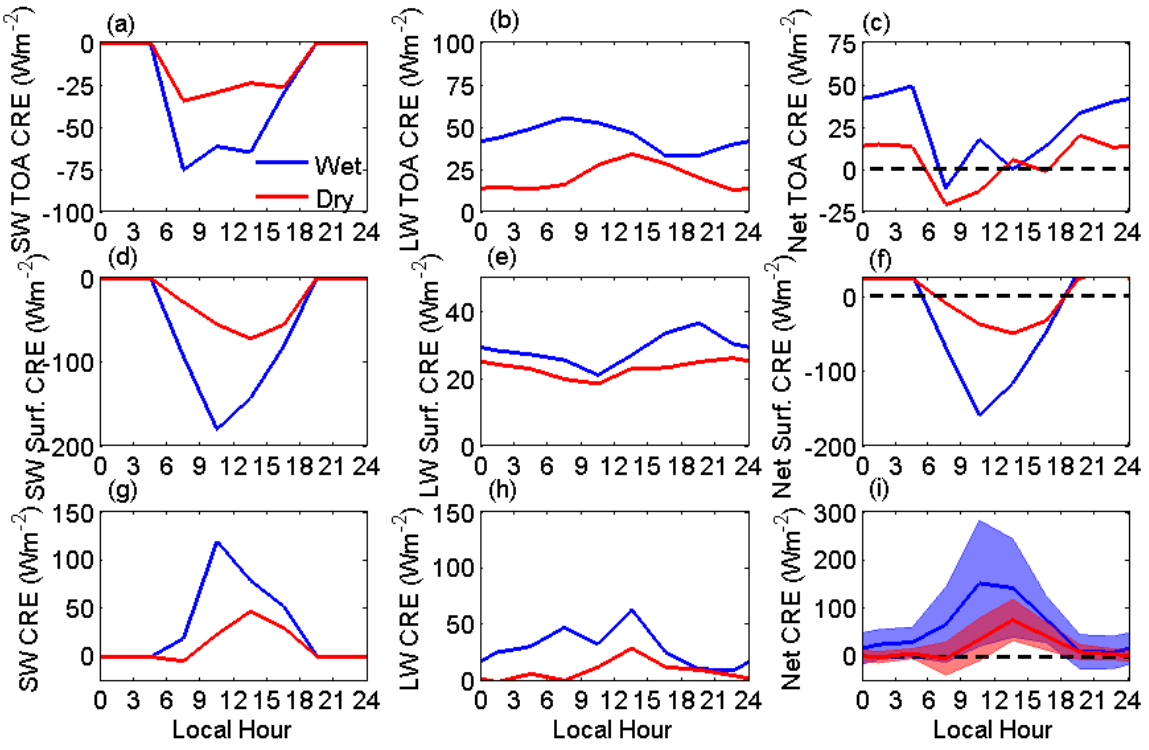

Figure 2.9: Diurnal cycle of (a) SW TOA CRE, (b) LW TOA CRE, (c) net TOA CRE, (d) SW surface CRE, (e) LW surface CRE, (f) net surface CRE, (g) SW atmospheric CRE, (h)

LW atmospheric CRE, and (i) net atmospheric CRE for the 2006 wet and dry season in Niamey, Niger. The shading in (i) represents plus or minus one standard deviation.

The LW TOA CRE exhibits a smaller diurnal amplitude than SW TOA CRE, but still influences the net TOA CRE (Figure 2.9c). In the pre-dawn hours, the absorption of LW radiation by the cloudy atmosphere makes the net TOA CRE positive, reaching a maximum of around 50 W m^{-2}. The early morning minimum in SW TOA CRE causes a minimum of ~-10 W m^{-2} in the wet season and ~-20 W m^{-2} in the dry season. While there are differences in wet and dry season SW and LW TOA CRE of over 50 W m^{-2} at dawn, the difference in sign and the respective phasing of the diurnal cycles result in a smaller difference in the net TOA CRE. Hence, cloud cover increases substantially from the dry season to the wet season, but this cloudiness increase produces no appreciable increase in net TOA CRE.

Clouds invoke a substantial surface CRE during the daytime during both seasons (Figures 2.9d-f), but particularly during the wet season. The wet season surface SW CRE remains negative throughout the day since the clouds have a higher albedo than the surface. The sharp morning minimum of -180 W m^{-2} occurs due to the daily maximum in cloud coverage at that time in combination with the daily change in solar insolation (Figure 2.9d). Dry season SW surface CRE follows the same pattern, but with a much smaller magnitude, reaching a minimum during the early afternoon. These seasonal peaks in the SW surface CRE correspond quite well with peaks in fractional cloudiness, as expected. A diurnal cycle is observed in the LW surface CRE, but its magnitude is minimal and represents only a fraction of the SW surface CRE (Figure 2.9e). Although the SW CRE is negative at the TOA and surface, the LW surface CRE is always positive. The LW surface CRE never

increases above 25 W m^{-2} during the dry season while during the wet season it peaks at only 36 W m^{-2} during the afternoon. While the diurnal cycles of the SW and LW surface CRE are relatively synchronized, the net surface CRE is dominated by the SW surface CRE (Figure 2.9f). There is a substantially greater surface CRE during the wet season indicating increased cooling of the surface by clouds, primarily in response to the SW surface CRE.

What is the effect of clouds on the column itself apart from the effects of clouds at the TOA and surface? The atmospheric CRE, which represents the effect of clouds on the radiation absorbed/emitted by the atmosphere, is shown in Figures 2.9g-i. A positive value of atmospheric CRE denotes absorption of radiation when there are more clouds resulting in increased warming of the atmospheric column. A negative value of atmospheric CRE denotes emission or reflection of radiation when there are more clouds resulting in increased cooling of the atmospheric column. Both the LW and SW atmospheric CRE are measured to be positive at all times during the dry and wet seasons over the Sahel (Figures 2.9g-h). Regardless of the season or time, the presence of an air mass somewhere in the atmospheric column that contains clouds is correlated with increased atmospheric absorption of radiation in the SW and LW (i.e. an increased atmospheric CRE). Diurnal cycles differ between the seasons, but the wet season possesses the most pronounced and highest amplitude cycle. The wet season SW atmospheric CRE peaks in the late morning, while the dry season SW and LW atmospheric CREs and the wet season LW atmospheric CRE peaks in the afternoon.

Only high level cirrus clouds were observed during the dry season with cloud coverage of ~20% during the night and a maximum of ~30% during early afternoon when the clouds were the thickest (not shown). The diurnal cycles of the SW and LW

atmospheric CREs correspond well with these changes in dry season cirrus cloudiness (Figures 2.9g-h). Similarly, the wet season SW atmospheric CRE diurnal cycle corresponds to the diurnal cycle of cloud coverage and thickness during that season. The SW atmospheric CRE, cloud coverage, and cloud thickness are all maximized during the morning (Figures 2.4a and 2.6a) and together with diurnal cycle of the solar insolation explain the diurnal cycle of the net atmospheric CRE (Figure 2.9g). There is little change in the cloud top height on the diurnal timescales during the dry season, which would impact the LW atmospheric CRE. This together with the minimal cloud coverage justifies the small impact of clouds on the LW atmospheric CRE on diurnal time scales (Figure 2.9h).

The diurnal cycle of net atmospheric CRE is strongly modulated by the SW atmospheric CRE during both seasons. Morning hours during the wet season experience the greatest net atmospheric CRE (Figure 2.9i) with an average approaching ~125 W m^{-2} and wide day-to-day variability as indicated by the envelope denoting the standard deviation. This wide variability is due to day-to-day variations in cloud cover. Also noteworthy is that the net SW atmospheric CRE is positive during the entire wet season diurnal cycle due to increased water vapor and cloudiness (Figures 2.4d and 2.6a). Minimal cloudiness and less water vapor in the column lead to a negligible net CRE at night during the dry season (Figure 2.9i). The radiative warming effects of cloud on the atmospheric column is significantly greater during the wet season over the Sahel and is maximized during the morning hours and minimized during the late afternoon. These measurements indicate that the diurnal cycle of cloudiness in the region is inexorably linked to and highly influences the diurnal cycle of radiative heating in the atmospheric column.

2.4 Summary

The diurnal cycle of the meteorology of the WAM monsoon circulation in the vicinity of the Sahel has been relatively well documented. Past studies and the current study show that when the convective boundary layer is deeper during the daytime monsoonal winds are relatively weak, which allows for moisture to mix vertically as the lower atmosphere heats and turbulent mixing is strong (Parker et al., 2005; Kalapureddy et al., 2009; Abdou et al., 2010; Pospichal et al., 2010). Overnight, monsoonal winds have been reported to strengthen as boundary layer turbulence weakens and horizontal advection becomes more important (Parker et al., 2005). These nighttime winds become southwesterly as the nocturnal jet between 200 and 600 m in altitude sets up north of the ITCZ and south of the ITF (Sultan et al., 2007; Lothon et al., 2008; Abdou et al., 2009; Kalapureddy et al., 2009). Enhanced nocturnal monsoonal winds increase moisture advection and in combination with destabilization caused by radiative cooling leads to a nocturnal maximum in precipitation that peaks during the early morning hours (Peyrillé and Lapore, 2007; Lothon et al., 2008) and the majority of this precipitation is associated with mesoscale convective complexes (Laing & Fritsch, 1993; Mohr, 2004). Virtually all of the observed attributes of the meteorological diurnal cycle observed in 2006 in Niamey, Niger are consistent with the descriptions from past studies leading us to conclude that our data set is somewhat representative of typical meteorological conditions in the region. Minor differences arise when compared to Gounou et al. (2012) however we attribute that to a using an average of the entire wet season.

Additional detail regarding diurnal variability in meteorological conditions over the Sahel based upon AMF observations included in the present study included wind profiles,

clouds, aerosols, integrated water vapor, and integrated liquid water. Wind profiles revealed directional and speed shear just above the surface to 1 km depth to be a predominant feature of the growing boundary layer in the dry season and, to a lesser extent, in the wet season. These winds likely contributed to the lofting of dust in both seasons, but especially during the dry season, and strong directional shear during wet season just above 1 km almost certainly lead to directional shearing of growing cumulus clouds.

Sensible and latent heat fluxes were consistent with past studies and sensible heating of the near-surface air mass beginning at daybreak was reflected in the diurnal cycle of the LCL, which increased by nearly 2 km during the boundary layer growth phase. Ultimately, the LCL height increased beyond the depth of the low-level moisture present during the wet season and into the SAL and an associated decrease in cloudiness was observed in accordance with this structural change. A significant diurnal cycle in large scale forcing during the wet season was also present in the NCEP Reanalysis data and corresponded with the rapid growth phase of the morning boundary layer and with increases in morning cloudiness in the mid- and upper levels of the Sahelian troposphere. The initial significant rainfall is required to change the dynamics of the system by providing enough moisture to fuel future rainfall events and lower the LCL height. Precipitation rate and cloud liquid water path measurements during the wet season showed a vague and rather noisy diurnal cycle.

There was a diurnal cycle in surface mixing ratio that was characterized by a decrease during the wet season afternoon. This decrease coincided with a significant latent heat flux and with a decrease in the boundary layer profiles of mixing ratio below 1 km during the afternoon. A slight increase in the integrated water vapor is suggested during

the afternoon, but the water vapor added by the surface latent heat flux is too small a percentage of the total integrated vapor to present a strong signature. By late morning, the surface heating and the subsequent surface sensible heat flux raise the LCL out of the low-level moisture and cloud coverage begins to decrease. Clouds remaining in the afternoon are largely in the mid- and high troposphere and are likely to be passive remnants of the nocturnal and morning convection and be composed of a large percentage of ice because the integrated liquid water path declines in lock-step with the increase in the LCL height into the SAL.

The goal of the present study was to capitalize on a unique opportunity to measure the diurnal cycle of the RFD and CREs on time scales resembling those of clouds, water vapor, and aerosols that interplay with the SW and LW radiation streams. Fortuitous geography enables the diurnal cycles observed during the wet and dry seasons over the Sahel to lie at two ends of the spectrum: near desert conditions and continental tropical conditions. Contrasting these two extremes in the diurnal cycles of meteorological variability and incoming and outgoing radiation streams was intended to expose sensitivities. The dry season has previously been analyzed by Milton et al. (2008) in this respect, however clouds, which can have a significant impact on diurnal time scales, are minimal during that time.

Clouds are shown to be an important surface cooling mechanism during the daytime (negative surface CRE), particularly during the wet season. Conversely, these same daytime clouds invoke negligible changes at TOA. This difference in boundary forcing results in a net radiative warming of the atmospheric column itself when clouds are present (positive atmospheric net CRE). Bouniol et al. (2012) reported that the diurnal LW surface

CRE could not be calculated accurately with available radiosonde temperature and water vapor data. To ameliorate this difficulty, we employed temperature and vapor profiles available from the AMF profiling microwave radiometer between radiosonde launches. This additional information enabled us to compute the LW surface CRE and our measurements are similar in magnitude to those presented in McFarlane et al. (2013) and other studies.

Based on measurements of the TOA, surface, and atmospheric CRE, the most pronounced cloud and radiation interactions on diurnal time scales involve the SW CREs. While diurnal cycles in the LW CRE were noted, in nearly all cases the SW impacts controlled the net CRE and many other associated variables.

A weakness of the present study is proper understanding of the diurnal cycle of dust and its seasonal differences. Dust is hard to quantify yet can have a profound impact on the radiation budget in the Sahel. Dry season dust storms in addition to the omnipresent dust year round should be quantified on a diurnal time scale. McFarlane et al. (2009), Turner (2008), and Milton et al. (2008) made great progress on the role of dust, however more work is needed. Without the use of a radiative transfer model, as in this study, it is very difficult to determine the exact radiative impact of dust.

CHAPTER 3: Seasonal and Diurnal Cycle of Meteorology, Clouds, and Radiation in the Amazon Rainforest of Brazil

As the AMF travels around the world, datasets for other regions have become available. This chapter discusses the observations from the first year of the GOAmazon deployment of the AMF in Manacapuru, Brazil. Monthly averaged meteorology and radiation variables as well as their diurnal cycles are presented. Local hour in Manacapuru, Brazil is four hours behind Coordinated Universal Time. The wet and dry seasons are reversed compared to the Sahel, with the wet season encompassing January, February, and March and the dry season including July, August, and September.

3.1 Seasonal Cycle of Meteorology

The annual progression of the monthly averages of surface air temperature, mixing ratio at 2 m, and wind speed and direction at 10 m are shown in Figure 3.1. The differences in the minimum and maximum values for each of these variables are minimal, with the spread in 2 m surface air temperature only encompassing 2 °C (Figure 3.1a). This is likely due to the presence of additional clouds in the wet season that prevents solar insolation from heating the surface (discussed later). Interestingly, the maximum surface mixing ratio occurs in the transition seasons, peaking in May and December (Figure 3.1b). But, over the course of the year the change in surface mixing ratio is very small, less than 1 g kg^{-1}. The annual minimum in surface mixing ratio does however occur at the height of the dry season as expected.

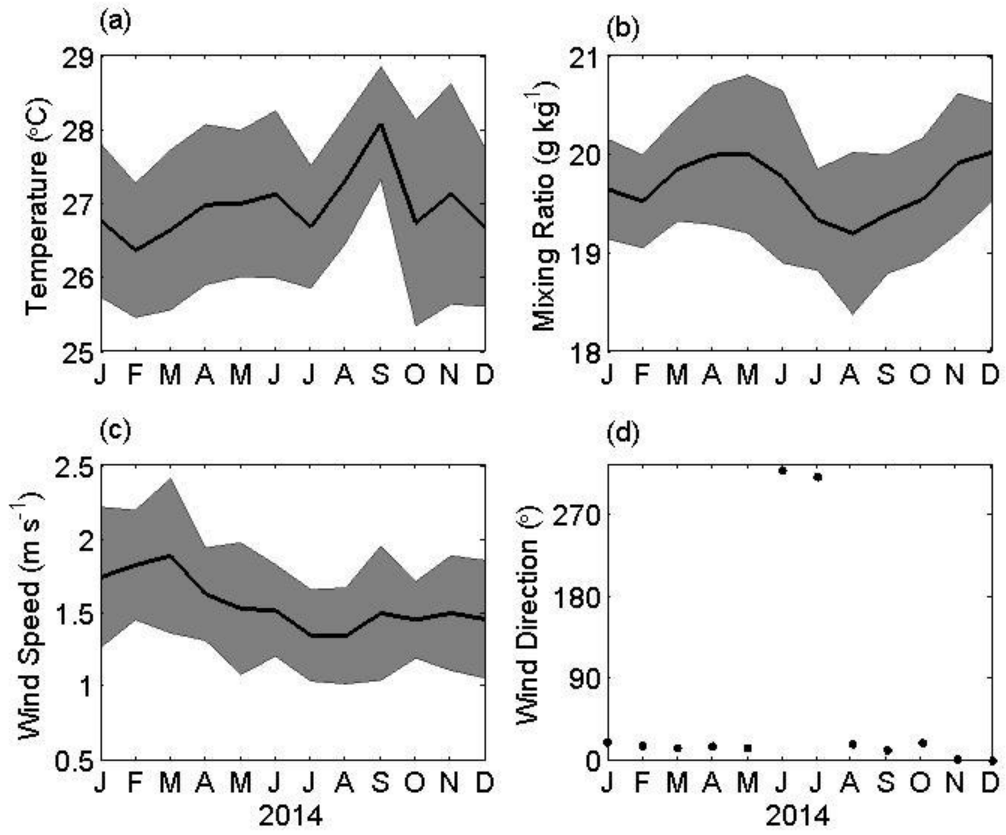

Figure 3.1: Monthly average (a) temperature at 2 m, (b) mixing ratio at 2 m, (c) wind speed at 10 m, and (d) wind direction at 10 m for the year 2014 in Manacapuru, Brazil. Shading represents plus or minus one standard deviation.

A seasonal cycle similar to that of the surface mixing ratio is present in the annual progression of surface wind speed, though the variation in surface wind speed is less than 1 m s^{-1} throughout the year (Figure 3.1c). The highest average wind speeds are recorded at the end of the wet season in March followed by a gradual decrease in wind speed through the transition into the dry season. Winds are primarily out of the north-northeast except for June and July when the winds take on a slight westerly component (Figure 3.1d). Overall the winds in this region can be described as very light and northerly.

The difference between the dry and wet seasons can be seen much easier in the annual progression of column integrated water (Figure 3.2). As in chapter 2, column integrated liquid water and water vapor will be termed liquid water path and integrated water vapor, respectively. Large values of liquid water path are present in the wet season, peaking in March, followed by a gradual decrease into the dry season when the annual minimum is reached in August. Integrated water vapor shows a similar pattern, except it remains nearly constant until May before decreasing for the dry season. The magnitudes of liquid water path and integrated water vapor in Manacapuru, Brazil are quite large year round. For comparison, the dry season integrated water vapor in Manacapuru, Brazil is nearly equivalent to the wet season value in Niamey, Niger and the wet season liquid water path is triple than what was observed in Niamey, Niger. Precipitation is recorded year round with larger precipitation rates in the wet season compared to the dry season and an annual maximum in March (not shown).

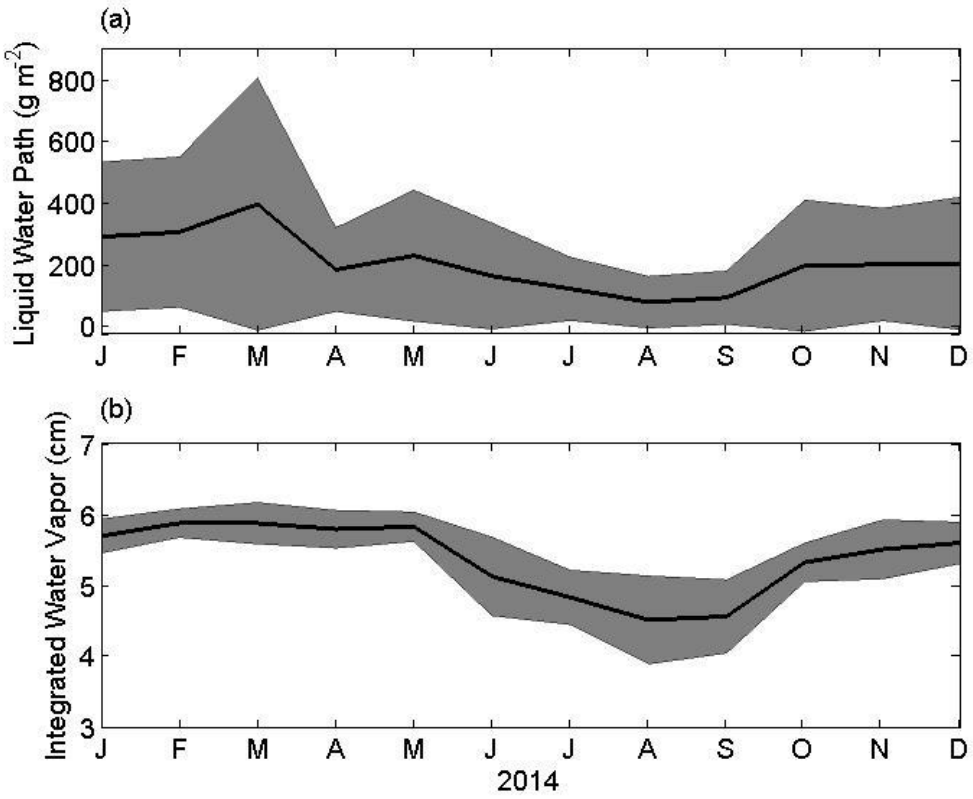

Figure 3.2: Monthly average (a) liquid water path and (b) integrated water vapor for the year 2014 in Manacapuru, Brazil. Shading represents plus or minus one standard deviation.

Although the dry season is not necessarily dry since there is appreciable precipitation, there is a decrease in moisture within the atmospheric column. The vertical profile of temperature is nearly constant throughout the year, but the profile of relative humidity shows considerable variability (Figure 3.3). There are periods of noticeable drying in the entire column between June and October with the most pronounced drying between 3 and 12 km. The main difference in large scale forcing that can influence the amount of moisture within the column is the Hadley circulation. This can be demonstrated by calculating back trajectories of an air parcel using the Hybrid Single Particle Lagrangian Integrated Trajectory Model (HYSPLIT; Draxler and Hess, 1997). Example back trajectories for the wet and dry season using conditions depicted in the NCEP Global Data

Assimilation System can be seen in Figures 3.4 and 3.5. During the wet season, the ascending branch of the Hadley cell lies over the region and one week prior to arriving in Manacapuru the air mass originates over the ocean at a lower altitude (Figure 3.4). Air that is 4 km above ground level was at the surface of the ocean. Surface moisture is then advected over land and rises within the column as it makes its way to the Amazon Rainforest. In the dry season, the ascending branch of the Hadley cell is no longer over the area so air parcels do not rise while they make their way towards the region (Figure 3.5). Upper level air over the ocean does not contain as much moisture as air just above the surface as influences from the Saharan air layer are present. As a result, moisture advection into the column above Manacapuru, Brazil decreases during the dry season.

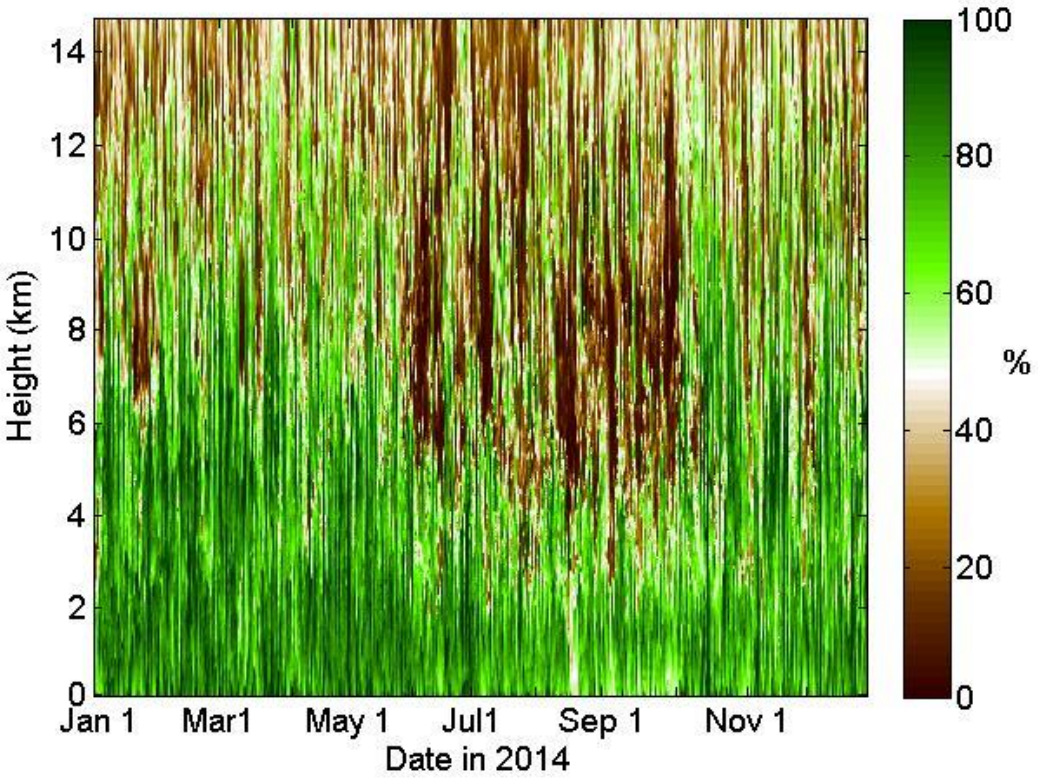

Figure 3.3: Time series of radiosonde observed relative humidity in the atmospheric column over Manacapuru, Brazil in the year 2014. Figure created by Lynne Trabachino.

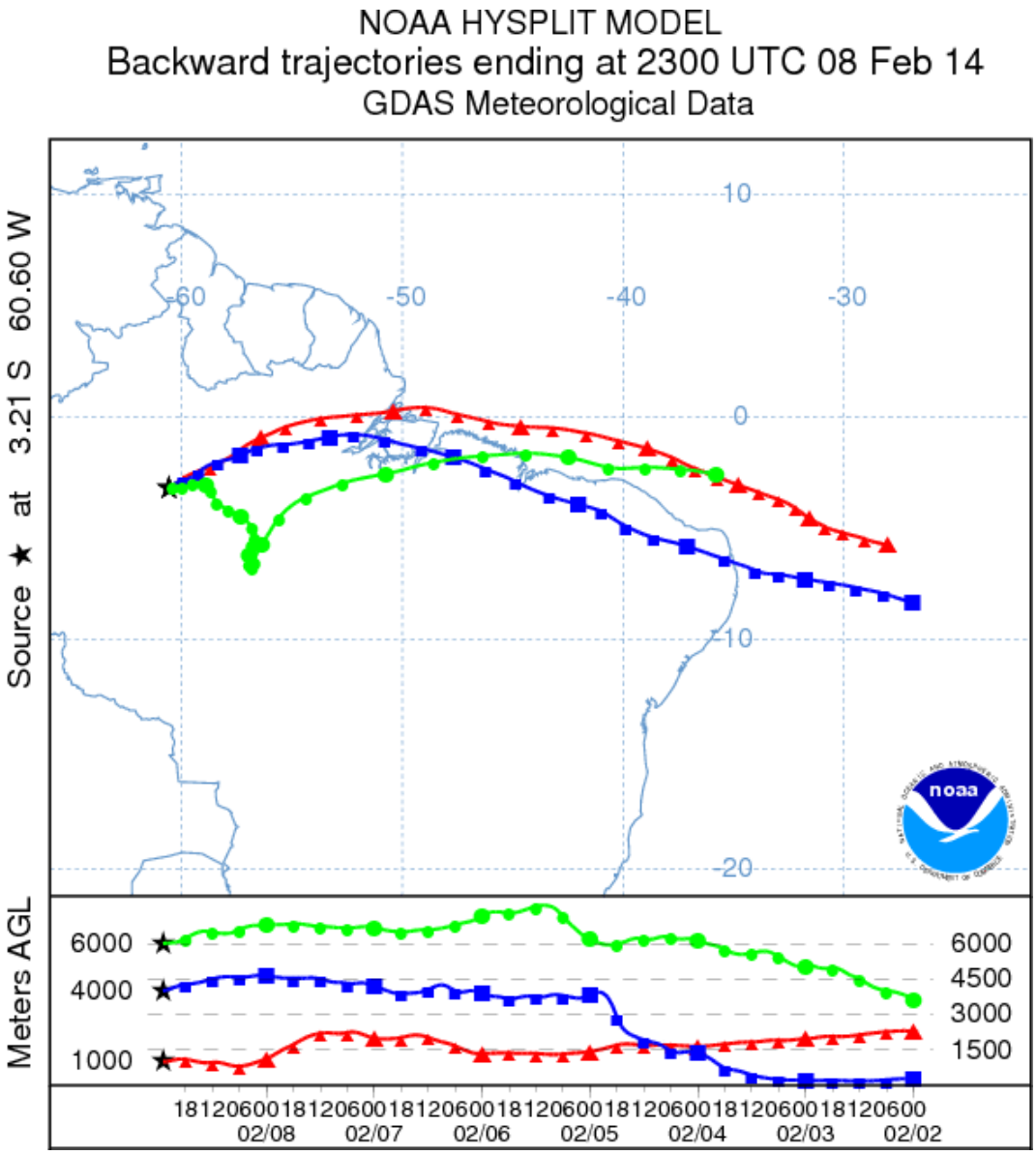

Figure 3.4: Back trajectory of an air parcel at 1000, 4000, and 6000 meters above ground level for the week ending February 8, 2014 at 2300 UTC in Manacapuru, Brazil.

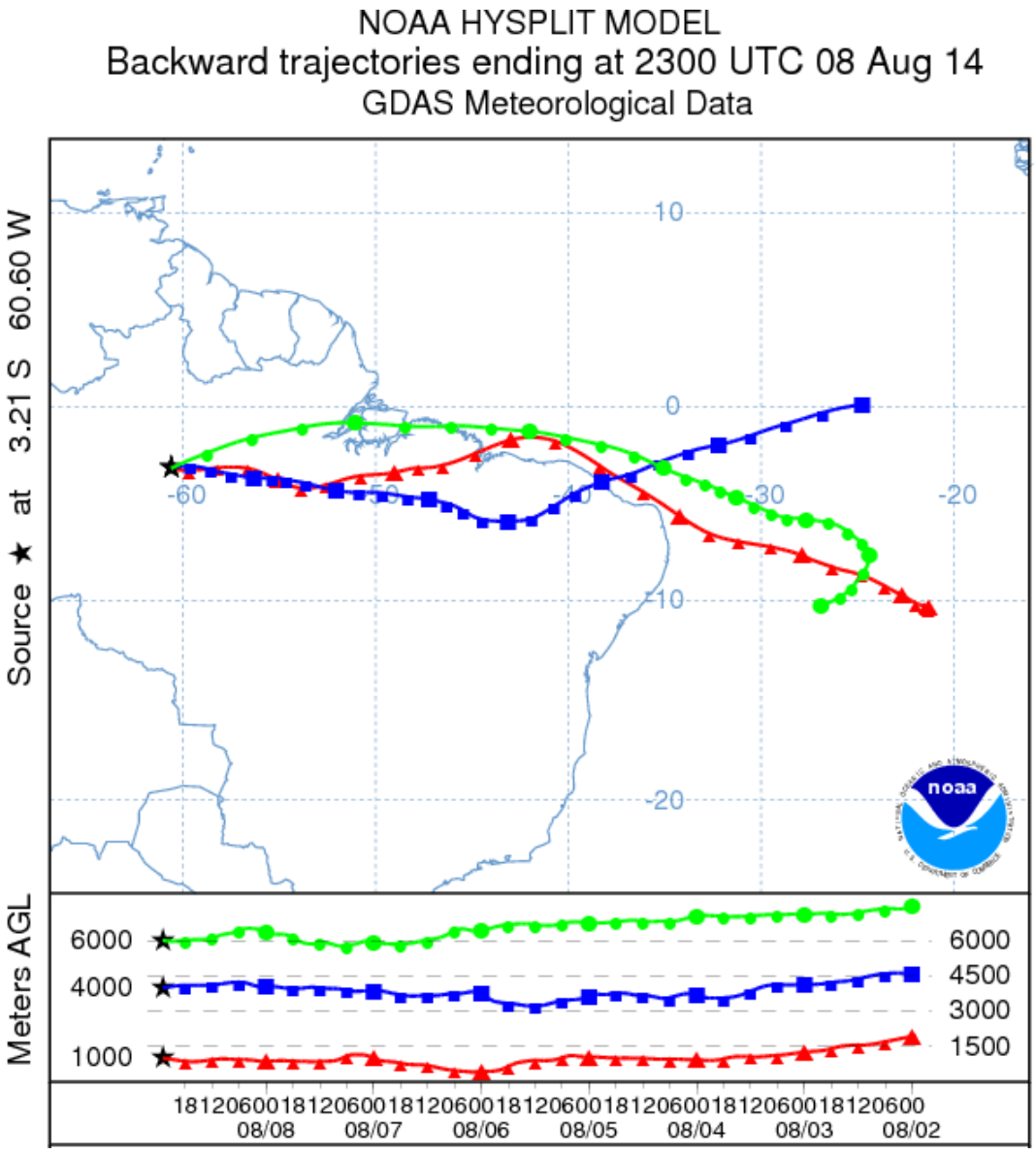

Figure 3.5: Back trajectory of an air parcel at 1000, 4000, and 6000 meters above ground level for the week ending August 8, 2014 at 2300 UTC in Manacapuru, Brazil.

Large amounts of moisture through the column are associated with clouds, which are a very common feature in the Amazon Rainforest. Cloud fraction, as shown in chapter 2, can be calculated for Manacapuru, Brazil using a number of observational techniques, three of which are presented in Figure 3.6. The first method used the AMF MPL backscatter data to create a cloud mask using an algorithm based on Wang and Sassen (2001). This

cloud mask is available as a value added product through ARM, that provides a quality controlled cloud field every 30 seconds; it is the only available measure of clouds that encompasses all of 2014 (Sivaraman and Comstock, 2011). The cloud radar became fully operational in the end of April 2014 and the data were combined with the MPL and ceilometer data in the ARSCL value added product, as was used for Niamey, Niger (Chapter 2; Clothiaux et al. 2001). The third data source for cloud fraction comes from the CERES geostationary enhanced product, SYN1Deg, which is available through July 2014 (Doelling et al., 2013). SYN1Deg temporally interpolates between CERES observations using observations from geostationary satellites. Regardless of the method used, substantial cloudiness is present in the wet season, peaking in February (Figure 3.6). A decrease in cloud fraction is observed through the transition season and into the dry season until the annual minimum cloud fraction is reached in September. Clouds begin to increase again as the transition is made to the following wet season. The differences between the results for the different instruments highlight the difficulty in accurately depicting whether a cloud is present. CERES underestimated dry season cloudiness, missing low level clouds and fog that were detected by the cloud radar and MPL. While these difference are present, it is important to remember that the mean plus or minus one standard deviation in cloud fraction for the three methods overlap one another, with the overall largest standard deviation in cloud fraction is present in the ARSCL algorithm.

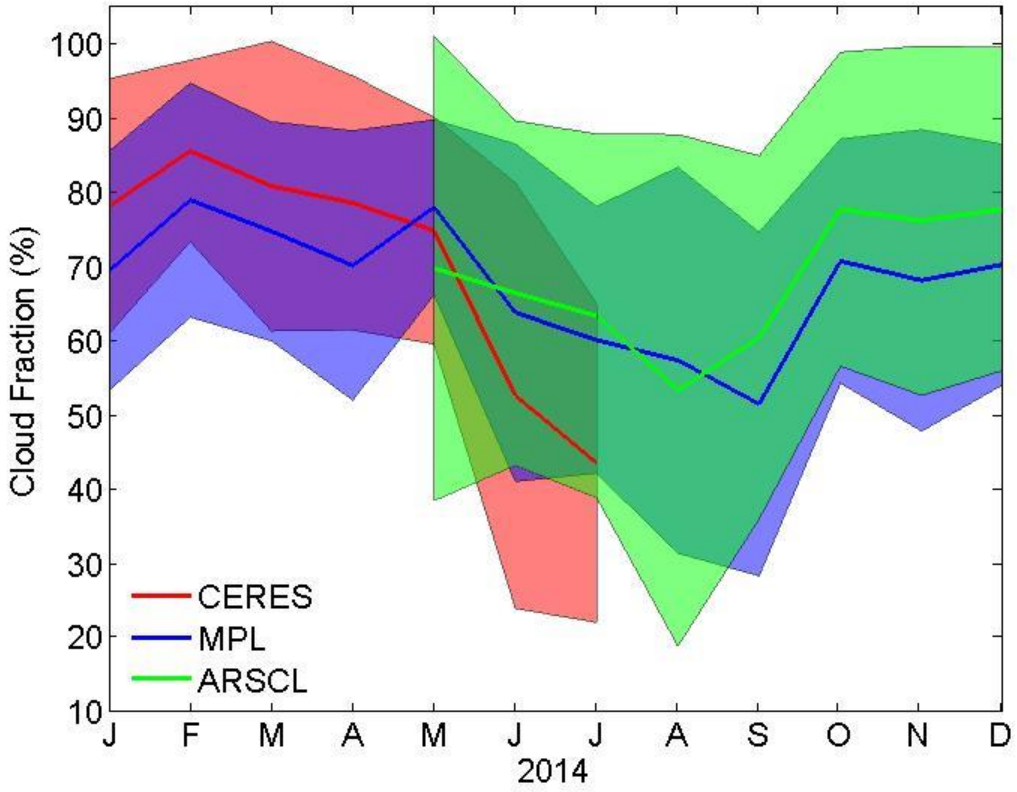

Figure 3.6: Monthly averaged cloud fraction as calculated by CERES (red), the Z. Wang micropulse lidar algorithm (blue), and the ARSCL algorithm (green) in Manacapuru, Brazil in the year 2014. Shading represents plus or minus one standard deviation.

One reason for the interest in the Amazon Rainforest within the field of climate science is the varying aerosol conditions. Air in the wet season is often considered pristine with aerosols limited to biogenic sources (Williams et al., 2002). Biomass burning becomes more common in the dry season, increasing the concentration of aerosols and therefore CCN. CCN concentrations gradually increase through the transition season with an abrupt increase in August at both 0.4 and 1.1 supersaturation (Figure 3.7). Daytime CCN concentrations peak in August while nighttime concentrations peak in September. The annual maximum daytime CCN concentration at 0.4 super saturation is rather large,

exceeding 1000 cm^{-3}, indicating that aerosols may have an impact on the absorption within the column as well as the reflectivity of clouds. Aerosol absorption coefficients from the particle soot absorption photometer were also analyzed but are not shown since the results are nearly identical to the CNN concentrations.

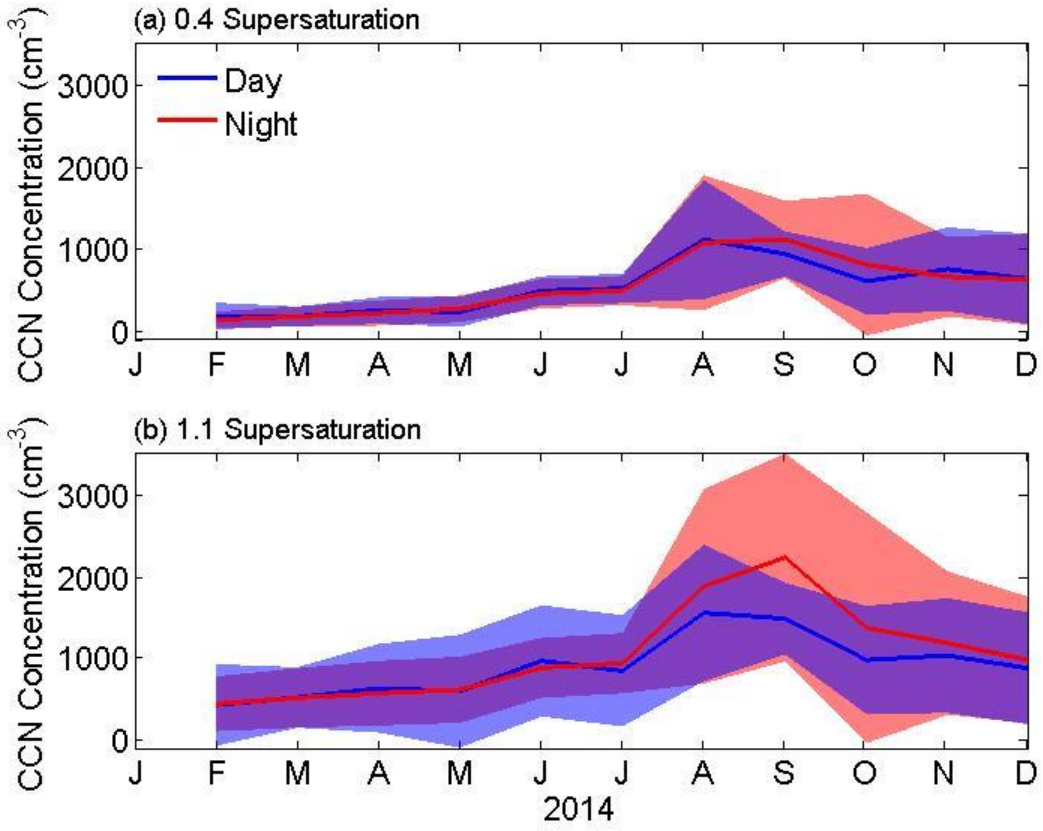

Figure 3.7: Monthly average CCN concentration at (a) 0.4 and (b) 1.1% supersaturation in Manacapuru, Brazil in 2014 during the day and at night. Shading represents plus or minus one standard deviation.

3.2 Diurnal Cycle of Meteorology

A noticeable diurnal cycle of meteorology is present in both the wet and dry season in Manacapuru, Brazil and can be seen in Figure 3.8. An early morning minimum in the air temperature at 2 m is seen with an afternoon maximum in both seasons (Figure 3.8a).

A larger range in the diurnal temperature is observed in the dry season. Increased wet season cloudiness prevents solar insolation from heating the surface during the day and longwave radiational cooling overnight. This same feature is observed in Niamey, Niger but is not as pronounced in Brazil.

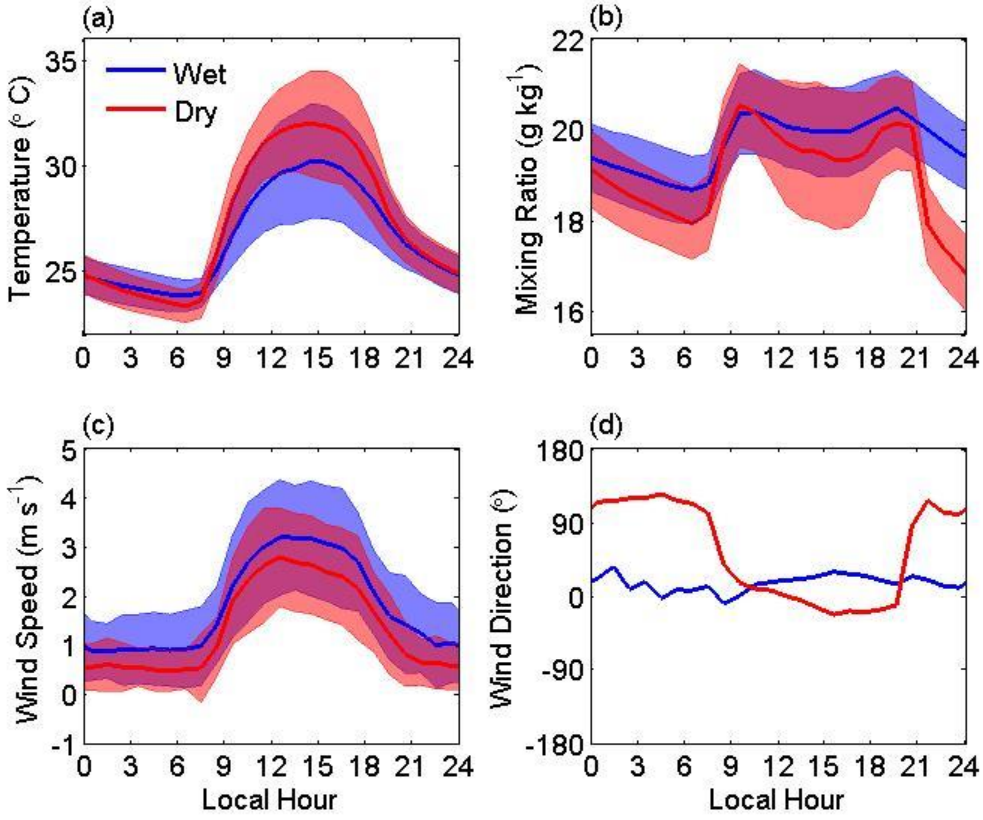

Figure 3.8: Diurnal cycle of (a) temperature at 2 m, (b) mixing ratio at 2 m, (c) wind speed at 10 m, and (d) wind direction at 10m for the 2014 wet and dry seasons in Manacapuru, Brazil.

The minimum in surface mixing ratio and temperature coincide during both seasons; it is cooler and drier just before dawn (Figure 3.8b). However, unlike surface temperature, the diurnal cycle in surface mixing ratio is bimodal with a secondary minimum in the afternoon and maximums in the late morning and evening hours. A sharp

increase due to evapotranspiration occurs in the morning, coinciding with sunrise and the presence of photosynthetically active radiation. Photosynthesis likely declines in the afternoon hours as the surface temperature peaks, resulting in stomatal closure and therefore a reduction in evapotranspiration (Koch et al., 1994). Surface mixing ratio then reaches a secondary maximum as soil moisture is replenished by afternoon rainfall in the dry season and plants are less stressed by environmental factors. Overnight, there is a gradual decrease in surface mixing ratio as the temperature cools and condensation occurs.

Wind speeds are relatively constant overnight, peaking in the late morning in the dry season and afternoon in the wet season with a gradual decrease into the nighttime hours (Figure 3.8c). Winds are always weaker in the dry season, with little change in direction throughout the day (Figure 3.8d). A river breeze circulation sets up in the dry season causing on average a shift in the wind direction exceeding 90° between the nighttime and daytime hours (Figure 3.8d). This shift is even more pronounced in the month of July with a 180° difference (not shown). Manacapuru sits just north of the Rio Solimões, a major tributary to the Amazon River (Figure 1.4b). Northerly winds occur during the day as the land heats more rapidly than the surface. Overnight, winds become eastward.

Liquid water path is characterized by a seasonally dependent diurnal cycle. It is relatively constant overnight in the dry season with an early afternoon peak while wet season exhibits a different diurnal cycle from the dry season with a morning maximum and evening minimum (Figure 3.9a). Neither season has a smooth cycle as deep convective events containing large amounts of liquid water are intermixed with scattered cumulus clouds and periods of clear skies. This also leads to a large standard deviation in the liquid water path, especially during the wet season. Unlike other variables, integrated water vapor

path shows a very weak diurnal cycle in the wet season (Figure 3.9b). It is nearly constant. In contrast, the dry season integrated water vapor echoes the diurnal cycle of liquid water path; constant in the morning followed by an increase in the afternoon.

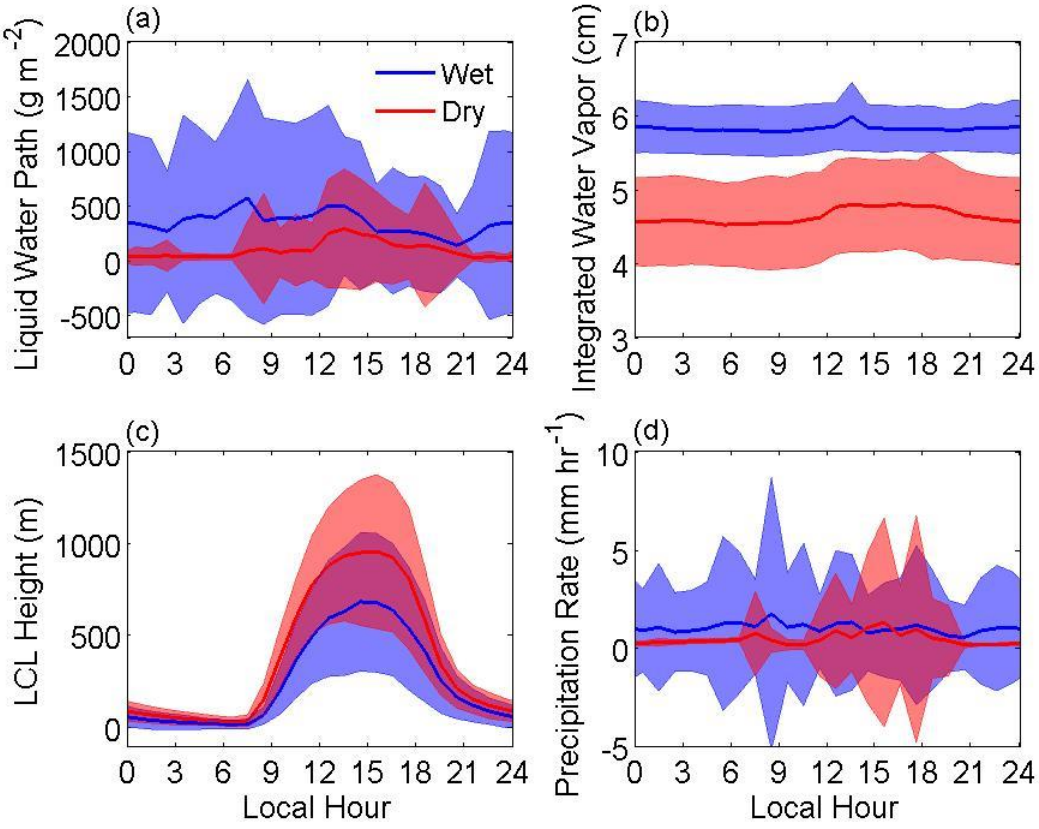

Figure 3.9: Diurnal cycle of (a) liquid water path, (b) integrated water vapor, (c) LCL height, and (d) precipitation rate for the 2014 wet and dry seasons in Manacapuru, Brazil. Shading represents plus or minus one standard deviation.

The height of the LCL is known to be highly correlated with the occurrence of convective clouds and precipitation in other parts of the continental tropics, such as the Sahel. The diurnal cycle of the height of the LCL is similar to temperature with an afternoon maximum (Figure 3.9c). The LCL is always higher in the dry season due to a combination of warmer daytime temperatures and less moisture. As the LCL gradually

raises throughout the day, wet season precipitation decreases (Figure 3.9d). Dry season precipitation has a more pronounced diurnal cycle than what is seen in the wet season with an afternoon peak.

The maximum in cloud fraction is out of phase with the maximum in precipitation for both seasons. During both seasons, cloud coverage peaks a few hours after the maximum precipitation is observed (Figure 3.10). Wet season morning low level clouds develop into afternoon deep convective clouds with the aid of a warming surface (Figure 3.10a). Some residual high level clouds are present overnight until low level clouds begin to form in the early morning hours. Dry season clouds are primarily in the upper troposphere with the highest cloud fraction between 1800 and 2100 h (Figure 3.10b). During the afternoon and evening hours there are some low and middle level clouds that are observed that are absent overnight and in the morning. Entrainment of dry mid-level air prevents clouds from being sustained throughout the entire day, like in the wet season.

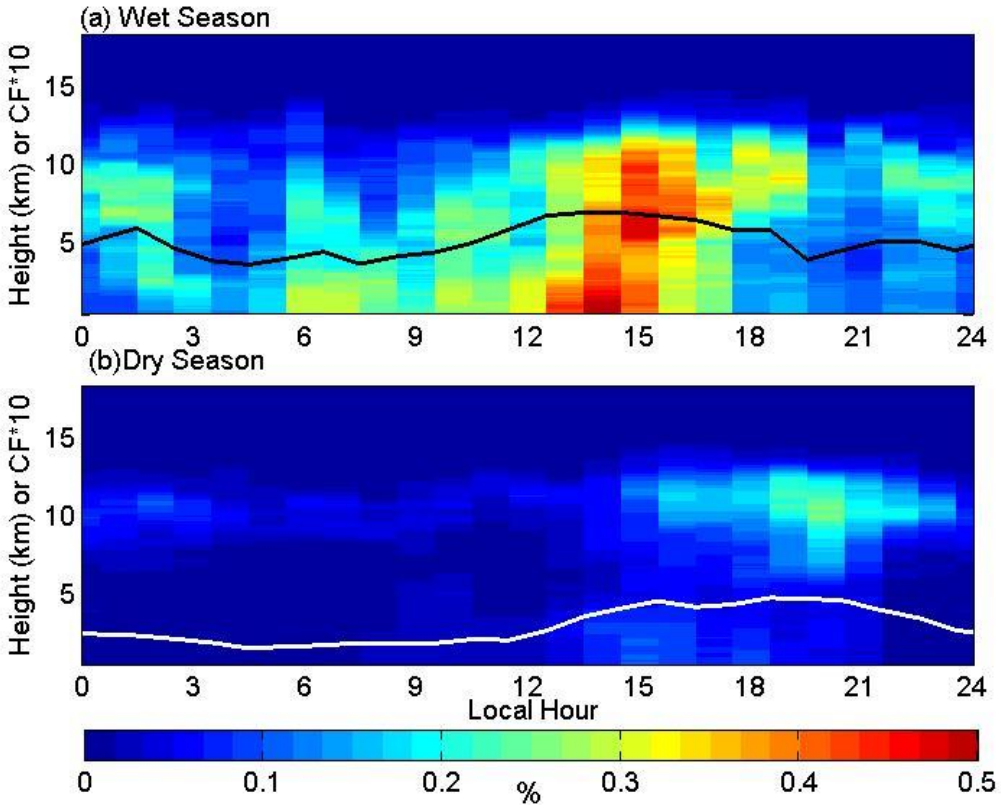

Figure 3.10: Diurnal cycle of total cloud fraction (solid black or white line) and cloud fraction with height for the 2014 (a) wet season and (b) dry season in Manacapuru, Brazil.

3.3 Monthly Averaged Radiation

Meteorological contrasts between the wet and dry seasons are associated with seasonal variations in the radiation budget at the TOA, surface, and within the atmospheric column. The radiative fluxes leaving at the TOA as measured by CERES can be seen in Figure 3.11. The SW and LW fluxes plotted are the monthly averages of the afternoon and overnight observations made by both Aqua and Terra. The TOA SW flux overnight is zero so only the afternoon observation is shown. Measurements are only available through October 2014 as the data for November and December for that year are not yet available. The annual maximum reflection of SW radiation occurs in February, which coincides with the annual maximum in cloud fraction and a general correlation can be seen between

reflected SW radiation and cloud fraction (Figures 3.6 and 3.11). An exception to this relationship occurs in the month of August, which has an increase in reflected SW radiation compared to July. But in this month the decrease in cloud fraction is counteracted by an increase in solar insolation that is greater between the months of July and August than August and September, thereby leading to the increase in upwelling SW radiation. The amplitude of the seasonal cycle in LW radiation emitted at the TOA is smaller than that for SW radiation, encompassing a spread of around 50 W m^{-2} (Figure 3.11). The influence of atmospheric moisture and clouds can easily be seen with a maximum of emitted LW radiation in the dry season and a minimum in the wet season. Despite year round cloudiness, the annual average TOA LW flux is very similar to the global annual mean.

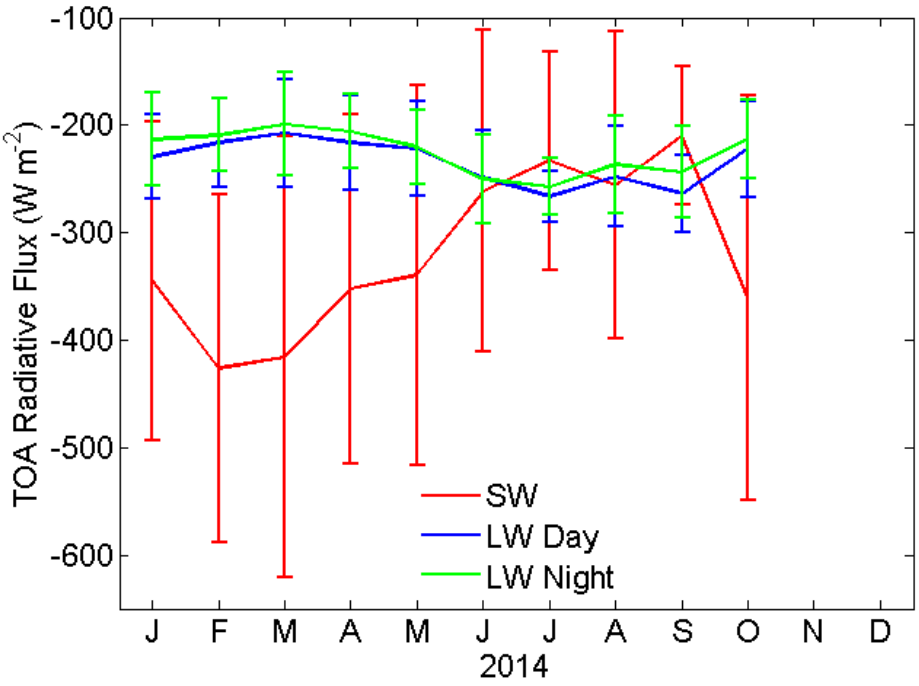

Figure 3.11: Monthly TOA outgoing daytime SW and daytime and nighttime LW radiative fluxes measured by CERES in the year 2014 over Manacapuru, Brazil. Error bars represent plus or minus one standard deviation.

Despite changes in clouds and moisture throughout the year, the variations in the surface radiative fluxes are very subtle (Figure 3.12). The only impact of clouds evident in these data is a slight increase in the downwelling component of the surface SW radiative flux in the dry season alongside a decrease in the standard deviation of the downwelling surface SW flux and an even smaller broad increase in the downwelling component of the surface LW radiative flux. An interesting feature of the radiation budget is the ratio of the upwelling and downwelling LW radiative fluxes. A very large percentage of the LW radiation emitted by the surface is absorbed by the atmosphere and emitted toward the surface as indicated by the net LW flux at the surface. Clouds and moisture prevent a large fraction of LW radiation from reaching the top of the atmosphere, thereby warming the troposphere and surface. The correlation coefficient between the surface downwelling LW flux and integrated water vapor is 0.62, which indicates a strong relationship between the two. The variability within the components of the surface LW flux is minimal, especially when compared to the variability with each month of the downwelling surface SW flux.

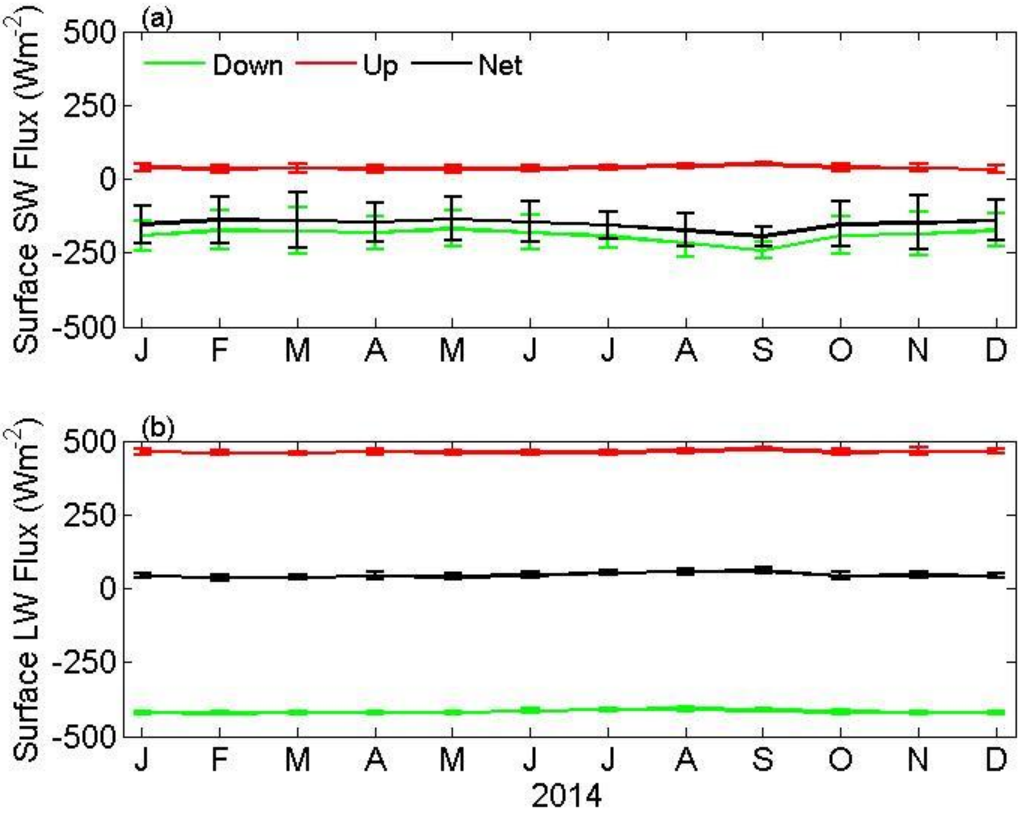

Figure 3.12: Monthly average surface upwelling, downwelling, and net SW (a) and LW (b) radiative fluxes in Manacapuru, Brazil during 2014. Error bars represent plus or minus one standard deviation.

Heating (or cooling) of the column gases can be quantified with the cross atmosphere RFD and is shown in Figure 3.13. Following the annual progression of solar insolation, the mid-day SW cross atmosphere RFD increases from February through April and decreases in May (Figure 3.13a). A second increase in seen from May to July as the vertical structure of clouds changes. Deep convective wet season clouds are more reflective than upper level dry season clouds sending more SW radiation to space that is therefore not available to heat the column. The SW RFD is stable in July and August, coinciding with a small increase in SW radiation emitted at the TOA although cloudiness decreases

slightly. The albedo of the atmosphere reaches its minimum in September and along with an increase in solar insolation result in a small increase in cross atmosphere SW RFD. In October the vertical structure of clouds begins to transition towards the wet season structure and the increased reflectivity leads to a decrease of cross atmosphere SW RFD into the wet season.

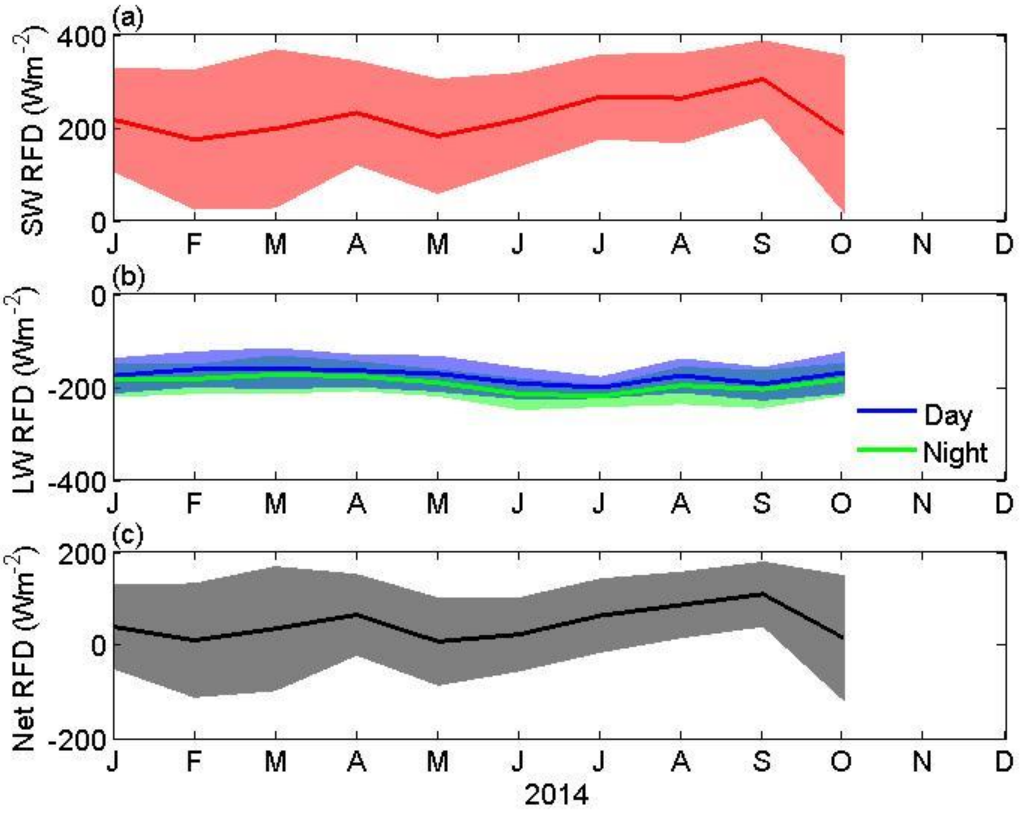

Figure 3.13: Monthly average (a) daytime SW, (b) daytime and nighttime LW, and (c) daytime net cross atmosphere radiative flux divergence over Manacapuru, Brazil during the year 2014. Shading represents plus or minus one standard deviation.

The LW RFD is roughly constant between January and April indicating that water vapor is playing a larger role on the absorption of LW radiation with the column than clouds (Figure 3.13b). The annual minimum LW RFD occurs June and July even though the

minima in clouds and moisture occur in August and September. This could be related to the annual maximum surface temperature occurring during August and September or the large increase in CCN concentrations seen during those two months.

Throughout the course of the year, the positive daytime net cross atmosphere RFD indicates that the column is warming radiatively mid-day (Figure 3.13c). Since the LW cross atmosphere RFD is constant in the wet season, the SW cross atmosphere RFD takes an active role in determining how the net cross atmosphere RFD will change. In the transition season and most of the dry season, competing changes in the LW and SW cross atmosphere RFD balance out the net cross atmosphere RFD at a nearly constant value. In the second half of the dry season, the LW cross atmosphere RFD becomes constant again, resulting in a small increase in the net cross atmosphere RFD in September associated with the increase in the SW cross atmosphere RFD.

The impact of clouds on the radiation budget in Manacapuru, Brazil can be seen in the CRE as presented in Figure 3.14. Maximum SW cooling at the surface at mid-day due to clouds occurs in the wet season and minimum cooling occurs in the dry season (Figure 3.14a). Through each season, the surface SW CRE is relatively constant with the changes occurring in the transition season, despite differences in cloud fraction within the seasons. LW warming at the surface due to clouds in constant throughout out the year and much smaller than the impact in the SW (Figure 3.14b). This results in a net cooling at the surface due to clouds, dominated by the surface SW CRE (Figure 3.14c).

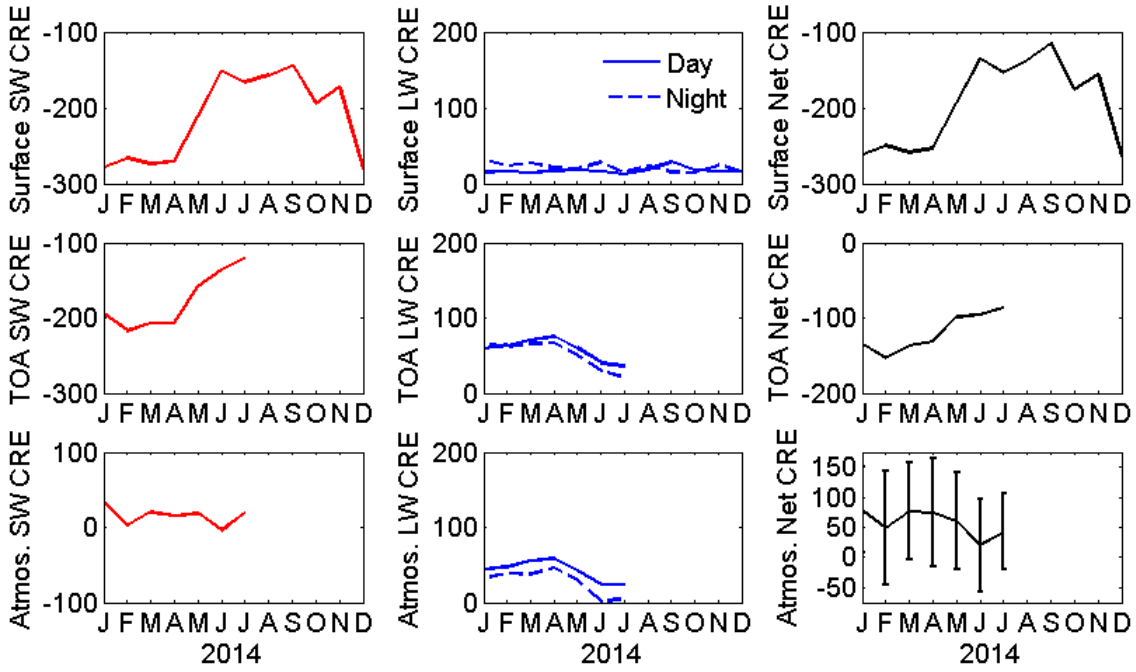

Figure 3.14: Monthly average SW (a), LW (b), and net (c) surface cloud radiative effect, SW (d), LW (e), and net (f) top of the atmosphere cloud radiative effect, and SW (g), LW (h), and net (i) atmospheric cloud radiative effect in Manacapuru, Brazil during the year 2014 in W m^{-2}. Error bars in (i) represent plus or minus one standard deviation.

Cooling of the Earth-atmosphere system also occurs at the TOA (Figure 3.14f). Since the CERES clear and all sky TOA fluxes are only available through July 2014, the mid-day TOA CRE cannot be calculated for the entire year. The largest TOA SW CRE occurs in February, coinciding with the annual maximum cloud fraction (Figure 3.14d). Clouds impose a smaller cooling at the TOA as the transition season progresses. Unlike at the surface, the TOA LW CRE is not constant throughout the year and is significant. While still smaller than the impact of clouds in the SW, the LW TOA CRE is roughly constant through the wet season but then decreases into the transition season (Figure 3.14e). The lack of deviation during the wet season indicates that water vapor dominates the LW TOA

CRE rather than clouds. There is a net cooling due to clouds at the TOA and although the SW and LW TOA CRE mirror one another, the seasonal cycle of clouds and moisture is evident in the annual progression (Figure 3.14f).

Although clouds are significantly cooling the Earth-atmosphere system in the SW at the surface and TOA they are either negligible or provide a slight warming in the column heat budget (Figure 3.14g). For example, clouds have a negligible impact on the atmospheric column in the SW during the month of February when the cloud fraction is the highest. Clouds reflect more SW radiation than is absorbed, leading to large changes at the boundaries, but small changes within the column itself. Radiation absorption when the atmosphere is cloudy is mostly occurring in the LW part of the spectrum with the daytime LW atmospheric CRE exceeding the SW atmospheric CRE each month (Figure 3.14h). These observations lie in sharp contrast to the Sahel, where the LW atmospheric CRE is essentially negligible compare to the SW atmospheric CRE. The annual progression of LW atmospheric CRE is similar to the surface LW CRE with water vapor being the main controlling factor. Neither LW atmospheric CRE nor SW atmospheric CRE dominate the net atmospheric CRE with impacts of both parts of the spectrum controlling the net (Figure 3.14i). The February and June minima in SW atmospheric CRE appear in the net, while the decrease in LW atmospheric CRE can be seen in the transition season.

3.4 Diurnal Cycle of Surface Fluxes

Since CERES only provides observations of the TOA radiative fluxes twice a day, this dataset is not compatible with a diurnal cycle study. On the other hand, surface radiative fluxes provided by the AMF can be analyzed on a diurnal time scale and are shown in Figure 3.15. The surface net SW radiative flux follows the curve for solar

insolation peaking around noon. There is some mismatch in the timing between the two seasons due to differing sunrise and sunset times. The amount of solar insolation is larger during the wet season however roughly 150 W m^{-2} less SW radiation reaches the surface due to the increased albedo of clouds.

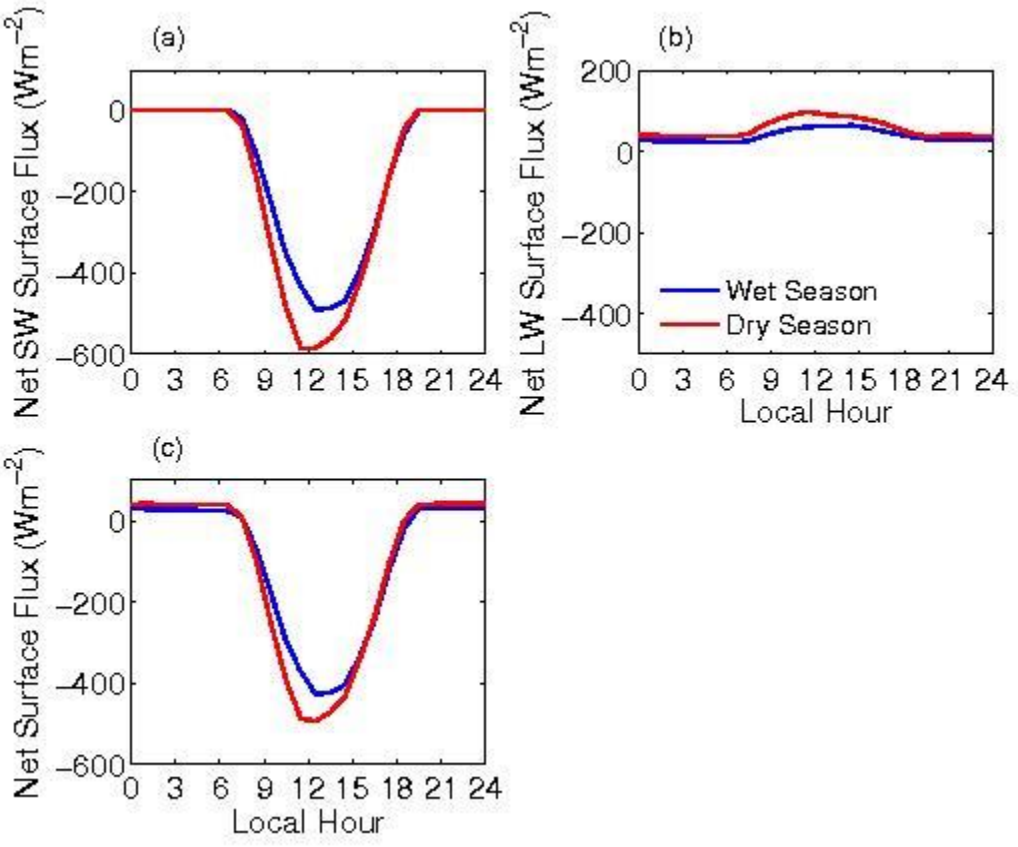

Figure 3.15: The diurnal cycle of the surface net SW (a), LW (b), and net (c) radiative fluxes during the 2014 wet and dry seasons in Manacapuru, Brazil.

The magnitudes of the surface net LW radiative flux between the wet and dry season are very similar and almost identical overnight (Figure 3.15b). The maximum deviation between the two seasons is only 38 W m^{-2}, occurring in the late morning hours. The larger deviation during the day is a result of an increase in integrated water vapor that

occurs in the daytime in the dry season, as well as a more pronounced diurnal cycle in temperature. The dry season has a slightly larger net LW since there is less water vapor within the column resulting in a smaller downwelling component of the LW radiative flux. In addition, warmer surface temperatures during the dry season result in a larger upwelling component of the LW radiative flux. These two impacts result in a similar diurnal cycle of net LW radiation. The diurnal cycle of the surface net radiative flux is dominated by the diurnal cycle of the net SW radiative flux, however overnight values are equal to the net LW radiative flux (Figure 3.15c). The large daytime net SW radiative flux in the wet season is somewhat balanced out by a larger net LW radiative flux in the wet season, to lessen the deviation between the two seasons.

3.5 Summary

Due to contrasting aerosol and thermodynamic conditions throughout the year, the Amazon Rainforest is an ideal location for observational studies on the radiation budget. A two year deployment of the AMF is providing valuable data that can be used to increase our understanding of the interaction between clouds, aerosols, and the radiation budget. Observations from the first year of this GOAmazon deployment have been presented in conjunction with TOA measurements of the radiative fluxes and cloud fraction from CERES. While rain falls in the area year round, a seasonal cycle in atmospheric moisture is seen, especially in the middle and upper troposphere. Moist surface maritime air is advected into the bottom layers of the atmosphere of Amazon Rainforest throughout the year. The wet season also sees rising surface air into the upper troposphere, acting as a moisture source. As the Hadley cell and ITCZ shift north for the Northern Hemisphere summer, middle and upper level air in the Amazon no longer originates near the surface,

but rather at the same height, lacking the moisture source of the ocean. Drying occurs throughout the entire column but is most pronounced above 4 km. Although this drying is present, the annual spread in mixing ratio only spanned 1 g kg^{-1}. There were also minimal changes in temperature, aside from a spike in August, likely related to increase SW absorption by biomass burning aerosols. Though it is hard to know for sure without observations of the surface heat fluxes, it can be suggested that an increase in the sensible heat flux and decrease in the latent heat flux contribute to the small increase in temperature in the dry season due to the small decrease in surface moisture. Winds were primarily from the north-northeast with a slight westward component in June and July when the river breeze begins to set up.

Integrated water vapor was roughly constant throughout the wet season and gradually decreased in the dry season. Liquid water path was a bit more variable but the pattern of an increase in the wet season and decrease in the dry season was present. The annual peak in cloud fraction was observed in February, while the minimum occurred in September. Although the annual peaks of integrated water vapor, liquid water path, cloud fraction, and precipitation differ, all of these variables show the same seasonal cycle.

The abundance of clouds and water vapor in the Amazon have a significant impact on both the SW and LW parts of the radiation budget, though aerosol concentrations must be considered as well. There are very small changes in the net surface radiation budget throughout the year however a small decrease in the mid-day net SW radiative flux and small increase in the mid-day net LW radiative flux occur in the second half of the dry season. These changes in the surface budget are matched by an increase in the mid-day outgoing LW radiative flux at the TOA and a decrease in the mid-day outgoing SW

radiative flux at the TOA. Additional clouds and water vapor in the wet season reflect SW radiation, preventing it from reaching the surface, as well as absorb LW radiation and reemit it back toward the surface. This same feature in the radiation budget occurs in the Sahel (Chapter 2; Miller et al., 2012). The small increase in mid-day reflected SW radiation and decrease in mid-day SW RFD observed in August coincide with the annual maximum daytime CCN concentration. It can be suggested that the larger concentration of CCN results in a larger amount of smaller cloud droplets, increasing the reflectivity of cloud (Twomey, 1977).

CHAPTER 4: Modeling the Radiation Budget with RRTM

4.1 Simulation of the SW Radiation Budget in Niamey Niger

Measurements of radiative fluxes at the TOA and surface enable us to measure the amount of heating or cooling within the atmospheric column. One downfall is that we do not know where within the column this heating or cooling is occurring. Using a simulation of the radiation budget with RRTM enables us to estimate the heating or cooling within each layer of the column based on its structure. There are multiple factors within the atmosphere that can impact heating or cooling and it is important to include all of these aspects in order to simulate the radiation budget correctly. A model also has the advantage of separating these factors to determine their individual effects as well as how they interact with one another. Unfortunately, measurements of aerosols, especially aerosol optical depth, are difficult or impossible to make when clouds are present. This is not a major issue during the dry season in Niamey, Niger, but can hinder measurements for a diurnal study in the wet season since there are not observations for each hour of each day. As a result the monthly average aerosol optical depth and Ångstrom exponent had to be used to represent the aerosols in RRTM.

Results validating this method can be found in Figure 4.1, which shows the diurnal cycle of the month average simulated cross atmosphere SW RFD for August 2006 in Niamey, Niger, compared to the observations. RRTM underestimates the SW RFD under clear skies and when only clouds or aerosols are included. However, when the monthly average aerosol properties are inserted along with hour averaged cloud properties throughout the month, RRTM does a credible job simulating the cross atmosphere SW RFD. This indicates that the cross atmosphere RFD is influenced by the interaction

between clouds and aerosols and not an effect from aerosols plus an effect from clouds. This is also further evidence that aerosols are an important factor in the wet season despite the increase in wet deposition.

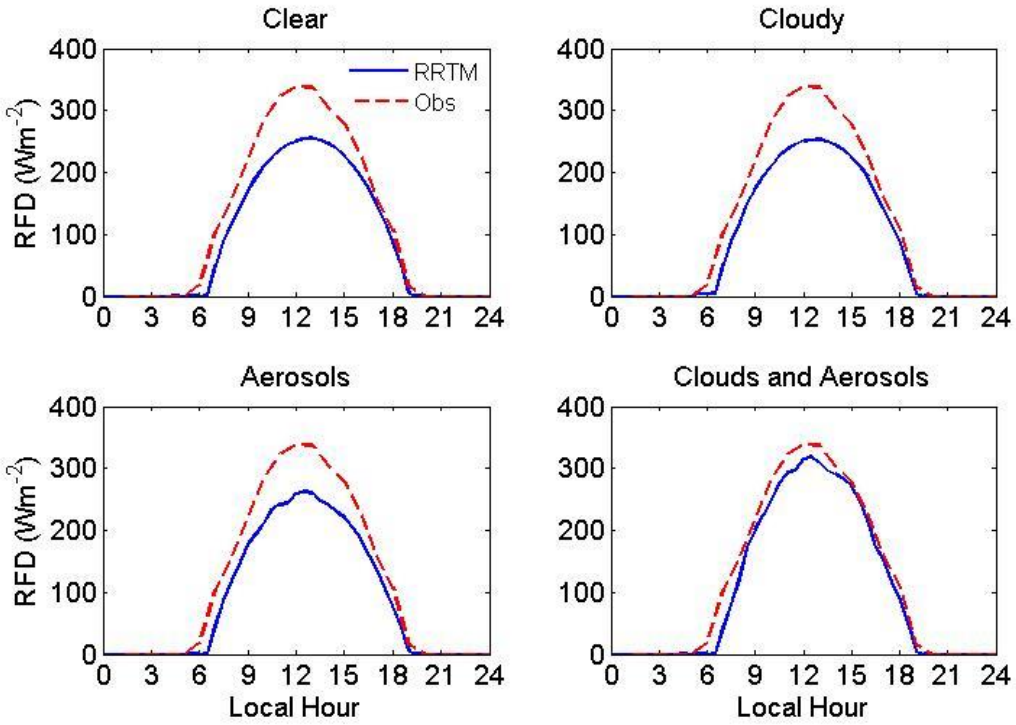

Figure 4.1: Monthly average RRTM calculated and observed SW cross atmosphere radiative flux divergences for August 2006 with (a) clear sky, (b) cloudy sky (c) aerosols present, (d) clouds and aerosols present.

To further analyze the interaction between clouds and aerosols with the radiation budget, heating profiles of the aerosol only, cloud only, and all sky scenarios were computed. By subtracting the aerosol only scenario or the cloud only scenario from the all sky scenario it is possible to see the impact clouds or aerosols have individually on the all sky heating profile (Figure 4.2). While heating occurs throughout the entire column there are two main layers of heating: near the surface due to aerosols and between 300 and 600 mb due to clouds. Cirrus clouds are often present around 12 km (Figure 2.6) while aerosols

are primarily in the bottom 1 km (McFarlane et al., 2009). Heating is largest around noon due to the diurnal cycle of solar insolation. A field of cirrus clouds allows solar insolation to pass through and reach the aerosol layer where a photon has a second chance to be scattered before reaching the surface. Some of this scattered radiation is directed back in the upward direction where it can then be absorbed or scatted by a cloud. As a result, aerosols result in heating near the surface and heating within the cloud layer (Figure 4.2a). In contrast, the effect of clouds on the all sky radiation budget can only be seen in the bottom of the cloud layer. Although aerosols are primarily located in the bottom 1 km, there are also aerosols present aloft that have the potential to allow for more absorption in the cloud layer.

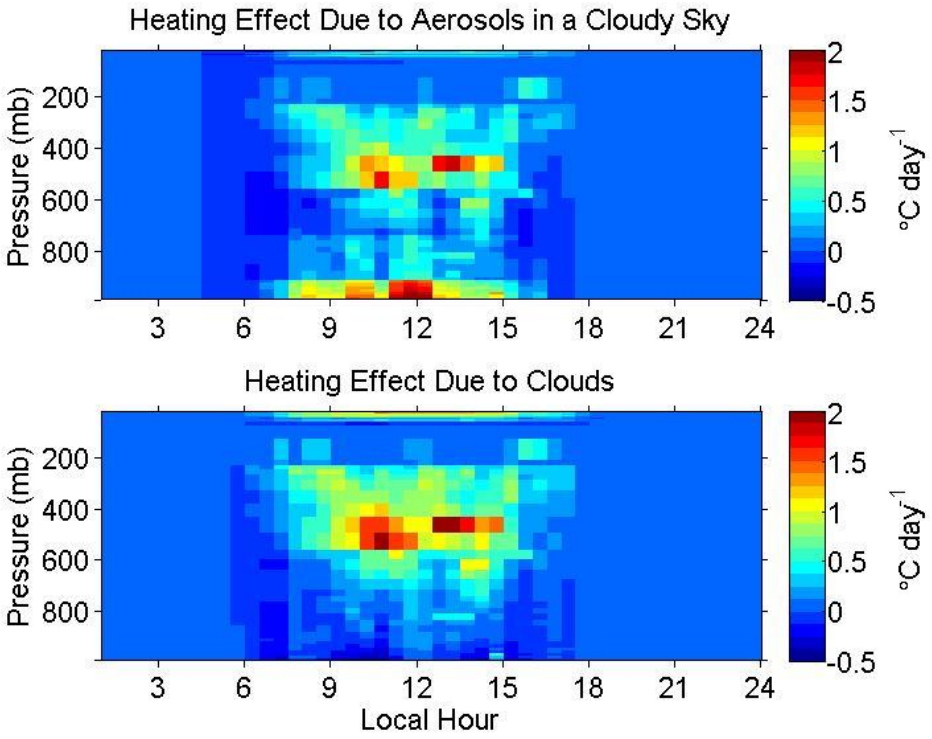

Figure 4.2: (a) Diurnal heating rate profile with clouds and aerosols minus the heating rate profile with clouds, (b) Diurnal heating rate profile with clouds and aerosols minus the heating rate profile with aerosols.

4.2 The Radiation Budget in a Changing Climate

One of the main questions in climate science is how the climate will change in the future, as a consequence of increasing concentrations of greenhouse gases emitted since the industrial revolution. GCMs are tools used to assess future climate scenarios and to understand processes that may impact the climate. One of the scenarios from CMIP5, deemed a high emission scenario, gradually increases the radiative forcing present in the preindustrial period until it reaches 8.5 W m^{-2} in the year 2100 (RCP8.5; Taylor et al., 2012). But a complication of GCMs is that it is difficult to isolate the effect of changes in radiative forcing on any one aspect of the climate system because there are many interconnected processes.

The likely susceptibility of the Sahel to climate change constitutes an imperative to better understand potential modifications to its sensitive climate as the planet warms. In an effort to determine how the radiation budget would change solely due a projected change in cloud fraction, four different experiments were originally proposed. The underlayment of these experiments was that projected changes in over cloudiness in GCMs could be mapped onto the existing measurements of cloud structure. This method assumes that the same cloud typed will be present in the future, but in differing amounts. The control scenario only used observations while the other three incorporated the total area cloud fraction from the Community Climate System Model 4.0 (CCSM4), Goddard Institute for Space Studies Model E-H (GISS EH), and the Hadley Centre Global Environment Model version 2 (HadGEM). Cloud fraction data from these models are available with a temporal resolution of three hours so RRTM was run every five seconds, the temporal resolution of the cloud radar, for a one hour period before and after the model data point. GCM output

from the last 20 years of the RCP8.5 scenario were used, encompassing the years 2081 through 2100. A 20 year average incorporating the years 1980 through 1999 from the CMIP5 historical scenario for each of the models was subtracted from the RCP8.5 output to determine the projected change in cloud fraction. By subtracting the historical mean from the RCP8.5 simulation any bias within the model is removed. Since only area cloud fraction output was available, the control scenario's layered cloud fraction was modified based on the projected change in three ways: cloud fraction was altered equally at all levels, altered only in the top layer that a cloud was predicted to be present, or only in the bottom layer a cloud was predicted to be present. This experimental design would allow us to assess whether the radiation budget is more sensitive to the location or fraction of a cloud.

The initial goal of projecting the cloud fraction changes from CMIP5 models onto the existing cloud structure proved to be a significant challenge. The first problem lies in the relationship between the cloud fraction in the historical runs of a CMIP5 model and the observations used to dictate the vertical structure of clouds. The experiment was designed such that the projected change in cloud fraction in the RCP8.5 scenario compared to a 20 year mean of the historical scenario would be mapped onto to the cloud fraction observed in 2006 by the cloud radar in Niamey, Niger. Unfortunately, the historical mean cloud fraction proved to be drastically different from the observations used to define the vertical profile of clouds. A comparison of the wet season average area cloud fraction for the CMIP5 models and the 2006 observations is found in Figure 4.3. Both HadGEM and GISS greatly overestimate the cloud fraction and all three models misrepresent the diurnal cycle. None of the models captured the evening minimum in cloud fraction, while CCSM4 and GISS actually have peaks at that time. This presents a substantial difficulty because the

diurnal cycle in the models must be in-phase with that in the observations to avoid phase noise in the calculation but most importantly the magnitudes must be similar. Before the analyzing how the diurnal cycle will change in the future more work is needed to make sure models are able to simulate the current diurnal cycle.

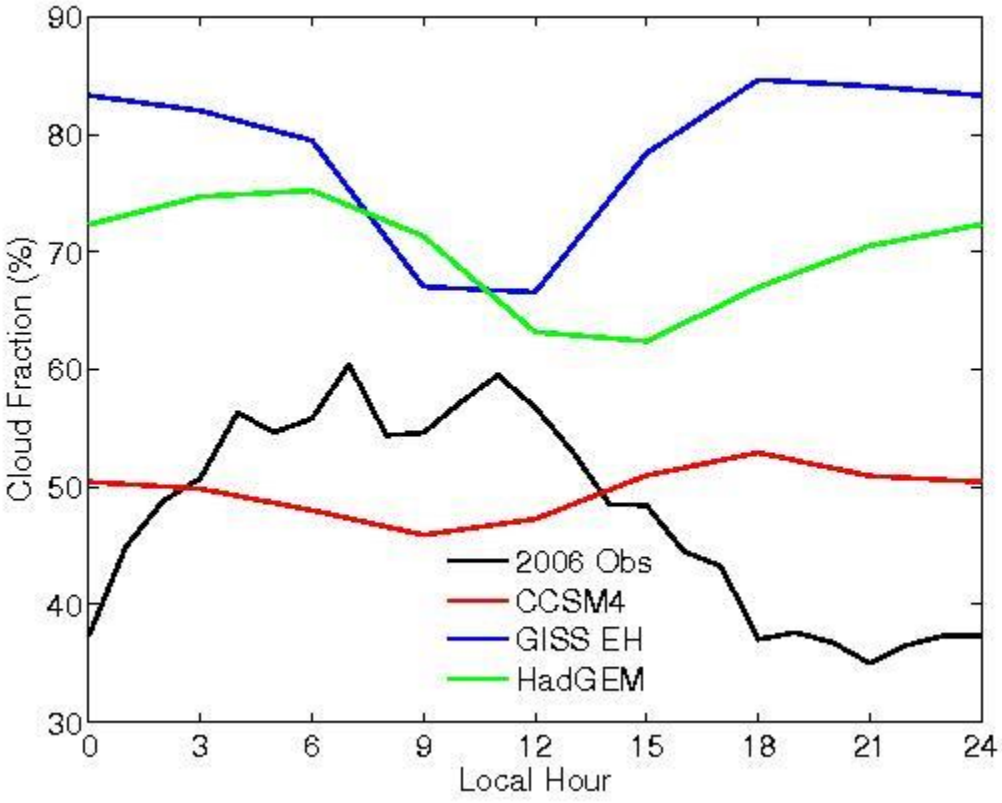

Figure 4.3: The diurnal cycle of the wet season average area cloud fraction from the 2006 observations and the 20 year mean of the historical scenario in CCSM4, GISS EH, and HadGEM.

By definition, cloud fraction is bound to being between 0 and 100% and therefore a decrease in cloud fraction cannot be larger than cloud fraction in the observations. Although the average projected cloud fraction in the selected CMIP5 models were larger than the historical scenario, there were many individual cases where the cloud fraction

decreased more than the total amount of clouds present in the observations, which are subject to radiation transfer calculations. To accommodate this issue, we attempted to place the residual decrease from days where additional clouds could not be physically removed on that day within a different year. But this scenario arose so often that the residual decrease in clouds accumulated in each hour calculation bin over the 20 year period of the study and could not be accounted for. In other words, the books couldn't be balanced over specific days and hours. By applying the additional decrease in clouds to a different day within the year, the average vertical structure of clouds was changed. Another proposed solution to this problem was to multiply the ratio of the observed cloud fraction to the mean historical cloud fraction by a normalization factor. Unfortunately, a control run would then be needed for each projected scenario run. At the present time the normalization factor is unknown, and work is ongoing on this subject as discussed in the future work section.

A further concern with the proposed experiment was the definition of the thickness of a vertical layer with RRTM. This is also a common problem in GCMs. When a cloud is inserted in a layer within RRTM it is assumed that the cloud thickness is equal to the layer thickness. In many cases, as in this one, layers closer to the surface are given a higher vertical resolution. It became apparent that the thickness of the layer became more important than the increase in cloud fraction or the microphysical properties of the cloud. For example, a thick layer of cirrus clouds became more radiatively important than a thin low level cloud. This contradicts previous work in cloud radiative forcing that shows cirrus clouds alloW more solar insolation to pass through the layer while lower level clouds tend to absorb and scatter more solar insolation. As a result, cloud optical depth must be conserved between scenarios and not the microphysical properties of the cloud. This

requires further assumption within the future projection in cloudiness and whether the optical thickness should represent a thick cirrus cloud or a thin low level cloud. These experiments exposed the sensitivity of this method to the complexity of the observed cloud filed relative to the simplicity of the simulated cloud field. It also exposed the large uncertainties that would accompany the forward cloud-radiation projections regardless of the method used to "adjust" the existing cloud structure. For the reasons, these experiments remain a work in progress.

CHAPTER 5: Summary and Conclusions

5.1 Comparison of the Sahel Region of West Africa and the Amazon Rainforest of Brazil

The Amazon Rainforest of Brazil and the Sahel region of West Africa are both tropical regions that experience a wet and dry season. However, the Sahel oscillates between desert-like and tropical water vapor loading while the Amazon always has an abundant supply of water vapor. A common link between the two regions is the dependence on the position of the ITCZ as a source of lift and moisture advection during the wet season. The advection of water vapor into each region during their respective wet seasons requires different processes. The climate in the Sahel is controlled by the phase of the WAM and relies on the advection of water vapor from the tropical Atlantic by southwesterly monsoonal winds following a complete 180° shift in the wind direction. Moisture is advected into a shallow layer near the surface beneath the Saharan Air Layer. The ITCZ provides a source of lift and aids in convection and the production of clouds and precipitation. In contrast to the Sahel, the direction of the horizontal wind is relatively constant throughout the year in the Amazon Rainforest. During the wet season the upward branch of the Hadley cell and the ITCZ are centered upon the region and transport moist surface air into the middle atmosphere. Drier air is advected into the middle and upper level of the troposphere during the dry season, while the surface air remains quite moist. These synoptic background flows allow precipitation to occur in the Amazon's dry season, but not during the Sahel's dry season.

Another similarity between the two regions is the change in diurnal cloud structure between the wet and dry season. Deep convection occurs in the wet season in both locations, peaking in the morning in the Sahel and afternoon in the Amazon. Some residual

cirrus clouds remain in both locations as the convection subsides in both regions. The dry season in both regions is characterized by the presence of cirrus clouds. These upper level clouds reach maximum coverage in the afternoon over the central Sahel but in the evening in the Amazon Rainforest. Thus, there is a phase lag between the maximum coverage of cirrus and the peak rainfall with deep convection preceding the cirrus maximum by a few hours. The timing of the maximum cloud fraction gives more of a marine-type feel to the wet season in the Sahel while, in contrast, the Amazon is more typical of a continental region.

Many aspects of the radiation budget in the Sahel region West Africa and the Amazon Rainforest are similar, but there are important differences. In both locations competing effects in the LW and SW parts of the spectrum balance yielding a RFD that does not change much throughout the year. Clouds reflect SW radiation and prevent it from reaching the surface, which decreases the RFD, while water vapor absorbs LW radiation, increasing the RFD. The balance between these two effects differs in implementation between the two regions. The large loading of water vapor in the Amazon Rainforest dominates the LW radiation budget and results in a very small net surface LW flux in the wet season that is nearly half of that observed in the Sahel and observed in the global annual average (Trenberth et al., 2009). The SW radiation budget is controlled by a mixture of clouds, aerosols, and solar insolation. In the Sahel, there is little change in aerosol optical depth throughout the year and therefore aerosols have a minimal impact on the seasonal variation in the SW RFD. More clouds are present in the Amazon than the Sahel which results in a more negative surface net SW flux in the Amazon for most of the year. An exception to this rule is seen in August and September when the two locations have nearly

identical net surface SW fluxes. This equality occurs when the Amazon has its annual minimum in cloud fraction, placing it more in line with the cloud fraction over the Sahel. Also worth noting is that the surface of the Sahel greens up during these months and its surface albedo is more consistent with that over the Amazon Rainforest. The difference in the surface SW budget is offset by a much larger amount of SW radiation leaving the TOA in the Amazon.

Estimates of the RFDs and the CREs have been attempted in the past using a combination of measurements and models, but discrepancies between radiation transfer models and observations are not uncommon (see McFarlane et al. 2008 for an excellent review). A recent study explored the potential sources of these model-observation discrepancies and concluded that proper averaging of surface data was a potential source of uncertainty in satellite-surface measurements of CRE over the Tropical Western Pacific and, presumably beyond (Parding et al. 2011). That study recommended that averaging times used to compute CRE be no less than 3-hours to diminish resolution-induced random errors, and we have heeded this advice in the present study. Another compelling reason to average the data over 3-hours is that the broadband TOA measurements used from GERB, like any satellite broadband radiation measurement, are subject to random error due to radiance-to-flux conversion (Clerbeaux et al, 2008a,b; Loeb et al, 2011).

Further uncertainty in the CRE in the Sahel arises when comparing observations from GERB with those from CERES polar orbiter observations and the CERES geostationary product (CERES Geo), which temporally interpolates in between CERES observations using narrow-band radiation measurements to provide an all sky and clear sky data point every three hours at the TOA. Monthly average TOA CRE in the Sahel as

calculated by Miller et al. (2012) using GERB is shown in comparison to CERES observations in Figure 5.1. Little difference between the observational techniques are seen in the dry season, however there are discrepancies in the wet season. A monthly average calculation of TOA SW CRE using only the observations made when CERES is overhead of the region significantly overestimates the wet season SW CRE at the TOA, especially in August. CERES passes overhead the Sahel in the late morning hours, coinciding with the diurnal maximum cloud fraction. In addition, values of solar insolation are larger at this time than in the early morning or late afternoon hours, further increasing the overestimation of CRE. The impacts of the exceptionally large TOA SW CRE observed by CERES can also be seen with a small overestimation of the wet season TOA SW CRE in CERES Geo.

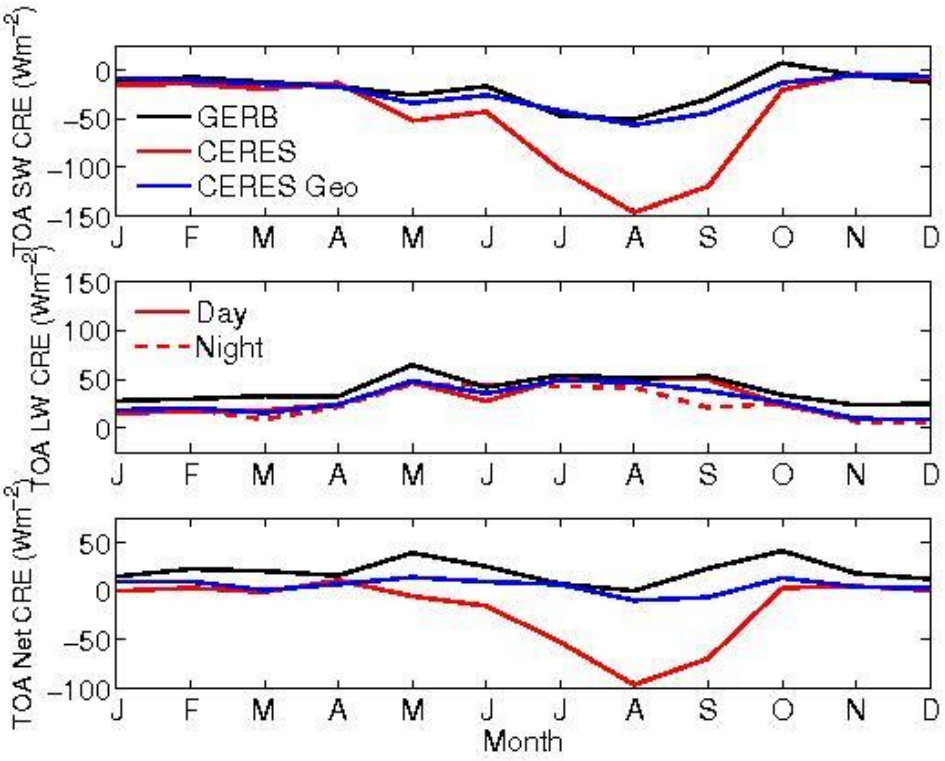

Figure 5.1: Monthly average TOA SW (a), LW (b), and net (c) CRE in Niamey, Niger during 2006 calculated using observations from GERB, CERES, and CERES Geo.

Through the year there is also a small underestimation of the TOA LW CRE by CERES when compared to GERB. CERES does a more reasonable job with the TOA LW CRE since the LW radiation budget does not vary as much through the course of the day as the SW radiation budget. Significant differences are also present in the TOA net CRE year round. The large cooling seen in the TOA SW CRE decreases the warming seen in the TOA net CRE, sometimes resulting in a net cooling. When only looking at the instantaneous observations from CERES a significant net cooling is seen at the TOA, which is not the reality. The instantaneous CERES observations can therefore not be used to calculate the RFD or CRE. The resulting influences of the instantaneous CERES observations on CERES Geo and the added uncertainty of converting narrowband radiance measurements to broadband make GERB a much more suitable source for observations of RFD and CRE.

Further differences in the technique used to calculate the atmospheric CRE can be seen in Figure 5.2. A one hour time period was used to calculate the clear sky fluxes in Miller et al. (2012), while a three hour time period was used in this study as recommended by Parding et al. (2011). The two techniques agree quite well in the calculation of the SW atmospheric CRE in the Sahel during the months of May, June, and July. During the other months of the year, a slightly smaller SW atmospheric CRE is seen when a three hour average is used. The different techniques result in different surface downwelling SW fluxes, and therefore different values for the clear sky surface upwelling and downwelling SW fluxes. The differences in the LW atmospheric CRE between the two averaging techniques are smaller (Figure 5.2b and c). But the comparison nonetheless shows that the calculation of CRE from a combination of satellite and surface observations is sensitive to

the averaging period, particularly in the SW, and again reinforces the fallacy of computing CRE from instantaneous polar orbiter snapshots.

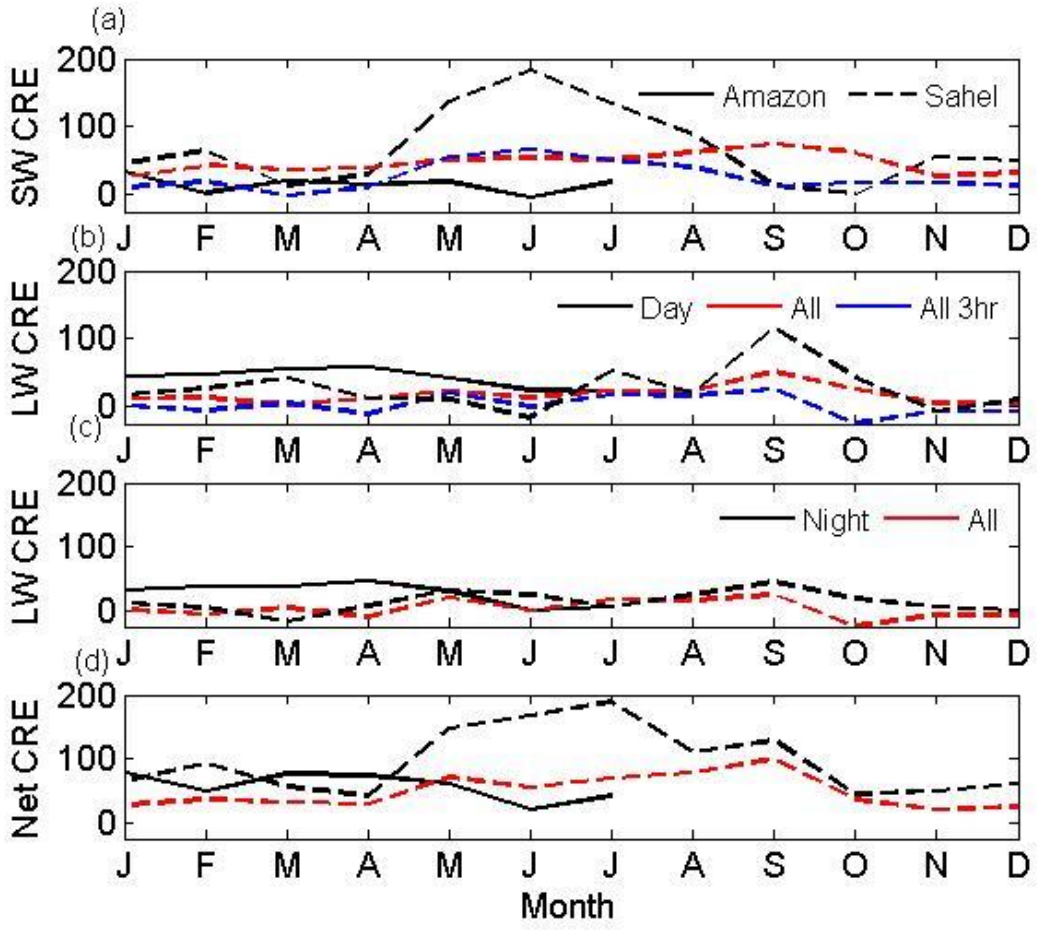

Figure 5.2: Month average SW (a), LW (b&c), and net (c) atmospheric CRE in W m^{-2} for the Amazon (solid line) and Sahel (dashed line) calculated for the CERES day or nighttime observation (black), a 1 hour average for determining clear sky fluxes using GERB (red), and a 1 hour average for determining clear sky fluxes using GERB (blue).

Regardless of the region, clouds result in cooling at the boundaries of the atmospheric column. The largest CRE in both the Sahel and the Amazon is at the surface in the SW spectrum. Wet season SW CRE can reach -140 W m^{-2} in the Sahel and be roughly double this amount in the Amazon. In contrast, the CRE at the TOA and in the LW is much

smaller in both regions. Although the LW CRE at the surface does not change with time of year or time or day in the Amazon, a diurnal and seasonal cycle in the LW CRE is present in the Sahel due to its large water vapor variability. Another difference in the CRE between the two locations is the role of SW and LW radiation in the net warming of the column. The majority of the warming in the column in the Sahel occurs in the SW, while in the Amazon it occurs in the LW (Figure 5.2). Furthermore, the LW CRE in the wet season of the Sahel is similar in magnitude to the dry season LW CRE in the Amazon (Figure 5.2b and c), though it should be noted that observational techniques used to compute CRE differ between the Amazon and Sahel. Though we do not expect the differing techniques to produce unreasonable uncertainty in our calculations, some uncertainty in these comparisons is inevitable.

Interpreting the results presented herein in the context of past studies of atmospheric CRE is difficult due to differences in methodology and location, but the current study suggests that when clouds are present in these tropical regions there is an increase in the average radiative heating by a few percent, which is somewhat consistent with the results of McFarlane et al. (2008). At the TOA, the wet season net CRE in the Sahel appears to be negligible on average, which is different than the significant periods of positive and negative CRE seen in the Amazon and during the summer season of the Indian monsoon (Thampi and Roca, 2014). This is likely due to less overall cloud coverage observed in the Sahel compared to other regions. On the other hand, competing impacts of the SW CRE and LW CRE at the TOA have also been noted by Berry and Mace (2014) using data from the Asian summer monsoon. At the surface, the diurnal cycle of the SW, LW, and net CRE in the Sahel is much smaller in magnitude than that observed during the

wet season of the Australian monsoon, and compliments the magnitude of the surface CRE during their monsoonal break periods, but not the variability in surface CRE (May et al., 2012). But the average value of surface SW CRE that is seen during the wet season of the Australian monsoon is similar to what is observed in the Amazon.

One aspect of the current study that makes it unique is the nearly complete reliance upon observations to measure CRE. An approach often taken in past studies is to compute the CRE on the basis of the difference between observed all-sky and computed clear-sky radiation. This approach may be perfectly acceptable (even preferable) to the approach taken here when it is applied in other locations, but would add considerable uncertainty in the Sahel and Amazon regions due to the heavy aerosol burden and ubiquitous thin cirrus. Attempts to define clear sky over the Sahel can best be defined as highly uncertain. Toward this end, we believe that it may be best to define the CRE in tropical areas as being the difference between atmospheric columns with minimal cloudiness and those with maximum cloudiness rather than using the term clear sky, which over the Sahel would be considered extremely rare if not non-existent due to the large, omnipresent aerosol burden. To observe CRE over the Sahel relies upon having a geostationary satellite overhead to measure the TOA radiative fluxes.

5.2 Answers to the Science Questions

1. What role does water vapor play in modulating the diurnal cycle of the radiation budget during the wet season over the West African Sahel?

There is no observable diurnal impact of additional water vapor present over the Sahel during the wet season. Furthermore, the overall radiative heating of the column itself

appears relatively constant through the year despite changing distributions of the individual components of the budget.

2. What influences the diurnal radiation budget at the TOA, surface, and within the atmospheric column over the West African Sahel and the monthly average radiation budget in the Amazon Rainforest of Brazil?

Clouds and the annual cycle of solar insolation control the *diurnal cycle* of the radiation budget at the surface, TOA, and within the column in the Sahel region of West Africa. The seasonal cycle of the radiation budget in the Amazon Rainforest of Brazil is also controlled by clouds and the annual cycle of solar insolation, however there are also impacts from column integrated water vapor and more variable aerosol loads in the Amazon Rainforest that are not observed in the diurnal cycle of the radiation budget in the Sahel.

3. How does the CRE compare in the West African Sahel region and Amazon Rainforest of Brazil?

Clouds have a warming effect on the atmospheric column in both the Sahel and the Amazon. The majority of this warming occurs in the LW in the Amazon and in the SW in the Sahel. Cooling in the SW is observed at the surface in both regions, however the impact during the wet season is nearly double in the Amazon compared to the Sahel due to much larger cloud coverage. The cloud radiative effect at the TOA is minimal in the Sahel, but there is considerable cooling at the TOA in the Amazon.

4. How will the radiation budget in the West African Sahel region respond to projected changes in climate, such as an increase or decrease in cloud fraction and thickness?

Evaluation of the radiation budget in a changing climate is ongoing and the role of a projected change in cloud fraction on the radiation budget is yet to be determined.

5.3 Future Work

This work may be expanded in future observational and modeling studies in both the Sahel region of West Africa and Amazon Rainforest of Brazil. Improved understanding of the CRE may also be gained through the observation of the diurnal cycle of RFD and CRE in other regions. Since rainfall varies in the Sahel on a year to year basis, it is difficult to quantify the extent to which the results presented here are representative of the overall climate in Niamey. The controlling factors in years with a failed monsoon remain a mystery, but an accurate forecast of the wet monsoon season will have numerous socioeconomic benefits. Additional data from a future AMF deployment in Niamey, Niger will allow us to add to our knowledge. Data are needed from a year where the monsoon is weak or fails so that it is possible to determine how the clouds and radiation budget are different. Additional data will also help quantify the impact of aerosols on the radiation budget and aerosol-cloud-climate interactions. This is particularly true in light of the fact that ARM has gained new equipment that significantly enhances its aerosol measurement capability. Alas, a second deployment in this region must await the resolution of geopolitical turmoil, which is perhaps the most significant impediment to further progress in understanding the climate of this sensitive region.

Additional modeling studies are also needed for the Sahel region. CMIP5 models have a demonstrably difficult time reproducing the diurnal cycle and magnitude of area cloud fraction. Although disk space is a necessity, it is imperative that large modeling groups save model output at a greater temporal resolution to allow for more detailed diurnal

cycle studies. Such studies have the greatest potential to improve parameterizations and radiation representations in the model. These detailed data will then allow for less complicated procedures in studying the role of projected changes in cloud coverage on the diurnal cycle of the radiation budget. A present option is to determine a normalization factor that can be used to adjust the historical mean cloud fraction for each year to the observations in the year being used as the control scenario. If such a normalization factor can be determined, projected changes in cloud fraction can be placed into RRTM and its role on the diurnal cycle of the radiation budget estimated. This process can then be repeated for the Amazon Rainforest.

Another desirable expansion of this study using RRTM involves future projections of the concentration of carbon dioxide in the Amazon Rainforest. It has been shown that the column is so heavily laden with water vapor, especially in the wet season, that the IR window is effectively closed. The downwelling component of the surface LW radiative flux is quite large due to the absorption by water vapor molecules. Since carbon dioxide also absorbs LW radiation it would be interesting to examine whether the presence of additional carbon dioxide would actually change the LW radiation budget in a meaningful way. In the event the infrared window is closed, as we postulate, and the increasing concentration of carbon dioxide has a negligible effect on the local radiation budget, an experiment could be designed to test how much the concentration of water vapor within the column would need to decrease before carbon dioxide becomes an important factor.

Surface observations are still being made by AMF1 in Manacapuru, Brazil and are expected to continue until December 2015. Another year of data will then be available for analysis. It was unfortunate that the GERB instrument on the newest Meteosat failed.

However, the legacy GERB instrument is still collecting data that due to budget issues remains unprocessed and therefore has not been released. In the meantime CERES provides an alternative for TOA radiative flux observations and has the benefit of sampling a larger percentage of the globe. Even with the development of geostationary enhanced product with a temporal resolution of 3 hours, this study suggest that CERES is not compatible with a diurnal cycle study. A single daytime measurement is made of reflected SW radiation with the rest of the day dependent on modeled radiation. Because the CRE has a diurnal cycle that is modulated by the diurnal cycle of cloud coverage and solar insolation, the two quantities must be considered as convoluted. As a result of this convolution, a single observation is unable to characterize the diurnal cycle of CRE, and as such, unable to determine its true role in the regional radiation budget. Accordingly, it is highly recommend that the United States' government agencies work together to place a broadband radiometer on their next geostationary satellite. With multiple permanent surface based radiation measurement cites owned by the Department of Energy, such a geostationary satellite broadband measurement system would allow the diurnal cycle of RFD and CRE to be resolved in more regions and enable studies over more climatologically meaningful periods.

APPENDIX 1: List of Acronyms

AEJ	African Easterly Jet
AMF	Atmospheric Radiation Measurement Program's Mobile Facility
AOD	Aerosol Optical Depth
ARSCL	Active Remotely-Sensed Cloud Locations
CCN	Cloud Condensation Nuclei
CCSM4	Community Climate System Model 4.0
CERES	Clouds and the Earth's Radiant Energy System
CERES Geo	CERES Geostationary Product
CMIP	Coupled Model Intercomparison Project
CRE	Cloud Radiative Effect
CRF	Cloud Radiative Forcing
ENSO	El Niño Southern Oscillation
GCM	General Circulation Model
GERB	Geostationary Earth Radiation Budget Instrument
GISS EH	Goddard Institute for Space Studies Model E-H
GoAmazon	Green Ocean Amazon
HadGEM	Hadley Centre Global Environment Model version 2
HYSPLIT	Hybrid Single Particle Lagrangian Integrated Trajectory Model
ITCZ	Intertropical Convergence Zone
ITF	Intertropical Front
LCL	Lifting Condensation Level
LW	Longwave
LWP	Liquid Water Path
MCC	Mesoscale Convective Complex
MPL	Micropulse Lidar
MWRP	Microwave Radiometer Profiler
NAO	North Atlantic Oscillation
NCEP	National Centers for Environmental Prediction
RFD	Radiative Flux Divergence
RRTM	Rapid Radiative Transfer Model
SAL	Saharan Air Layer
SEVIRI	Spinning Enhanced Visible and Infrared Imager
SW	Shortwave
TOA	Top of the Atmosphere
WAM	West African Monsoon

REFERENCES

Abdou, K., D. J. Parker., B. Brooks, N. Kalthoff, and T. Lebel, 2010: The diurnal cycle of lower boundary-layer wind in the West African monsoon. *Quart. J. Roy. Meteorol. Soc*., **136**, 66–76, doi:10.1002/qj.536.

Berry, E., and G. G. Mace, 2014: Cloud properties and radiative effects of the Asian summer monsoon derived from A-Train data, *J. Geophys. Res*.., **119**, 9492–9508, doi:10.1002/2014JD021458.

Bock, O. et al., 2008: The West African Monsoon observed with ground-based GPS receivers during AMMA, *J. Geophys. Res*., **113**, D21105, doi: 10.1029/2008JD010327.

Bolton, David, 1980: The Computation of Equivalent Potential Temperature. *Mon. Wea. Rev*., **108**,1046–1053, doi: http://dx.doi.org/10.1175/1520-0493(1980)108<1046: TCOEPT> 2.0.CO;2.

Bouniol, Dominique et al., 2012: Diurnal and season cycles of cloud occurrences, types, and radiative impact over West Africa. *Journal of Applied Meteorology and Climatology*, **51**, 534-553, doi: 10.1175/JAMC-D-11-051.1.

Cauduro Dias de Paiva, Eloiza M., Robin T. Clarke, 1995: Time trends in tainfall records in Amazonia. Bull. Amer. Meteor. Soc., 76, 2203–2209.

Cess, R. D., et al., 1995: Absorption of solar radiation by clouds: Observation versus models, *Science,* **267**, 496-499.

Chu, Pao-Shin, Zhi-Ping Yu, Stefan Hastenrath, 1994: Detecting climate change concurrent with deforestation in the Amazon Basin: Which way has it gone?. *Bull. Amer. Meteor. Soc*., **75**, 579–583.

Clerbaux, N., et al., 2008: Unfiltering of the Geostationary Earth Radiation Budget (GERB) Data. Part I: Shortwave Radiation. *J. Atmos. Oceanic Technol*., **25**, 1087–1105.

Clothiaux, E.E. et al., 2001: The ARM millimeter wave cloud radars (MMCRs) and the active remote sensing of clouds (ARSCL) value added product (VAP). *DOE Tech. Memo*., ARM VAP-002.1.

Collow, A. M., V. P. Ghate, M. A. Miller, and L.Trabachino, 2015: A one-year study of the diurnal Cycle of meteorology, clouds, and radiation in the West African Sahel region. *Q.J.R. Meteorol. Soc*., submitted.

Coulter, R., 2012a: Radar wind profiler and RASS handbook, ARM Climate Research Facility, DOE/SC-ARM/TR-044.

Coulter, R., 2012b: Micropulse lidar (MPL) handbook, ARM Climate Research Facility, DOE/SC-ARM/TR-019.

Culf, A. D., G. Fisch, J. Lean, and J. Polcher, 1998: A comparison of Amazonian climate data with general circulation model simulations. J. Climate, 11, 2764-2773.

D'Almeida, C., Vörösmarty, C. J., Hurtt, G. C., Marengo, J. A., Dingman, S. L. and Keim, B. D., 2007: The effects of deforestation on the hydrological cycle in Amazonia: a review on scale and resolution. Int. J. Climatol., 27, 633–647, doi: 10.1002/joc.1475.

Del Genio, A. and M.S. Yao, 1988: Sensitivity of a global climate model to the specification of convective updraft and downdraft mass fluxes. *J. Atmos. Sci*., **45**: 2641-2668.

Dewitte, S., N. Clerbaux, L. Gonzalez, A. Hermans, A. Ipe, A. Joukoff, and G. Sadowski, 2000: Generation of GERB unfiltered radiances and fluxes. In Proc. 2000 EUMETSAT Meteorological Satellite Data Users' Conf, 29-72.

Dias, M. S., P.S. Dias, M. Longo, D.R Fitzjarrald, & A.S. Denning, 2004: River breeze circulation in eastern Amazonia: observations and modelling results. *Theoretical and Applied Climatology*, **78**, 111-121.

Doelling, D.R. et al., 2013: Geostationary Enhanced Temporal Interpolation for CERES Flux Products. *J. Atmos. Oceanic Technol*., **30**, 1072–1090, doi: http://dx.doi.org/10.1175/JTECH-D-12-00136.1.

Draxler, R.R.,and G.D. Hess, 1997, Description of the Hysplit_4 modeling system, *NOAA Technical Memorandum ERL ARL-224*, December, 24p.

Dunn, M., K. Johnson, and M. Jensen, 2011: The microbase value-added product: A baseline retrieval of cloud microphysical properties. ARM Climate Research Facility, DOE/SC-ARM/TR-095.

Eck, T. F., B. N. Holben, I. Slutsker, and A. Setzer, 1998: Measurements of irradiance attenuation and estimation of aerosol single scattering albedo for biomass burning aerosols in Amazonia, J. Geophys. Res., 103, 31865–31878, doi:10.1029/98JD00399.

Giambelluca, T. W., et al., 1997: Observations of Albedo and Radiation Balance over Postforest Land Surfaces in the Eastern Amazon Basin. *J. Climate*, **10**, 919–928. doi: http://dx.doi.org/10.1175/1520-0442(1997)010<0919:OOAARB>2.0.CO;2.

Gounou, A., F. Guichard and F. Couvreux, 2012: Observations of diurnal cycles over a West African meridional transect: Pre-monsoon and full-monsoon seasons. *Boundary-Layer Meteorol*., **144**, 329-357. doi: 10.1007/s10546-012-9723-8.

Guichard, F. et al., 2009: Surface thermodynamics and radiative budget in the Sahelian Gourma: Seasonal and diurnal cycles, *Journal of Hydrology*, **375**, 161-177.

Hahmann, Andrea N., Robert E. Dickinson, 1997: RCCM2–BATS Model over Tropical South America: Applications to Tropical Deforestation. J. Climate, 10, 1944–1964.

Harries, J.E et al., 2005: The Geostationary Earth Radiation Budget Project, *Bull. Amer. Meteor. Soc*., 86, 945-960, doi:10.1175/BAMS-86-7-945.

Hengsdijk, H. and H. van Keulen, 2002: The effect of temporal variation on inputs and outputs of future-oriented land use systems in West Africa. *Agriculture, Ecosystems & Environment*, **9**, 245-259.

IPCC, 2013: Summary for Policymakers. In: Climate Change 2013: The Physical Science Basis. Contribution of Working Group I to the Fifth Assessment Report of the Intergovernmental Panel on Climate Change [Stocker, T.F., D. Qin, G.-K. Plattner, M. Tignor, S.K. Allen, J. Boschung, A. Nauels, Y. Xia, V. Bex and P.M. Midgley (eds.)]. Cambridge University Press, Cambridge, United Kingdom and New York, NY, USA

Joly M. and A. Voldoire, 2009: Influence of ENSO on the West African monsoon: temporal aspects and atmospheric processes, *J. of Climate*, **22**, 3193-3210, doi:10.1175/2008JCLI2450.1.

Kalapureddy, M. C. R., M. Lothon, B. Campistron, F. Lohou, and F. Saïd, 2010: Wind profiler analysis of the African Easterly Jet in relation with the boundary layer and the Saharan heat-low. *Q.J.R. Meteorol. Soc*., **137**, 77-91, doi: 10.1002/qj.494.

Kandji, S., L. Verchot, and J. Mackensen, 2006: Climate change and variability in the Sahel region: Impacts and adaptation strategies in the agricultural sector. U.N. Environmental Programme and World Agroforestry Centre Tech. Rep., 48 pp.

Kim, K., W.K.-M. Lau, Y.C. Sud, and G.K. Walker, 2010: Influence of aerosol-radiative forcings on the diurnal and seasonal cycles of rainfall over West Africa and Eastern Atlantic Ocean using GCM simulations. *Climate Dynamics*, **35**, 115-126, doi:10.1007/s00382-010-0750-1.

Koch, G. W., J. S. Amthor, and M. L. Goulden, 1994: Diurnal patterns of leaf photosynthesis, conductance and water potential at the top of a lowland rain forest canopy in Cameroon: measurements from the Radeau des Cimes, *Tree Physiology*, **14**, 347-360.

Kollias, P., M.A. Miller, K.L. Johnson, M.P. Jensen, and D.T. Troyan, 2009: Cloud, thermodynamic, and precipitation observations in West Africa during 2006. *J. Geophys. Res*., **114**, D00E08, doi:10.1029/2008JD010641.

Koster, R.D. and coauthors. 2005: GLACE: The global land-atmosphere coupling experiment. Part I: overview, *J. Hydrometeorology*., **7**, 590-610.

Laing, A.G., J. M. Fritsch, 1993: Mesoscale convective complexes in Africa. *Mon. Weather Rev*., **121**, 2254 – 2263.

Le Barbé, L.,T. Lebel, and D. Tapsoba, 2002: Rainfall variability in West Africa during the years 1950-90. *J. Climate*, **15**, 187-202.

Lebel, T. and A. Ali, 2009: Recent trends in the Central and Western Sahel rainfall regime (1990-2007), *Journal of Hydrology*, **375**, 52-64.

Lélé, I. and P. Lamb, 2010: Variability of the Intertropical Front (ITF) and Rainfall over the West African Sudan–Sahel Zone. *J. Climate*, **23**, 3984–4004, doi:http://dx.doi.org/10.1175/2010JCLI3277.1.

Li, Huanlian, Huijun Wang, and Yizhou Yin, 2012: Interdecadal variation of the West African summer monsoon during 1979–2010 and associated variability. *Climate Dynamics*, **39**, 2883-2894, doi: 10.1007/s00382-012-1426-9.

Liljegren, James C., 2002: Evaluation of a neW multi-frequency Microwave Radiometer for measuring the vertical distribution of temperature, water vapor, and cloud liquid water. ARM Climate Research Facility.

Loeb, N.G., S. Kato, K. Loukachine, and N.Manalo-Smith, 2005: Angular distribution models for top-of-atmosphere radiative flux estimation from the Clouds and the Earth's Radiant Energy System Instrument on the Terra satellite. Part I: Methodology. *J. Atmos. Oceanic Technol*., **22**, 338–351, doi: http://dx.doi.org/10.1175/JTECH1712.1

Lothon, M., F. Saïd, F. Lohou and B. Campistron, 2008: Observation of the diurnal cycle in the low troposphere of West Africa. *Mon. Wea. Rev*., **136**, 3477–3500.

Machado, L. A. T., H. Laurent, and A. A. Lima, 2002: Diurnal march of the convection observed during TRMM-WETAMC/LBA, *J. Geophys. Res*., **107**(D20), 8064, doi:10.1029/2001JD000338.

Machado, L.A.T., H. Laurent, N. Dessay, and I. Miranda, 2004: Seasonal and diurnal variability of convection over the Amazonia: A comparison of different vegetation types and large scale forcing. Theor. Appl. Climatol., 78, 61–77, doi:10.1007/s00704-004-0044-9.

Malhi, Y., E. Pegoraro, A. D. Nobre, M. G. P. Pereira, J. Grace, A. D. Culf, and R. Clement, 2002: Energy and water dynamics of a central Amazonian rain forest, J. Geophys. Res., 107, D20, 8061, doi:10.1029/2001JD000623.

Mallet, M., P. Tulet, D. Serça, F. Solmon, O. Dubovik, J. Pelon, V. Pont, and O. Thouron, 2009: Impact of dust aerosols on the radiative budget, surface heat fluxes, heating rate profiles and convective activity over West Africa during March 2006, *Atmos. Chem. Phys. Discuss*., **9**, 2967-3006, doi:10.5194/acpd-9-2967-2009.

Mather, J. H., McFarlane, S. A., Miller, M. A., and Johnson, K. L., 2007: Cloud properties and associated radiative heating rates in the tropical western Pacific. *J. Geophys Res.*, **112**, D05201, doi:10.1029/2006JD007555.

Mather, J. H. and J. W. Voyles, 2013: The Arm climate research facility: A review of structure and capabilities, *Bull. Amer. Meteor. Soc*., **94**, 377-392, doi:10.1175/BAMS-D-11-00.18.

May, P. T., C. N. Long, and A. Protat, 2012. The diurnal cycle of the boundary layer, convection, clouds, and surface radiation in a coastal monsoon environment (Darwin, Australia). *Journal of Climate*, **25**: 5309-5326.

McFarlane, S. A., J. H. Mather, T. P. Ackerman, and Z. Liu, 2008: Effect of clouds on the calculated vertical distribution of shortwave absorption in the tropics. *J. Geophys. Res*., **113**, D18203, doi:10.1029/2008JD00979I.

McFarlane, S. A., Kassianov, E. I., Barnard, J., Flynn, C., & Ackerman, T. P. (2009). Surface shortwave aerosol radiative forcing during the Atmospheric Radiation Measurement Mobile Facility deployment in Niamey, Niger. *J. Geophys. Res*., **114**, D00E06, doi:10.1029/2008JD010491.

McFarlane, S. A., C. N. Long, J. Flaherty, 2013: A Climatology of Surface Cloud Radiative Effects at the ARM Tropical Western Pacific Sites. *J. Appl. Meteor. Climatol*., **52,** 996–1013. doi: http://dx.doi.org/10.1175/JAMC-D-12-0189.1.

Miller, M. A. and A. Slingo, 2007. The ARM Mobile Facility and its first international deployment: measuring radiative flux divergence in West Africa, *Bull. Amer. Meteor. Soc*., 88:1229–1244, doi: 10.1175/BAMS-88-8-1229.

Miller, Mark A., Virendra P. Ghate, Robert K. Zahn, 2012: The radiation budget of the West African Sahel and its controls: A perspective from observations and global climate models. *J. Climate*, 25, 5976–5996, doi: http://dx.doi.org/10.1175/JCLI-D-11-00072.1.

Miller, R.L., A. Slingo, J.C. Barnard, and E. Kassianov, 2009: Seasonal contrast in the surface energy balance of the Sahel, *J. Geophys. Res*., **114**, D00E05, doi:10.1029/2008JD010521.

Milton, S. F., G. Greed, M. E. Brooks, J. Haywood, B. Johnson, R. P. Allan, A. Slingo, and W. M. F. Grey, 2008: Modeled and observed atmospheric radiation balance during the West African dry season: Role of mineral dust, biomass burning aerosol, and surface albedo, *J. Geophys*. *Res*., **113**, D00C02, doi:10.1029/2007JD009741.

Mlawer, E.J., S.J. Taubman, P.D. Brown, M.J. Iacono and S.A. Clough, 1997: RRTM, a validated correlated-k model for the longwave. *J. Geophys. Res*., **102**, 16,663-16,682.

Mlawer, E.J., and S.A. Clough, 1998: Shortwave and longwave enhancements in the rapid radiative transfer model, in Proceedings of the 7th Atmospheric Radiation Measurement (ARM) Science Team Meeting, U.S. Department of Energy, CONF-970365.

Mohr, K.I., 2004: Interannual, monthly, and regional variability in the wet season diurnal cycle of precipitation in sub-Saharan Africa. *J. Climate*, **17**, 2441 – 2453.

Morris, V. R., 2006: Microwave radiometer (MWR) handbook, ARM Climate Research Facility, ARM TR-016.

Morris, V. R., 2012: Vaisala ceilometer (VCEIL) handbook, ARM Climate Research Facility, DOE/SC-ARM-TR-020.

Neelin, J. D., M. Münnich, H. Su, J. E. Meyerson, and C. E. Holloway, 2006: Tropical drying trends in global warming models and observations, *Proceedings of the National Academy of Sciences*, **103,** 6110-6115, doi: 10.1073/pnas.0601798103.

Negri, Andrew J., Emmanouil N. Anagnostou, and Robert F. Adler, 2000: A 10-yr Climatology of Amazonian Rainfall Derived from Passive Microwave Satellite Observations. *J. Appl. Meteor*., **39**, 42–56. doi: http://dx.doi.org/10.1175/1520-0450(2000)039<0042:AYCOAR>2.0.CO;2.

Nicholson, S. E., 1981: The nature of rainfall fluctuations in subtropical West Africa. *Mon. Wea. Rev*., **108**, 473–487.

Oliveira, A. P., & Fitzjarrald, D. R.,1993: The Amazon river breeze and the local boundary layer: I. Observations. *Boundary-Layer Meteorology*, **63**, 141-162.

Parding, K., L. M. Hinkelman, T. P. Ackerman, and S. A. McFarlane, 2011: Shortwave absorptance in a tropical cloudy atmosphere: Reconciling calculations and observations, *J. Geophys. Res*., **116**, D19202, doi: 10.1029/2011JD015639.

Parker, D.J., C. Thorncroft, R.R. Burton, and A. Diongue-Niang, 2005a: Analysis of the African easterly jet, using aircraft observations from the JET2000 experiment, *Q. J. R. Meteorol. Soc*., **131**, 1461–1482, doi:10.1256/qj.03.189.

Parker, D. J. et al., 2005b. The diurnal cycle of the West African Monsoon circulation, *Q.J. R. Meteorol. Soc.*, 131: 2839-2860, doi: 10.1256/qj.04.52.

Peyrille, P. and J-P. Lapore, 2007: An idealized two-dimensional framework to study the West African Monsoon.Part II: Large-scale advection and the diurnal cycle, *Journal of Atmospheric Sciences*, **64**, 2783-2803, doi: 10.1175/JAS4052.1.

Pospichal, B. et al., 2010: Diurnal cycle of the intertropical discontinuity over West Africa analyzed by remote sensing and mesoscale modelling, *Q. J. R. Meteorol. Soc*., **136**, 92-106, doi: 10.1002/qj.435.

Ramanathan, V., R. D. Cess, E. F. Harrison, P. Minnis, and B. R. Barkstrom, 1989: Cloud- radiative forcing and climate: Results from the Earth Radiation Budget Experiment. *Science,* **243**, 57-63.

Ramier D. et al., 2009: Towards an understanding of coupled physical and biological processes in the cultivated Sahel - 1. Energy and water. *J. Hydrology*, **375**, 204-216.

Rao, V. B., I. F. Cavalcanti and K. Hada, 1996: Annual variation of rainfall over Brazil and water vapor characteristics over South America. *J. of Geophys. Res*., **101**, D21, 26539-26.

Reda, I. and A. Andreas, 2008: Solar Position Algorithm for Solar Radiation Applications, *National Renewable Energy Laboratory*, NREL/TP-560-34302.

Rickenbach, T., R. Nieto Ferreira, N. Guy, and E. Williams, 2009: Radar-observed squall line propagation and the diurnal cycle of convection in Niamey, Niger, during the 2006 African Monsoon and Multidisciplinary Analyses Intensive Observing Period, *J. Geophys. Res.*,**114**, D03107, doi:10.1029/2008JD010871.

Rosário, N. E., Yamasoe, M. A., Brindley, H., Eck, T. F., & Schafer, J., 2011: Downwelling solar irradiance in the biomass burning region of the southern Amazon: Dependence on aerosol intensive optical properties and role of water vapor. J. of Geophys. Res., 116, D18.

Russell, J. E., J. E. Harries, and N. Clerbaux, 2006: Geostationary Earth Radiation Budget (GERB) data. 36th COSPAR Scientific Assembly, 36, 2490.

Sandford, M.C.W. et al., 2003: The geostationary Earth radiation budget (GERB) instrument on EUMETSAT's MSG satellite. *Acta Astronautica*, **53**, 909-915.

Sapucci, L. F., L. A. T. Machado, J. F. G. Monico, and A. Plana-Fattori, 2007: Intercomparison of Integrated Water Vapor Estimates from Multisensors in the Amazonian Region. J. Atmos. Oceanic Technol., 24, 1880–1894.

Schafer, J. S., B. N. Holben, T. F. Eck, M. A. Yamasoe, and P. Artaxo, 2002: Atmospheric effects on insolation in the Brazilian Amazon: Observed modification of solar radiation by clouds and smoke and derived single scattering albedo of fire aerosols, J. Geophys. Res., 107, D20, 8074, doi:10.1029/2001JD000428, 2002.

Sivaraman, C. and J. Comstock, 2011: Micropulse lidar cloud mask- value added product technical report, DOE/SC-ARM/TR-098.

Slingo, A., H. E. White, N. A. Bharmal, and G. J. Robinson, 2009: Overview of observations from the RADAGAST experiment in Niamey, Niger: 2. Radiative fluxes and divergences, *J. Geophys. Res*., **114**, D00E04, doi:10.1029/2008JD010497.

Stephens, G. L., et al., 2012: An update on Earth's energy balance in light of the latest global observations. *Nature Geoscience*, **5**, 691–696, DOI: 10.1038/NGEO1580.

Sultan, B., S. Janicot and A. Diedhiou, 2003: The West African Monsoon dynamics. Part 1: Documentation of Intraseasonal variability. *J. Climate*, **16**, 3389-3406.

Sultan, B. and S. Janicot, 2003. The West African Monsoon dynamics. Part II: The "preonset" and "onset" of the summer monsoon. *J. Climate*, **16**: 3407-3427.

Taylor, Karl E., R. J. Stouffer, G. A. Meehl, 2012: An Overview of CMIP5 and the Experiment Design. *Bull. Amer. Meteor. Soc.*, **93**, 485–498. doi:http://dx.doi.org/10.1175/BAMS-D-11-00094.1.

Taylor, P. C., 2012: Tropical outgoing longwave radiation and longwave cloud forcing diurnal cycles from CERES. *Journal of the Atmospheric Sciences*, **69**, 3652-3669.

Thampi, B. V. and R. Roca, 2014: Investigation of negative cloud radiative forcing over the Indian subcontinent and adjacent oceans during the summer monsoon season. *Atmospheric Chemistry and Physics*, **14**, 6739-6758.

Timouk, F. et al., 2009: Response of surface energy balance to water regime and vegetation development in a Sahelian landscape. *Journal of Hydrology*, **375**, 178-189, doi: 10.1016/j.jhydrol.2009.04.022.

Thorncroft, C.D. and M. Blackburn, 1999: Maintenance of the African easterly jet. *Q. J. R. Meteorol. Soc*., **125**, 763-786.

Trabachino, L. and M. A. Miller: Thermodynamic profiling capabilities of the microwave radiometer profiler in various locations of interest for atmospheric model development. *Atmospheric System Research Science Team Meeting*, Potomac, Maryland, March 10 - March 14, 2014.

Trenberth, K. E., J. T. Fasullo, J. Kiehl, 2009: Earth's Global Energy Budget. *Bull. Amer. Meteor. Soc*., **90**, 311–323. doi: http://dx.doi.org/10.1175/2008BAMS26 34. 1.

Turner, D.D., 2008: Ground-based infrared retrievals of optical depth, effective radius, and composition of airborne mineral dust above the Sahel. J. *Geophys. Res*., **113**, D00E03, doi:10.1029/2008JD010054.

Twomey, S., 1977: The influence of pollution on the shortwave albedo of clouds. *Journal of the Atmospheric Sciences*, **34**, 1149-1152.

Wang, Z, and K Sassen. 2001: Cloud type and macrophysical property retrieval using multiple remote sensors. *Journal of Applied Meteorology*, **40**, 1665–1682.

Widener, K.B. and K. Johnson, 2006: W-band ARM Cloud Radar (WACR) Handbook. ARM Climate Research Facility, ARM-TR-073.

Wielicki, B.A., B. R. Barkstrom, E. F. Harrison, R. B. Lee III, G. L. Smith, and J. E. Cooper, 1996: Clouds and the Earth's radiant energy system (CERES): An Earth observing system experiment. *Bull. Amer. Meteor. Soc*., **77**, 853–868, doi: http://dx.doi.org/10.1175/1520-0477(1996)077<0853:CATERE>2.0.CO;2.

Williams, E., et al., 2002: Contrasting convective regimes over the Amazon: Implications for cloud electrification, *J. Geophys. Res*., **107**(D20), 8082, doi:10.1029/2001JD000380.

Zipser, E. J., C. Liu, D. J. Cecil, S. W. Nesbitt, and D. P. Yorty, 2006: Where are the most intense thunderstorms on Earth?. *Bull. Amer. Meteor. Soc*., **87**, 1057–1071. doi: http://dx.doi.org/10.1175/BAMS-87-8-1057.